



THE HONG KONG
POLYTECHNIC UNIVERSITY

香港理工大學

Pao Yue-kong Library

包玉剛圖書館

Copyright Undertaking

This thesis is protected by copyright, with all rights reserved.

By reading and using the thesis, the reader understands and agrees to the following terms:

1. The reader will abide by the rules and legal ordinances governing copyright regarding the use of the thesis.
2. The reader will use the thesis for the purpose of research or private study only and not for distribution or further reproduction or any other purpose.
3. The reader agrees to indemnify and hold the University harmless from and against any loss, damage, cost, liability or expenses arising from copyright infringement or unauthorized usage.

IMPORTANT

If you have reasons to believe that any materials in this thesis are deemed not suitable to be distributed in this form, or a copyright owner having difficulty with the material being included in our database, please contact lbsys@polyu.edu.hk providing details. The Library will look into your claim and consider taking remedial action upon receipt of the written requests.

**INVESTIGATIONS OF THE MECHANICAL
RELAXATION OF GLASSES AT HIGH
TEMPERATURES**

JIANBIAO WANG

PhD

The Hong Kong Polytechnic University

2021

The Hong Kong Polytechnic University
Department of Mechanical Engineering

**Investigations of the mechanical relaxation of
glasses at high temperatures**

Jianbiao WANG

A thesis submitted in partial fulfillment of the requirements for the degree
of Doctor of Philosophy

July 2020

Certificate of Originality

I hereby declare that this thesis is my own work and that, to the best of my knowledge and belief, it reproduces no material previously published or written, nor material that has been accepted for the award of any other degree or diploma, except where due acknowledgement has been made in the text.

Signed: _____

Name: Wang Jianbiao

Abstract

Glasses are in daily use by virtually all humanity and have dramatically expanded the frontiers of industry and science as well. Owing to the developments of newest technologies, especially for fifth-generation (5G) wireless communication and artificial intelligence (AI), the demand for glass-based optical devices and structural components has sharply increased. This leads to new challenges to large-scale precision manufacturing as the mechanical behaviors of glass are complex during its thermal history. In this thesis, I attempt to explore the mechanical relaxation of glass at high temperatures, which not only benefits important industrial demands but also helps understand essential questions associated with glass transition. This thesis summarizes my efforts in performing mechanical experiments and theoretical modeling to promote the understanding of glass relaxation and transition.

(1) Primary (α) relaxation was studied experimentally using the impulse excitation technique (IET) in borosilicate and chalcogenide glasses. The glass transition point (T_g) determined from temperature-dependent Young's modulus was found to be close to that determined by viscosity in borosilicate glasses. A non-destructive and instantaneous measurement method for determining viscosity is proposed for borosilicate glasses that have little non-exponentiality. This method can be explained by the implicit features in the Burgers model and a physics-based minimal model that considers the solid-like to liquid-like behavior transition. For chalcogenide glass, a striking non-exponential relaxation was found using the Cole–Davidson (CD) function, and the non-exponential

estimate agrees well with previous research.

(2) A new mechanism for the mechanical secondary (β) relaxation was established based on the normal mode analysis of a potential energy landscape and experimentally confirmed by the predicted double-peak phenomenon in the Fourier spectrum of a fluorosilicate glass beam. This leads to a new method for probing β relaxation. Using the proposed model, the β relaxation in the fluorosilicate glass is found to be negatively temperature-dependent and can be explained based on the picture of fragmented oxide-network patches in liquid-like regions, which broadens the understanding of β relaxation.

(3) A long-expected phenomenon of non-zero to zero transition around T_g was firstly observed in structural glass, and the Kovacs' paradox was firstly confirmed in inorganic glasses by monitoring the relaxation of Young's modulus of an As_2Se_3 glass in two-step aging experiments. The effective relaxation time and Young's modulus at a quasi-equilibrium state obtained from long-term aging are both found to be dependent on the thermal history. The effect of thermal history is found to be related to the survival parts of glass after aging (i.e., the persistent memory). An elasticity-based relaxation model is proposed to explain the relationship behaviors, and a Mori–Tanaka (MT) analysis is used to determine the volume fraction of the local survival parts. The obtained memory persistence from either analysis agrees well with each other. With a series of experiments that change the aging temperature, it is found that structural memory persists below a critical temperature $T_p \sim T_g$ and becomes zero above T_p .

(4) A birth–death model is proposed to reveal the coupling effects between elastic

modulus relaxation and local heterogeneity, of which the analytical solution can be obtained. A preliminary examination shows that the model can capture the normal and anomalous relaxation of different glasses. Based on the birth–death model, a non-Gaussian distribution of microscopic elastic modulus can be obtained which was found in previous molecular dynamic simulations.

With novel experiments and theoretical inspections, an in-depth understanding of glass relaxation and transition is explored. The findings of this thesis could help industrial glass communities that need reliable but facile mechanical relaxation models. This investigation also provides new ideas on probing the glass transition, which can benefit the basic science in the future.

Keywords: Glass relaxation, β relaxation, Kovacs' paradox, memory effects, birth–death model, Young's modulus, impulse excitation technique

Publications arising from the thesis

Journal papers:

[1] **J. Wang**, H. Ruan, X. Wang, J. Wan, Investigating relaxation of glassy materials based on natural vibration of beam: A comparative study of borosilicate and chalcogenide glasses, *Journal of Non-Crystalline Solids*, 500 (2018) 181-190.

[2] **J. Wang**, X. Wang, H. Ruan, On the mechanical β relaxation in glass and its relation to the double-peak phenomenon in impulse excited vibration at high temperatures, *Journal of Non-Crystalline Solids*, 533 (2020) 119939.

[3] **J. Wang**, X. Wang, H. Ruan, Ergodicity breaking of an inorganic glass in aging near T_g probed by elasticity relaxation, arXiv:2006.04434, (2020), *Physical Review Materials* (under revision).

[4] M. Yang, X. Liu, Y. Wu, H. Wang, **J. Wang**, H. Ruan, Z. Lu, Elastic modulus change and its relation with glass-forming ability and plasticity in bulk metallic glasses, *Scripta Materialia*, 161 (2019) 62-65.

[5] X. Wang, J. Wan, **J. Wang**, L. Zhu, H. Ruan, Anomalous sudden drop of temperature-dependent Young's modulus of a plastically deformed duplex stainless steel, *Materials & Design*, 181 (2019) 108071.

Conference paper:

[1] **J. Wang**, H.H. Ruan, Probing Temperature-Dependent Viscoelastic Properties of Glassy Materials Using Impact Induced Vibration-Theory and Experiments, in: *Key Eng. Mater., Trans Tech Publ*, 2017, pp. 116-121.

Conference presentations:

[1] **J. Wang**, X. Wang, H. Ruan, The double-peak spectra of a fluoroborosilicate glass and its implication of the viscoelastic behavior, *25th international congress on glass (ICG2019)*, Boston, USA (2019)

[2] **J. Wang**, X. Wang, H. Ruan, The split frequency of beam vibration and the corresponding Young's modulus in the high temperature IET experiments, *The 8th East Asia Mechanical and Aerospace Engineering Workshop*, Hong Kong, China (2018)

[3] **J. Wang**, H. Ruan, M. Yang, Z. Lu, The molecular dynamics simulations and experiments of the temperature-dependent Young's modulus of high entropy alloy (随温度变化的高熵合金弹性模量的分子动力学模拟与实验研究), *Chinese Materials Conference 2017*, Yin Chuan, China (2017)

Acknowledgements

At this moment, I recall the first day when I came to The Hong Kong Polytechnic University, and the day is like today, having bright sunlight and soft wind. There are too many unforgettable people and events that have already grown up in my mind.

I would like to address the most sincere gratitude to my supervisor Dr. Haihui Ruan for the valuable guidance, consistent supports, and warm-hearted encouragements. Dr. Ruan is a talented and knowledgeable scholar who can find directions in the mist. Without his help, it would be very hard for me to climb the mountain of knowledge. His academic attitude is meticulous, and his vision is ambitious, which are all the treasures of my future works and life. Besides, Dr. Ruan also concerns my life in Hong Kong and helped me a lot on many issues. I would like to address the thanks to Dr. Ruan again.

I would like to address the same gratitude to my co-supervisor Dr. Haimin Yao for his valuable guidance and supports. Dr. Yao is a keenly penetrating scholar. He supported me a lot in the experiments and helped me a lot in academic thinking. His creativity and confidence influence me in many aspects in the past and will continue to influence my future.

I would also like to express my deep appreciations to the collaborators and team workers, Dr. Xu Wang, Dr. Jianquan Wan, Dr. Ming Yang, Dr.

Chen Lin, Mr. Jinan Liu, Mr. Yi Yang, Mr. Awis Mkhtar, Mr. Suo Zhang, Mr. Jens Krarup, and Mr. Saad Ahmed Sheikh. It was a happy time to work together with them, and their constructive ideas greatly promoted my thesis.

I would also like to thanks Prof. Chi-Hang Lam, Dr. Matteo Lulli, Dr. Weidong Liu, Dr. Linli Zhu, Mr. Kuo-Hao Lee, Ms. Ai-xi Zhang, and Ms. Jing Li for valuable discussions.

Special thanks to all the technical staffs in the Department of Mechanical Engineering, the Research Office (Graduate School), and the Human Resources Office at The Hong Kong Polytechnic University who actively helped me a lot with this thesis.

Last but not least, I would like to express my thanks to my family and friends for their continuous support for my Ph.D. study.

Table of Contents

Abstract	I
Publications arising from the thesis	IV
Acknowledgements	VI
Table of Contents	- 1 -
Chapter 1 Research background	1
1.1 Introduction	1
1.2 History of glass	2
1.3 Large-scale manufacturing based on precision glass molding in modern industry	3
1.4 Glass state as a mystery in physics	5
1.5 Research scope and objectives	6
Chapter 2 Literature review	9
2.1 Introduction	9
2.2 Glass, glass transition, and glass relaxation	9
2.3 Phenomenological models of α-relaxation	13
2.4 Activation energy scenario for the Arrhenius and non-Arrhenius laws 17	
2.4.1 Free-volume models.....	17
2.4.2 Entropy models	17
2.4.3 Energy models	18
2.4.4 Elastic models	18
2.5 Nonlinear relaxation associated with thermal history	20
2.5.1 Tool–Narayanaswamy–Moynihan (TNM) model.....	20
2.5.2 Kovacs–Aklonis–Hutchinson Ramos (KAHR) model	22

2.6 Understanding glass relaxation from heterogeneity (I): Statistical scenarios	22
2.6.1 Mode-coupling theory.....	23
2.6.2 Coupling model.....	24
2.6.3 Other models.....	25
2.7 Understanding glass relaxation from heterogeneity (II): Stochastic scenarios	25
2.7.1 Energy-controlled stochastic process.....	25
2.7.2 Volume-controlled stochastic process.....	28
2.7.3 Rational thermodynamics	28
2.8 Machine-learning approach	29
2.9 Summary	30
Chapter 3 Experimental design based on impulse excited technique (IET): Theories and applications extended to glass at high temperatures	31
3.1 Introduction: Impulse excited technique (IET)	31
3.2 Vibrations of a viscoelastic beam with free-free end boundary conditions	34
3.3 Damping effects of support lines	39
3.4 Shoulder peak phenomenon	40
3.5 Summary	46
Chapter 4 Glass transition and primary (α) relaxations revealed by Young's modulus and decay rate in <i>in situ</i> experiments	47
4.1 Introduction	47
4.2 Experimental results of time-dependent Young's modulus and decay rate 49	
4.3 Discussion (I): The viscoelastic relaxations of phenomenological models	54

4.3.1	Finding viscosity from the results of IET experiments.....	54
4.3.2	The temperature-dependent viscosity determined from IET	58
4.4	Discussions (II): The physics picture under the phenomenological models.....	60
4.4.1	Simplified model for transition from solid-like to liquid-like behaviors	60
4.4.2	Effect of non-exponential relaxation	64
4.5	Summary	69
Chapter 5	The secondary (β) mechanical relaxation in glass and its performance in IET experiments	71
5.1.	Introduction	71
5.2.	Phenomenological modeling in the differential form	74
5.2.1	Mathematical derivations.....	74
5.2.2	Primary experimental examination	77
5.2.3	Beta relaxation revealed by the model.....	78
5.3.	Modeling mechanical β relaxation using PEL	80
5.4.	Experimental results of double peaks.....	87
5.5.	Physical understanding of the temperature dependence of the mechanical β relaxation in the fluorosilicate glass.....	90
5.6.	Conclusions	94
Chapter 6	Ergodicity breaking of an inorganic glass in aging near T_g probed by elasticity relaxation	95
6.1	Introduction	95
6.2	Temperature jump experiments.....	98
6.3	The relation between relaxation time and elasticity	102
6.3.1	Global elastic model	102
6.3.2	Mori-Tanaka (MT) analysis of glass after aging.....	104
6.4	Ergodicity breaking origin to dynamic heterogeneity	108

6.5	Conclusions	110
Chapter 7	Birth–death model of glass relaxation related to local elastic heterogeneity	111
7.1	Introduction	111
7.2	Mathematical modeling	113
7.2.1	Birth–death process at a constant temperature.....	113
7.2.2	Variation in survival ratio at varying temperatures.....	118
7.3	Numeric validation with stochastic simulation	121
7.4	Applications of the BD model and discussions	124
7.4.1	Prediction on the temperature-dependent Young’s modulus.....	124
7.4.2	Relationship between relaxation time and mixing rules	128
7.4.3	Distributions of the local elasticity heterogeneity due to VRH approximation	130
7.5	Conclusions	134
Chapter 8	Conclusions and future works	135
8.1	Conclusions	135
8.2	Future works	137
8.2.1	Probing elasticity relaxation of glass by the birth–death model	137
8.2.2	Mechanisms and applications of the rate-dependent viscosity of chalcogenide glasses	138
References	141

Chapter 1 Research background

1.1 Introduction

With the rapid development of modern technology, especially for fifth-generation (5G) wireless communication technologies and artificial intelligence (AI), an increasing number of optical products are in demand [1, 2]. This makes traditional materials such as glass, which is already used daily by most people, show valuable prospects in the future. If glasses were to be stripped from our society, mirrors, eyeglasses, televisions, cell phones, and many others all disappear. If we recollect, Galileo, Descartes, Newton, Fraunhofer, and many other early scientists devoted significant effort in producing glass lenses [3, 4], which then remarkably improved the research of modern science as the commonly used devices in research communities, including microscopes, telescopes, barometers, thermometers, and vacuum chambers, which are all dependent on glass products [1]. In 2014, Mauro and Zanotto [5] summarized 15 critical issues of future glass research, including combatting global warming, renewable energy, new energy storage methods, water and air pollution mitigation, energy consumption reduction, human health, information and communication technology, architecture, and other structural applications

However, unlike the abundance of glass applications and massive future demands, our beings' understanding of glass is immensely insufficient. In 2005, the question of 'What is the nature of the glassy state' was suggested to be one of the greatest scientific conundrums for the 125th anniversary of science [6]. The Nobel laureate P. W.

Anderson stated '*The deepest and most interesting unsolved problem in solid state theory is probably the theory of the nature of glass and the glass transition*' [7]. At present, many remarkable glass-related questions still exist, calling more efforts to untie them.

1.2 History of glass

Although some types of glass, such as perlite, obsidian, and tektites exist in nature [8], most glasses used are artificial. This important material has a long history. The estimated date of origin of man-made glass is from 4000 BCE in Mesopotamia [9]. Archaeological discoveries suggest that Egyptians could make glass vessels between the 14th and 16th century BCE. The technology then spread to Syria, Cyprus, and other eastern Mediterranean regions around the 11th century BCE. After 1000 BCE, Syria and Palestine began to be the primary source of glass products, and around 400 BCE, Macedonia and Greece also emerged as centers of glassmaking. Syria and Palestine developed the technique of glass blowing, which renders it much easier to fabricate glass products with complex shapes. Also, Greeks developed a new technology called the sandwiching technique by which gold layers were trapped between clear glass parts. In China, the evidence of glass usage was recovered from graves of 6th century AD [10]. Interestingly, further analysis revealed that the discovered glasses containing lead and barium were first used in the 2nd and 3rd century BCE. After a long period of human effort, glass can now be produced in large-scale industrialization. In the modern glass industry, glass is generally produced by using several cooling techniques, including the

Fourcault process [11], Colburn process [12], and float process, which is the most used method [13]. Another newly developed method is the sol–gel process [14].

The early glass was not transparent and, thus, became an alternative to pottery or precious stone replicas [15]. The desire for clear and transparent glass comes with the growth of blown glass production [3]. Thereafter, it was realized that purification and the proportion of raw materials are important in the making of clear glass [16, 17]. With increasing efforts, the optical applications for glass have become increasingly popular, leading to the current understanding of glass.

1.3 Large-scale manufacturing based on precision glass molding in modern industry

Two primary approaches have been used to make products from glass materials. The first is through material-removal processes, such as grinding, polishing, and lapping. This method can be adapted to various products, but it is costly and time-consuming, especially for hard glass and products with complex shapes [18]. The other method is thermoforming, such as glass blowing, cold bend, and precision glass molding (PGM). Thermoforming is less costly in both time and materials, but the process control may be complicated and the accuracy may not be satisfactory. In addition, the thermoformed glass workpiece may require further polishing to become transparent. This is the reason that PGM, which can realize efficient manufacturing in a single step, was proposed and has become one of the most active research areas [19, 20].

Fig. 1.1 shows a typical process for making a lens through PGM. The chamber of the PGM machine is filled with inert gas, such as nitrogen, during all heating and

molding processes to protect the sample from oxidation. The molding temperature should be above the glass transition temperature (T_g) to ensure glass viscosity is maintained in the range from 10^7 to 10^8 Pa·s. The molding process is then conducted with precision control. Upon completion of molding, the lens is first slowly cooled until the glass temperature has dropped to the strain point of the glass, and then the compressive force can be removed. Such a process has a higher production efficiency when a fast cooling rate is applied in the demolding process [21].

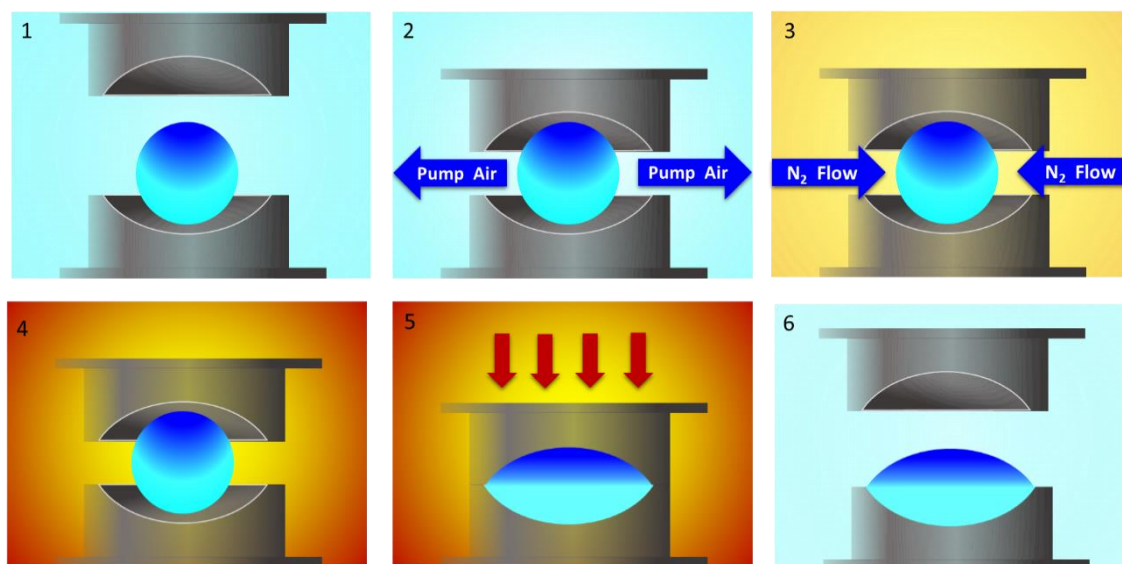


Fig. 1.1. Typical PGM process. (1) place the sample into the chamber, (2) pump out the air, (3) inject the inert gas, (4) heat the sample to the required temperature, (5) compress it with the designed mold, and (6) demold after cooling.

However, many technical challenges occur in PGM. Firstly, PGM is generally conducted at temperatures higher than T_g , and the product property is significantly dependent on the thermal history during cooling through T_g . Besides, the mechanical compressive process is related to the visco-elasto-plasticity of the sample, while a consensus of the constitutive relations of different glass is still lacking. Finding a suitable constitutive model for moldable glass is critical to the final products. However,

this process is difficult owing to the insufficient knowledge of glass relaxation/transition. A PGM process leads to residual stresses and shapes distortion in a molded glass piece, causing unexpected changes in density and refractive index. In the worst cases, molding may fail because of material breakage [22]. Conversely, glass production is a highly energy-intensive process [23]. The ongoing increase in world glass demand implies that this industry's energy use and CO₂ emissions will continue to grow without additional measures toward energy efficiency. In the PGM process, significant energy is used to maintain the plastic glass state, and multiple attempts are generally needed. A good understanding of the materials can help design a heating process that requires less energy and is environmentally friendly.

Traditionally, PGM is used for silica-based glass, while in recent years, the PGM of chalcogenide glass has drawn increased attention. Chalcogenide glass is an infrared optical product alternative to germanium crystal, which is rare and expensive [24]. The massive application of molding for chalcogenide glass makes civilian use possible, for example, living body recognition in autonomous vehicles [25]. However, the molding of chalcogenide glass has unresolved issues. The logarithmic viscosity of chalcogenide glass is linear to temperature [26, 27], which is dissimilar to that of Angell's predictions for most glass [28, 29]. Furthermore, chalcogenide glass breaks more easily during the molding process even when the temperature is higher than T_g or may oxidize, gasify or adhere to a mold surface when the temperature goes even higher [22].

1.4 Glass state as a mystery in physics

Before people realized the structural difference between glass and crystalline solids, glass is a commonly used term for describing a transparent or diaphanous material. It is well known that the macro properties of materials are determined by their

inner microstructures. Glasses are impressive because they share similarities with crystalline solids since they are both mechanically rigid at the macro level, while they share similarities with liquids by having disordered micro-level structures [30, 31]. However, the latter leads to difficulty in achieving an analytical description of the former because of a lack of mathematical amenities arising from structural periodicity [32]. Hence, the glass research community has more experience than knowledge. In 1932, Zachariasen stated that *‘It must be frankly admitted that we know practically nothing about the atomic arrangement in glasses’* when he started the classic paper [33].

It is generally believed that glassy formers can avoid crystallization due to the sharply increased viscosity near T_g during fast cooling [34]. Below T_g glass is ‘stuck’ on the way to its equilibrium state. That is, glass has high free energy and tends to relax. However, many glasses relax to the amorphous state of supercooled liquids instead of crystallization, although the latter should have the lowest free energy. In 2017, Zanutto and Mauro [35] summarized a paradoxical ultimate fate of glass, either supercooled liquid or crystallization. Although numerous efforts have been devoted to glass research, there are also many unsolved problems associated with glass relaxation, including memory effects [36, 37], Kovacs’ paradox [38-41], hierarchical relaxation [42-44], and dynamic and static heterogeneity [45-49]. The understanding of these issues will not only provide a physical picture of glass relaxation but also have direct benefits to glass manufacture.

1.5 Research scope and objectives

To help address these fundamental problems of glass, the viscoelastic property of glass influenced by thermal history is very interesting to consider. Previously, the glass processing community has focused more on phenomenological models, which may be

easily applied to glass processing, while the glass physics community focuses more on mathematical models that may reflect the nature of amorphous states. The gap between essential glass properties and phenomenological viscoelastic behaviors is far from being closed, leading to the reality that the models used in the industry may not be very reliable, while the physical discussions of glass are far from practical applications. Therefore, the traditional phenomenological viscoelastic property of glass will be understood in more physical approaches in this thesis, which helps reveal the connections between the macro mechanical response and the microphysical mechanism, and in turn, helps build more reliable models.

In this thesis, I attempt to achieve a better understanding of glass relaxation at high temperatures where the glass is usually processed. I will first review the literature on both phenomenological models and the understanding of glass physics in Chapter 2. Next, the experimental designs based on the impulse excitation technique (IET) will be introduced in Chapter 3. A revisit of viscoelastic beam vibration is provided, which helps us better understand the experimental results. In Chapter 4, the primary (α) relaxation of glass is discussed based on IET results. As viscosity is one of the most important factors in glass processing, a variety of spring-dashpot systems are examined to check if the short-term response in IET can be used to determine viscosity and the rationale of choosing a simplified viscoelastic model is provided. In Chapter 5, the secondary (β) relaxation of glass will be modeled in two different ways, that is, the integral-type viscoelastic model from the bottom of physics and the differential-type viscoelastic model based on a traditional phenomenological linear relation, and then the two methods are both examined based on the experimental results to determine their connections. In Chapter 6, the effort will be devoted to how the phenomenological measurable quantity reflects the micro relaxation process in physics. The time-

dependent relaxation of Young's modulus under different thermal conditions will be measured, and the physics close to the equilibrium state will be discussed in detail. Based on the physical findings in the previous chapters, a simple birth–death model is proposed and preliminarily studied in Chapter 7. Finally, the results are summarized, and future research topics are proposed in Chapter 8.

Chapter 2 Literature review

2.1 Introduction

In this chapter, the works associated with glass transition and glass relaxation are summarized. In Section 2.2, the basics of glass and glass transition will be introduced. The phenomenological models of glass relaxation will be summarized in Section 2.3, and the physical modeling will be summarized in Section 2.4. In Section 2.5, the latest research on machine learning related to glass will be summarized.

2.2 Glass, glass transition, and glass relaxation

Several standard terms are used to describe glass, including supercooled liquid [34, 50], amorphous state [31], non-crystalline materials [51], and disordered materials [52]. With a less strict distinction, these terms have similar meanings, and the difference is related to the environments of different research groups or disciplines. Some physical differences between these terms will be mentioned later. To show the particularity of glass at the micro-level, the state of the atomic configuration of glass, that is, the disordered configurations in the long-range distance can be called a glassy state. However, it should be noted that someone may argue that glass is only considered as a disordered material obtained by cooling liquids. For example, *Encyclopædia Britannica* states that glass is an inorganic solid material made by cooling molten ingredients [53]. With an understanding of disordered materials, glass can be made by constituents ranging from inorganic minerals and polymers to metals [54], and glass making is not

limited to cooling methods [55-57]. In addition, some biological materials have glassy states [58-60]. These glasses all correspond to certain disordered atomic or molecular structures, thus called structural glass. Several non-structural configurations can also be called ‘glass’, for example, spin glass [61], charge-density glass [62], orientational glass [63], and vortex glass [64], to describe their disordered state. Either structural or non-structural glass shares many similar phenomenological regularities and can be collectively called glassy state materials. Therefore, in this thesis, glass is defined as the material of (1) macroscopically solid-like property (that is, it can resist shear force in the experimental period) and (2) microscopically a lack of long-range order in atomic and/or molecular structures. Unless otherwise mentioned, only structural glass is considered in this thesis.

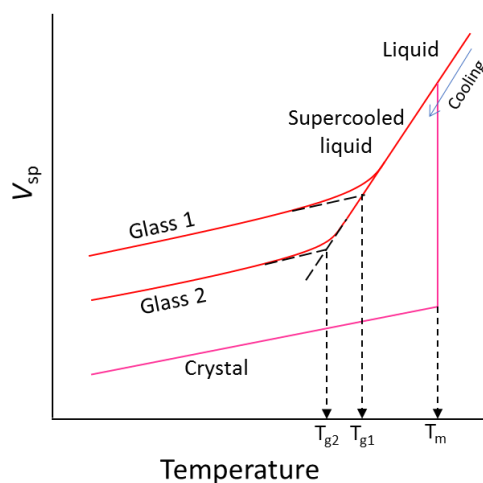


Fig. 2.1 Schematic representation of phase and glass transition: the specific volume (V_{sp}) changes with temperature.

Glass transition is a unique property of glass that differs from traditional solid and liquid materials. With temperature change, materials may change between different

phases due to thermodynamics, thus leading to changes in the material properties. Fig. 2.1 shows the change in the specific volume V_{sp} with temperature for a typical liquid undergoing a cooling process. When the temperature reaches the melting point T_m , the liquid may crystallize. However, since crystallization is a kinetic process that rests with several different factors, the liquid may avoid crystallization when the temperature is below T_m , leading to supercooled liquid. If the temperature continually decreases, the supercooled liquid will soon become a solid-like material, glass, and the temperature-dependent property changes. The transition from supercooled liquid to glass is the so-called glass transition. Generally, the volume expands linearly with the temperature for both the supercooled liquid and glass. Therefore, if we extend the temperature dependence curve of supercooled liquid and glass, a cross will be obtained. The temperature corresponding to the cross is called 'glass transition temperature', T_g , as shown in Fig. 2.1.

Generally, the transition at T_g is considered a result of sharply increased viscosity, which prevents the system from achieving an equilibrium state [34]. However, T_g is not a well-defined concept as the obtained value of T_g depends on thermal history. For example, if the cooling rate is different, T_g is different. As shown in Fig. 2.1, faster cooling and slower cooling will lead to Glass 1 and Glass 2, respectively. This is because, at a lower cooling rate, the glass system has more time to reach its equilibrium state; thus, the temperature dependence of V_{sp} will continue its tendency as a supercooled liquid. A similar transition can also be found in volume [65], enthalpy [66], refractive index [67], viscosity [28, 29], elastic modulus [68, 69] or other macroscopic

properties [70]. To understand the transition from the microstructures of glass, diffraction methods [71] and spectroscopy [72] were used in early studies. Several atomic models are used, including Monte Carlo Simulations [73] and molecular dynamics simulations [74]. As proposed by Rouxel [75], the structure in glass can be separated into four relevant scales: (i) atomic, over 1.5–2.5 Å; (ii) molecular, from 2.5 to 4.5 Å; (iii) ‘network’, within a few nanometers; and (iv) continuum scales, over a hundred nanometers. Scales (i) and (ii) are in the short range, and scale (iii) is in the medium range. On these scales, we can obtain some structural messages [76]. Meanwhile, on the scale (iv), we still do not know anything except for some empirical relaxation theories [33]. Surprisingly, no significant differences exist in the micro configurations between the supercooled liquid state and the glassy state. Therefore, glass can be treated as supercooled liquids out of equilibrium state due to their high viscosity [34].

The glassy system departing from an equilibrium state is always on a path to equilibrium, known as glass relaxation. Such a relaxation process can be found by monitoring the macro properties mentioned previously. It is known that the relaxation process is not only related to understanding the basics of glass transition but also related to industrial applications. Therefore, the relaxation behaviors of glass should be investigated.

Experiments have shown that relaxation occurs in almost all timescales, which can roughly be separated into three types when it is close to the T_g [44, 77]. (1) The primary, referred to as α -relaxation with a typical timescale of $>10^{-3}$ s, is associated with

structural relaxation and plays the primary role in glass transition. (2) The secondary relaxation with a timescale of 10^{-8} – 10^{-3} s, which is often called (slow) β relaxation, is related to localized atomic motion through a mechanism that is still vague. (3) The relaxation with a timescale of 10^{-8} – 10^{-12} s, usually called fast β relaxation, could be related to the rattling motion of caged particles [78].

2.3 Phenomenological models of α -relaxation

As an empirical fact, the relaxation process is faster if the current state is further from the equilibrium state. Therefore, one can define a relaxation process as

$$\frac{dP}{dt} = \frac{P_{\infty} - P}{\tau}, \quad (2.1)$$

where $P = P(t)$ is the monitored property, $P_{\infty} = P(t \rightarrow \infty)$ is the property at equilibrium state, t is time, and τ is a parameter that shows the relaxation speed. If τ is constant at a specified temperature T , the above equation can be solved as

$$\dots \quad (2.2)$$

where A is a parameter determined by initial conditions. This is an exponential process. When the temperature is close to T_g , the strain relaxation of SiO_2 glass [79], the refraction index relaxation of GeO_2 glass [80], and the enthalpy relaxation rate of RbCN [81] are exponential functions of time. However, most relaxation behaviors of glass are non-exponential [82]. The most frequently used non-exponential functions are the stretched exponential and power law functions. The stretched exponential function is also called the KWW function after Kohlrausch–Williams–Watts [83] and can be written as:

$$P(t) = P_\infty + A \exp \left[- \left(\frac{t}{\tau} \right)^n \right], \quad (2.3)$$

where n is the non-exponential index. Power law functions have more flexible forms; for example [84],

$$P(t) = P_\infty + \frac{A}{(1+t/\tau)^n}, \quad (2.4)$$

where n is the power index. In Eqs. (2.3) and (2.4), we still consider the parameter τ as the relaxation time. However, its physical meaning is different from that in Eq. (2.1).

τ may be related to the environmental conditions, for example, temperature T . If a certain form with a specified index n can well describe the relaxation at different temperatures in an investigation, the relaxation function defines a master curve because of its uniformity. If we chose a relaxation process at $T = T_r$ as a reference relaxation curve, all the relaxation processes will be equal to a reference relaxation by changing $\tau(T)$ (relaxation time at temperature T) to $\tau(T_r)$ (relaxation time at temperature T_r) by using the following ratio:

$$a_T = \frac{\tau(T)}{\tau(T_r)}. \quad (2.5)$$

The a_T term is generally called ‘shift factor’ because it helps ‘shift’ the relaxation curves to that of the reference. Based on the above assumption, a_T is related to T instead of T_r , that is, $a_T = a_T(T)$. Thus, one can calculate the relaxation process at any temperature if $a_T(T)$ and $\tau(T_r)$ are known. This is especially important for predicting the properties of glass under complex thermal history. With the help of $a_T(T)$, the relaxation process at any temperature can always be considered as a continuous process at the reference temperature. This is the so-called ‘time-temperature superposition principle’. One

frequently used expression of $a_T(T)$ is the Williams–Landel–Ferry(WLF) equation [85].

$$\log a_T(T) = \frac{C_1(T - T_r)}{C_2 + T - T_r}, \quad (2.6)$$

where C_1 and C_2 are experimentally determined parameters.

Other forms of $a_T(T)$ are frequently presented by an equivalent question: How does τ change with T ? The simplest relation was suggested by Arrhenius [86].

$$\tau = \tau_0 \exp\left(\frac{\Delta E}{k_B T}\right), \quad (2.7)$$

where ΔE is the energy barrier. However, the Arrhenius law only works for a few glassy formers, for example, pure silica (a-Si), silicon oxide (a-SiO₂), or phosphor pentoxide (a-P₂O₅) [87] (herein, ‘a’ is short for ‘amorphous’). The relaxations of most glassy formers are non-Arrhenius. Walther [88] in 1931 suggested that

$$\tau = \tau_0 \exp\left(\frac{C}{T^n}\right), \quad (2.8)$$

where C and n are the fitting parameters. Further, the Vogel–Fulcher–Tammann (VFT) law suggests that

$$\tau = \tau_0 \exp\left(\frac{A}{T - T_0}\right), \quad (2.9)$$

where A and T_0 are the fitting parameters.

Based on Maxwell [89], a relaxation process is associated with viscosity η . In a glass, the relation between viscosity and relaxation time is [89, 90]

$$\eta = G\tau, \quad (2.10)$$

where G is the instantaneous shear modulus. In most thermal histories, the variation in elasticity will not cover more than one order of magnitude. Therefore, Arrhenius and non-Arrhenius laws are also applicable to viscosity. Angell et al. [28, 29, 91] found that

glass transition generally occurs at $\eta \approx 10^{12}$ Pa s, as shown in Fig. 2.2(a). For Arrhenius law, the viscosity change with temperature is ‘steady’ near T_g , while for strong non-Arrhenius law, it is ‘sharp’. Figuratively speaking, the glassy formers are ‘strong’ to keep its viscosity property for Arrhenius law while being ‘fragile’; that is, its viscosity property for non-Arrhenius law is difficult to maintain. Angell [92] supposed that the structures of strong and fragile glasses are different, which was experimentally proved by Mauro [93]. Angell [28] defined ‘fragility’ M to show the property of temperature dependence of viscosity by [94]

$$M = \left. \frac{\partial \log \eta}{\partial (T_g/T)} \right|_{T=T_g}, \quad (2.11)$$

which is the slope at $T = T_g$ in the Angell plot.

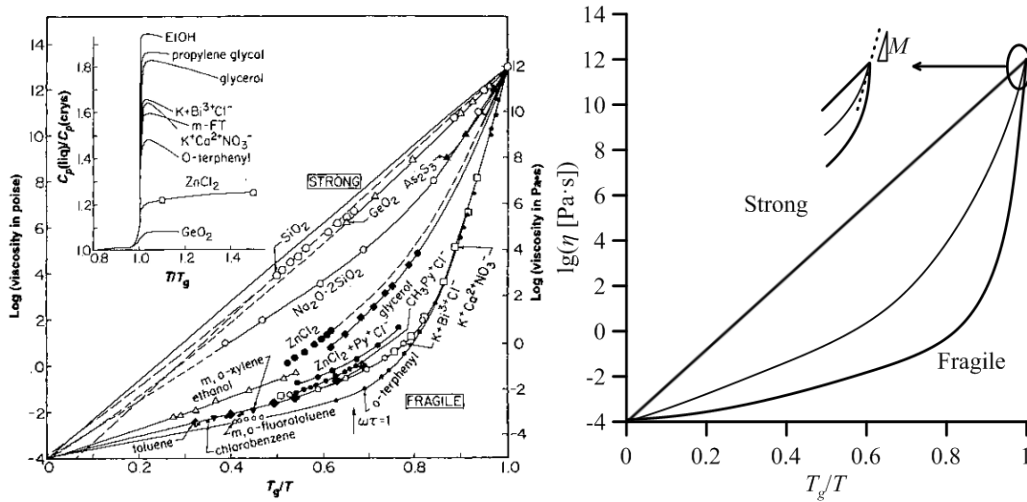


Fig. 2.2 The temperature dependence of viscosity: (a) Angell's plot of the temperature dependence of viscosity of various glasses (copied from Angell [28]) and (b) sketch of strong and fragile glass (fragility).

2.4 Activation energy scenario for the Arrhenius and non-Arrhenius laws

Although the VFT model is empirical, many theoretical derivations have reached the same form [95-97]. This shows that the phenomenological models may have a physical background. To understand the non-Arrhenius behavior in glass, the first physical intuition is ΔE , which is not a constant because some physical quantities controlling ΔE are related to temperature, that is, $\Delta E = \Delta E(T)$. Researchers have attempted to understand the controlling quantities from different aspects.

2.4.1 Free-volume models

This model addresses the situation from the perspective of individual molecules, which are assumed to arrange with a certain amount of available volume. The ‘available volume’ should not be occupied by other molecules thus called ‘free volume’, v_f that decreases as the liquid contracts on cooling. It is predicted that [98-100]

$$\tau = \tau_0 \exp\left(C/v_f(T)\right), \quad (2.12)$$

where C is the parameter determined by experimentation.

2.4.2 Entropy models

When a molecular transport occurs in the glassy system, it is on the route determined by the free volume. Conversely, the motion of the molecule in the glass is confined by its neighbors. Therefore, molecule must reorient in combination with a certain number of its neighbors instead of self reorient, which is the so-called ‘cooperatively rearranging region’ (CRR). Before and after the local relaxation, the configurational states are different. The activation energy for transitions between system states $\Delta E \sim 1/S_{\text{conf}}$, where S_{conf} is the configuration entropy [95, 96]. Therefore,

the temperature dependence of the relaxation time is

$$\tau = \tau_0 \exp\left(\frac{C}{TS_{\text{conf}}}\right), \quad (2.13)$$

where C is the parameter determined by experimentation. Although this model has some problems [101], the entropy model was very popular in the field and defined a paradigm.

2.4.3 Energy models

In addition to volume and entropy, using energy as the controlling variable leads to the third class of models of this type. In the simplest version, it supposes a CCR should overcome a specific barrier energy E_0 before a local relaxation event can occur. It is assumed that that such a CCR contains several molecules with the most likely energy which is close to its average energy $\bar{E}(T)$. Then the activation energy can be simplified as [102]:

$$\Delta E = E_0 - \bar{E}(T). \quad (2.14)$$

However, the assumption of $\langle E \rangle \sim E(T)$ can only be used when the CRR is quite small [103], in which the the predicted linear response of these models can match experimental results.

2.4.4 Elastic models

From the perspective of molecules or atoms, the motion is very fast. However, the glass relaxation near T_g can be sensed in macro time. As the activation energy is assumed in terms of the short-term system elastic properties, elastic models can reveal the connections between the slow and fast system freedom degrees. Generally high-frequency shear and bulk moduli (G_∞, K_∞), and the speed of sound c_∞ can be used in

the model because the atomic arrangements happen in a very short time thus the rest of the glass formers have no time to relax and look like a rigid bulk.

Tobolsky *et al.* [104] in 1943 suggested that the activation energy can be calculated by the short-time elastic properties, appearing to be harmonic models. It used the square wells which are separated by an average configuration space coordinate distance, and the configuration space coordinates are characterized by a Gaussian distribution. With those ideas, the relaxation time is derived to be proportional to the inverse of the Gaussian probability of finding the system a distance from the mean value:

$$\tau = \tau_0 \exp\left(\lambda_1 a^2 / \langle x^2 \rangle\right), \quad (2.15)$$

where x is the reaction coordinate, λ_1 is a numerical factor of order one, and $\langle x^2 \rangle$ is the thermal root mean square (RMS) average distance of the system from an equilibrium state. Referring to Eq. (2.7) provides the activation energy

$$\Delta E = \lambda_1 k_B T \frac{a^2}{\langle x^2 \rangle}. \quad (2.16)$$

In supercooled liquids, it is expected that the activation energy increases upon cooling, which is consistent with the prediction that the thermal RMS average $\langle x^2 \rangle$ usually decreases faster upon cooling than the thermal equilibrium result $\langle x^2 \rangle \sim T$. If the relevant energy landscape is assumed to be spatial, the activation energy ΔE should be related to instantaneous shear deformation, resulting in the energy of the form [104]

$$\Delta E = \lambda_2 a^3 G_\infty, \quad (2.17)$$

where λ_2 is a number in the order of one, a is a microscopic length scale, and G_∞ is the instantaneous liquid shear modulus.

During a local relaxation event, thermal fluctuations generate a local expansion exceeding a certain critical value, the local motion can break its original structure and

a local molecular rearrangement occurs. Mooney [105] estimated the probability of these relaxation events interfering with the thermal longitudinal sound waves and found that

$$\Delta E = \lambda_3 m c_\infty^2, \quad (2.18)$$

where λ_3 is a unitless parameter of order one, m is the molecular mass, and c_∞ is the speed of longitudinal sound waves at high frequency.

The shoving model considers another physical picture that is similar to the local expansion model. The dominant activation energy is the energy that expends on ‘shoving’ aside from the immediate nearest neighbors to rearrangements of a molecule. Then the activation energy is again derived to be proportional to the high-frequency liquid shear modulus G_∞ [106].

$$\Delta E = \frac{2}{3} G_\infty(T) \frac{(\Delta V)^2}{V} \quad (2.19)$$

2.5 Nonlinear relaxation associated with thermal history

It should be noted that glass may need appreciable time to reach equilibrium when the temperature is near or lower than T_g . Therefore, the properties of glass will depend on the thermal history because of memory effects. This suggests that the relaxation time in Eq. (2.1) is related to thermal history, which makes the relaxation nonlinear. At present, the most widely used model to understand this issue is the Tool–Narayanaswamy–Moynihan (TNM) model [107–109] and the Kovacs–Aklonis–Hutchinson Ramos (KAHR) model [110].

2.5.1 Tool–Narayanaswamy–Moynihan (TNM) model

The idea was first proposed by Tool [107] that the property of glass at the current

temperature corresponds to a fictive temperature T_f at which the equilibrium state has the same value as the specified property. If we suppose that the relaxation ‘speed’ is directly proportional to the difference between the current and equilibrium properties, T_f can be derived as

$$\frac{dT_f}{dt} = \frac{T_f - T}{\tau}. \quad (2.20)$$

Under Tool’s hypothesis, τ is only related to the temperature, which can be described by the Arrhenius equation. However, in many cases, the simple exponential function of τ does not work well. Based on thermorheological simplicity, Narayanaswamy [108] proposed a new description of τ

$$\tau = \tau_0 \exp \left[\frac{x\Delta H}{RT} + \frac{(1-x)\Delta H}{RT_f} \right], \quad (2.21)$$

where τ_0 is a constant, ΔH is the activation energy, R is the ideal gas constant, and x is a constant reflecting the influence of temperature and structure. For an arbitrary temperature history, the fictive temperature is given by

$$T_f(\xi) = T - \int_0^\xi M(\xi - \xi') \frac{dT}{d\xi'} d\xi'. \quad (2.22)$$

Here, ξ is the reduced time given by

$$\xi = \int_0^t \frac{\tau_r}{\tau} dt = \int_0^t \frac{\tau_r}{\tau[T(t')]} dt', \quad (2.23)$$

and $M(\xi) = \frac{p - p_2}{p_1 - p_2} = \frac{T_f - T_2}{T_1 - T_2}$ is the relaxation core, which can be used in the form

of

$$M(\xi) = \exp \left[-(\xi / \tau_r)^\beta \right]. \quad (2.24)$$

In these equations, τ_r is the relaxation of a reference temperature and β is constant.

2.5.2 Kovacs–Aklonis–Hutchinson Ramos (KAHR) model

The TNM model is phenomenological, and no specified physical factors are considered during the derivation. The frameworks of KAHR and TNM are the same, while the KAHR model provides a new aspect from the viewpoint of temperature and pressure. In the KAHR model, the volume recovery behavior is defined by a normalised parameter $\delta_V(t) = (V(t) - V_\infty)/V_\infty$, where $V(t)$ is the instantaneous specified volume and V_∞ is the equilibrium specified volume. When the temperature and pressure both vary, the volume can be written as [111]

$$\delta_V(t) = \int_0^\xi \left[-(\alpha_l - \alpha_g) \frac{dT}{d\xi'} - (k_l - k_g) \frac{dP}{d\xi'} \right] M(\xi - \xi') d\xi', \quad (2.25)$$

where the suffixes l and g indicate the liquid and glassy state, respectively; α is the isobaric thermal expansion coefficient; k is the isothermal compressibility; M is the kernel relaxation function defined by Eq. (2.24) as well as the same definition of ζ in Eq. (2.23). The relaxation time in Eq. (2.23) is written as:

$$\tau(T, \delta_V) = \tau_r \exp[-\theta(T - T_r)] \exp\left[\frac{-\theta(1-x)\delta_V}{\alpha_l - \alpha_g} \right], \quad (2.26)$$

where θ is a material constant and x is a partition parameter ($0 \leq x \leq 1$).

2.6 Understanding glass relaxation from heterogeneity (I): Statistical scenarios

Glass is spatially heterogeneous in both structure and dynamics in microscales. Therefore, the global property is a superposition result of every local part, which leads to the mean-field theories that help understand the complex behaviors of glass relaxations.

2.6.1 Mode-coupling theory

Mode-coupling theory (MCT) [112, 113] is famous for a ‘first principle’ theory of glass because it starts from the density states of glass without any empirical assumption.

The particle density in a glass former can be defined as:

$$\rho(\mathbf{r}, t) = \sum_j^N \delta(\mathbf{r} - \mathbf{r}_j(t)), \quad (2.27)$$

whose Fourier transform is expressed as:

$$\rho(\mathbf{k}, t) = \int d\mathbf{r} \rho(\mathbf{r}, t) \exp(i\mathbf{k} \cdot \mathbf{r}) = \sum_j \exp[i\mathbf{k} \cdot \mathbf{r}_j(t)], \quad (2.28)$$

where N is the total number of particles in the liquid above, $\mathbf{r}_j(t)$ is the position of particle j at time t , and \mathbf{k} is the wavevector used in the Fourier transform. The time-dependent correlations between these collective density modes can be probed by the intermediate scattering function [114]:

$$F(\mathbf{k}, t) = \frac{1}{N} \langle \rho_{-\mathbf{k}}(0) \rho_{\mathbf{k}}(t) \rangle \quad (2.29)$$

For simple liquids, MCT provides a damped harmonic oscillator relation [115]:

$$\ddot{F}(\mathbf{k}, t) - \gamma(\mathbf{k}) \dot{F}(\mathbf{k}, t) + \omega^2(\mathbf{k}) F(\mathbf{k}, t) = 0, \quad (2.30)$$

where $\gamma(\mathbf{k})$ is the damping coefficient and $\omega(\mathbf{k})$ is the mode frequency in question, which for simple liquids is $\omega(\mathbf{k}) = ck$, where c is the adiabatic sound speed.

Eq.(2.30) can be written in a more generalized form that can describe more complex liquids, including highly viscous supercooled liquids, by replacing $\omega(\mathbf{k})$ with a more generalized function $\Omega(\mathbf{k})$, and $\gamma(\mathbf{k})\dot{F}(\mathbf{k}, t)$ by a convolution of $\dot{F}(\mathbf{k}, t)$ that has a memory function $M(\mathbf{k}, t)$ controlling the effects of the thermal history on the system.

Then Eq.(2.30) changes to:

$$\ddot{F}(\mathbf{k}, t) + \Omega^2(\mathbf{k})F(\mathbf{k}, t) - \int_0^t dt' M(\mathbf{k}, t-t') \dot{F}(\mathbf{k}, t') = 0 \quad (2.31)$$

To obtain $\Omega(\mathbf{k})$ and $M(\mathbf{k}, t)$ in the model, one can use the theoretical generation method or the parameter fitting of empirical functions. In some cases, these functions are hardly obtained theoretically, thus some approximations can be made. In the model, $\gamma(\mathbf{k})\delta(t)$ provides the usual linear damping term and $\Omega^2(\mathbf{k})m(\mathbf{k}, t)$ can be written in a leading order in terms of pair interactions between particles in the liquid.

MCT provides a remarkable set of accurate predictions, including dynamic glass transition T_c , cage effects, and secondary relaxation (β relaxation) of glass formers. Furthermore, its predictions on the non-exponential and non-Arrhenius laws are completely consistent with experiments and simulations. However, MCT is generally available at a temperature much higher than T_g ; thus, some modified MCTs have been proposed, including extended MCT, generalized MCT, and inhomogeneous MCT [116].

2.6.2 Coupling model

The coupling model (CM) may be confusing with MCT in the name, while they are built from completely different perspectives. The derivation of CM still lacks the mathematical rigor of MCT [117], while many issues are explained by the model, including the non-exponential mechanism, α - β relaxation, and Kovacs' paradox [39, 118]. It can be dated back to Ngai [119] which considered the cooperative (or coupling) dynamics in the relaxation of a complex system. The relaxation process defined by CM can be written as [120]:

$$\phi(t) = \begin{cases} \exp\left(-\frac{t}{\tau_0}\right) & , \omega_c t < 1 \\ \exp\left[-\left(\frac{t}{\tau^*}\right)^{1-n}\right] & , \omega_c t > 1 \end{cases}, \quad (2.32)$$

where τ_0 is a constant and $\tau^* = [(1-n)\omega_c^n \tau_0]^{1/(1-n)}$; $1/\omega_c$ is a characteristic time when

intermolecular cooperative activities become important and $0 < n < 1$.

2.6.3 Other models

Other methods used to understand the complex glass relaxations are the energy landscape approach [121], random first-order transition theory [122], entropic barrier hopping theory [46], and frustration-based models [123].

2.7 Understanding glass relaxation from heterogeneity (II): Stochastic scenarios

The modeling based on statistics and stochastics cannot be fully separated because all the statistical models are started from assumed stochastic processes. However, if the stochastic process is too complex, the mean-field solutions are difficult to reach with mathematics. To bypass the difficulties, more consideration is placed on the stochastic process instead of mean-field mathematics.

2.7.1 Energy-controlled stochastic process

The simplest stochastic model considers a two-level system (TLS) where the local phase transforms between two distinguishable states [124, 125]. As shown in Fig. 2.3(a), the two states have different energy conditions and they can jump between each based on the probability controlled by the energy barrier. The TLS model sufficiently describes many glass properties at low temperatures [124, 125]. For example, the linear temperature dependence of the specific heat and related memory effects [126]. Based on the measurements of the internal friction and speed of sound variation on varying amorphous materials, Topp *et al.* [127] suggested that when the temperature is below 5

K (Kelvin), showing that the standard tunneling model is universal for disordered materials below ~ 5 K, while internal friction above ~ 10 K for different materials displays a wide range of magnitudes and temperature dependence that no universal principles can be concluded. In 1992, an extended tunneling model was developed by Tielburger *et al.* [128] who provided the possibility of describing the acoustic behavior of vitreous silica at higher temperatures in general. Using the developed model, Tielburger *et al.* [128] described the tendency of Brillouin-scattering experiments on vitreous silica to be performed at temperatures between 50 and 300 K and pressures up to 3 GPa.

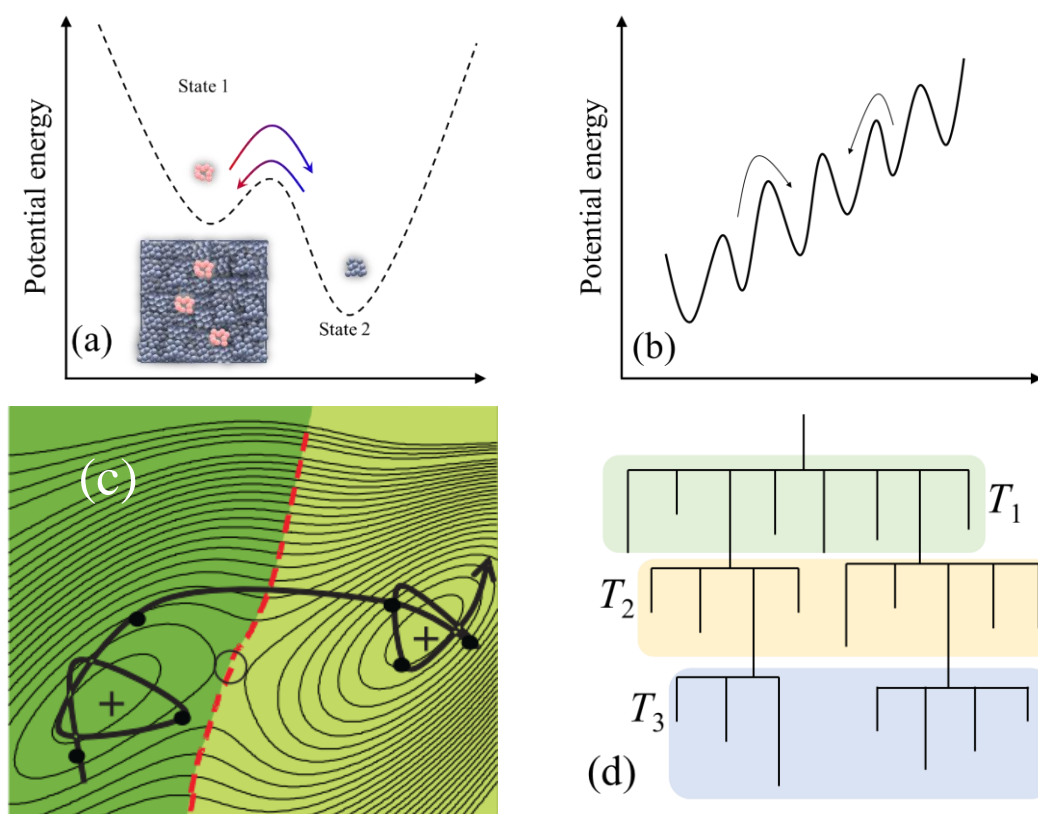


Fig. 2.3 Sketches of energy controlled stochastic models where the states have different energy conditions and they can jump to each other based on the probability controlled by the energy barrier: (a) two-level system (TLS); (b) multi-level system (MLS), (c) energy surface in phase space (reproduced from Fig. 3 in Ref. [121]), and (d) hierarchical tree representation of rugged funnel energy surface (reproduced based on Fig. 1 in Ref. [37]).

The key point that makes the TLS model successful is when thermal activation is considered. However, the predicted values are not satisfactory when the temperature is higher than 100 K. For example, anomalous tunneling phenomena are overserved in numerous works [129, 130]. This is because the phase configuration is more complex than only two levels. To extend the application of energy barrier hopping, multiple energy barrier models are considered, as shown in Fig. 2.3(b). In 1987, a master equation approach was developed by Dyre [131] to study glass transition based on the energy phase space hopping. A similar idea was then used to investigate energy [132] and Kovacs effects [133]. However, these models do not have easily found solutions. In 2011, Ruan and Zhang proposed a Monte Carlo method to overcome these challenges [134].

The real potential energy surface is high dimensional; thus, a more complex modeling approach was proposed based on the hypersurface of energy, as shown in Fig. 2.3(c). Relaxation events occur following the hypersurface, and the local minimal and saddle points are critical to the relaxation property. These configurations help us solve many important issues in glass [121]. Similar ideas were also used in other glass systems, for example, spin glasses. Compared with structural glasses, spin glasses have a more unique definition of a glass transition point (T_C , similar to T_g in structural glass), and the relaxation is incomplete after aging [102]. To explain this, the potential energy landscape (PEL) was assumed to be very complex with a hierarchical schedule, as shown in Fig. 2.3(d). The energy state hopping is hierarchical, and the routes between different hierarchies are limited.

2.7.2 Volume-controlled stochastic process

Owing to the success of free volume theory, many studies have been encouraged to consider the volume hopping as a feature of local relaxation. In 1984, Richard *et al.* [135] proposed a stochastic model based on free volume to study the aging process of glass. In the model, the global volume relaxation is a result of the transition of the local specified volume in the phase space. A similar idea was inherited by Medvedev *et al.* [65] in 2012, who proposed a novel stochastic model by adding the effects of macro volume to local relaxation time. Only a single relaxation time, instead of a built-in relaxation spectrum, was used in Medvedev *et al.* [65], and the time-shift relaxation spectrum is a consequence of the fluctuations in a specific volume.

2.7.3 Rational thermodynamics

The above models associated with a ‘material clock’ can predict some features of glass relaxation but not all features as they are designed to capture only a portion of the overall spectrum. The rational mechanics framework provides a possibility for the global understanding of glass relaxation, including enthalpy, volume, and stress–strain response. The thermodynamic consistency for nonlinearly viscoelastic materials was developed by Coleman and Noll [36, 136]. After the nonlinear relaxation models of TNM and KAHR, Lustig *et al.* [137] extended the rational mechanics framework to a thermoviscoelastic model that considers the history-dependent material clock. In 2004, [138] introduced a novel shift factor that is similar to the WLF function in the framework of Lustig *et al.* [137]. As the stochastic model [65] in Section 2.7.2 also defines a shift factor, Medvedev and Caruthers [139] extended the model to be a full

tensorial and thermodynamically consistent constitutive model.

2.8 Machine-learning approach

Machine learning is a newly developed method for understanding glass relaxation, especially in the last three years. This tendency seems to be related to the so-called ‘New Industrial Revolution’, which may erupt from artificial intelligence (AI). At present, machine learning can be considered as a multivariate statistical question where the neural networks provide a function containing the possible relation between input and output. This is extremely suitable for glass research where too many things are unknown, for example, the relation between ‘random’ local configuration and a specified macro property. The earliest research may belong to Brauer *et al.* [140] who modeled the solubility in the system $\text{P}_2\text{O}_5\text{--CaO--MgO--Na}_2\text{O--TiO}_2$ using artificial neural networks. Subsequently, the machine learning approach was used to predict the glass-forming ability [141], glass transition temperature [142, 143], elasticity [144], plasticity [145], etc.

Combining molecular dynamics (MD) simulations and machine learning is another trend because the former can provide significant data required by the latter. This helps overcome the data deficiency problem in material research. In 2016, Schoenholz *et al.* [146] used the support vector machine method to identify the ‘hard/soft’ points by simulating the bi-disperse Kob–Andersen Lennard–Jones glass. In 2019, Ivancic and Riggleman [147] identified shear banding in a model polymer. A breakthrough was made by Bapst *et al.* [148] that the static initial structures can be used to predict the

long-term dynamics of glass. As commented by Biroli, this indicates that the information of the initial structures is not forgotten in the subsequent relaxation process [149], bringing a new understanding of glass relaxation.

2.9 Summary

In this chapter, I introduced the theoretical understanding of glass transition and relaxation. It first provides the kinetic process of glass transition and then summarises the present phenomenological and physics-based modeling. Finally, the newly developed machine learning approaches are summarized.

Chapter 3 Experimental design based on impulse excited technique (IET): Theories and applications extended to glass at high temperatures

3.1 Introduction: Impulse excited technique (IET)

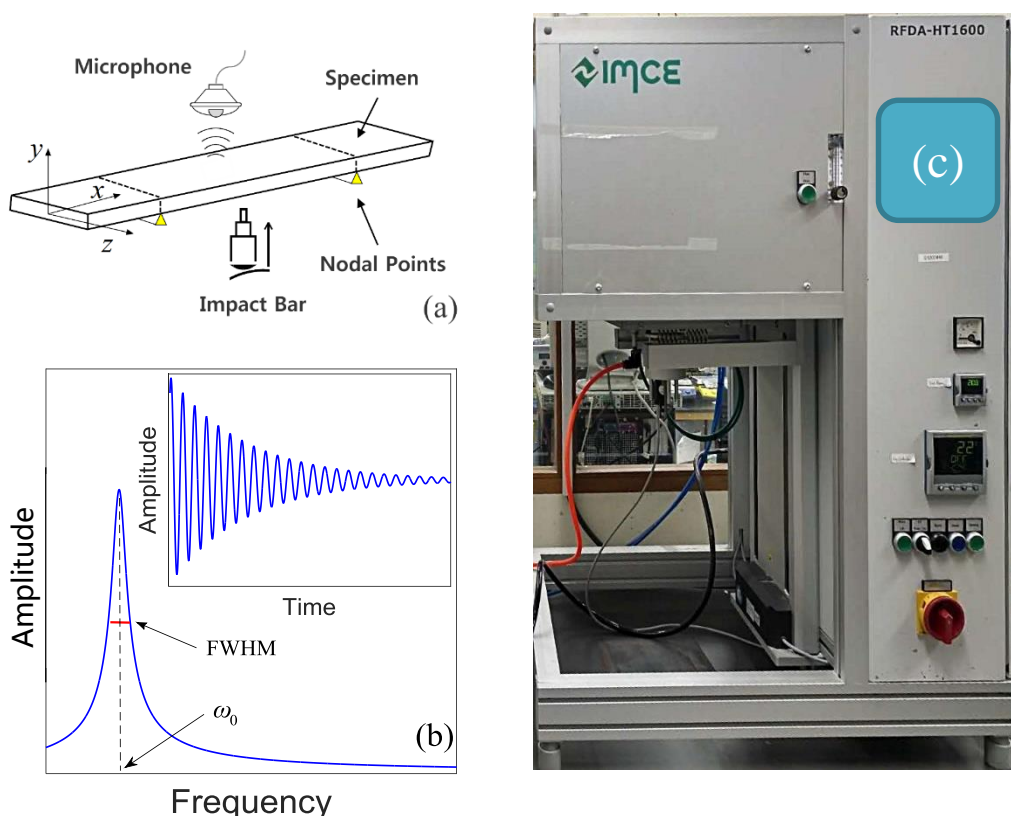


Fig. 3.1 IET experiment: (a) IET setup, (b) typical acoustic signal and its energy spectrum, and (c) IET equipment (RFDA-HT1600 from IMCE, Belgium) used in this thesis.

The impulse excited technique (IET) [150] is a widely used method to measure the elastic and damping properties of materials. It was first proposed by Förster [151] in 1937 and has now been included in the ASTM and ISO standards [152, 153] as an accurate approach to determine the elastic moduli of materials after the improvement

by Pickett [154] and Spinner and Teft [155]. Fig. 3.1 shows the IET experimental schematics. All the units shown in Fig. 3.1(a) were installed in a closed furnace to study the temperature dependence. To avoid external influence beyond the materials, a beam-like sample with free–free ends is required in the experiments. Once the impact bar strikes the specimen, there will be a damped acoustic signal excited owing to beam vibration (the inset of Fig. 3.1(b)), which can be converted by Fourier transform to the energy spectrum shown in Fig. 3.1(b). Fig. 3.1(c) shows an image of the IET equipment used in the thesis. Based on the Euler–Bernoulli beam theory, two motionless points exist at $0.224L$ and $0.776L$ (where L is the beam length) in the first-order flexible vibration mode of an elastic free–free beam. These two points are named as nodal points in Fig. 3.1(a), where the beam is hung with thin metal wires, rendering the approximate boundary condition of the free–free beam.

The signal intensity shown in Fig. 3(b) can be mathematically expressed using the formula for a 1-D damped system

$$y(t) \propto \exp(-\beta t + i\omega_d t), \quad (3.1)$$

where i is the imaginary unit, t is time ($t \geq 0$), and ω_d and β are the vibration frequency and decay rate, respectively. The reference frequency is expressed as follows:

$$\omega_0 = \sqrt{\omega_d^2 + \beta^2}, \quad (3.2)$$

which is the natural frequency of an undamped 1-D system. Based on the Euler–Bernoulli beam theory, the natural frequency of a pure elastic free–free beam is expressed as

$$\omega_E = \sqrt{\lambda_n^4 E_0 I_z / \rho L^4}, \quad (3.3)$$

where E_0 , I_z , and ρ are Young's modulus, the second moment of area, and linear density, respectively, and λ_n is the modal parameter satisfying $\cos\lambda_n \sin\lambda_n = 1$ for a free-free beam and $\lambda_n = 4.73$ for the first-order flexible vibration mode. For the 1-D system described by Eq. (3.1), the energy spectrum of the Fourier transform will peak at the frequency ω_0 and the decay rate k is approximately the half width at half maximum (HWHM) of the peak, as shown in Fig. 3.1(b). In the case where k is much smaller than ω_0 for a solid, generally assumed as $\omega_d \cong \omega_0 \cong \omega_E$ in practice. This notion that the frequency at the energy spectrum peak is approximately the natural frequency of the pure elastic beam is adopted in IET to determine the natural frequency of the beam and decay rate, which are converted to Young's modulus using Eq. (3.3). If the beam is too short or too thick, a correction factor based on the Timoshenko beam theory should be applied [152].

If the IET setups are installed inside a controlled furnace, the experiment can be conducted at various temperatures and different heating/cooling rate. In 1988, Heritage *et al.* [156] reported temperature-dependent Young's modulus of pure aluminum in the temperature range of 20–300 °C using IET. Currently, IET experiments can be conducted at temperatures as high as 1750 °C [157], and suitable for various marco materials. If samples are too small or too thin, it would be difficult to obtain strong acoustic signals for analysis. Knowledge of the elastic and damping properties as a function of temperature provides the basic data for designing high-temperature applications [150] and helps probe the internal structure evolution of the materials. For example, IET can be used to probe the reversible closure and opening of pre-existing micro cracks in silica ceramics [158], phase transformation in zirconia ceramics [159], glass transition, crystallization [160, 161] and structural relaxation [68, 162, 163] of

glassy materials.

However, some outstanding issues associated with IET remain. Firstly, the standard measurement methods [152, 153] on elasticity measurement are only available to elastic bodies with low internal friction, while glassy materials are viscoelastic, especially at high temperatures. Naturally, considering the viscoelastic vibration of beam-like samples is necessary. At present, most theoretical works of the viscoelastic beam are based on specified viscoelastic models, as summarized by Adhikari [164, 165]. This leads to only simple models that can be derived, and the quantitative comparison between different viscoelastic models is knotty. Conversely, some issues associated with IET have not been clarified theoretically, especially for the effects of support lines and the signal acquisition process. For example, the experiments of Roebben [150] in 1997 showed that support wires can introduce significant damping. However, how the process occurred has not been discussed theoretically until today. These issues are technical, but their influence on the understanding of obtained datum is significant in many cases. To reach the quantitative utilization of IET experiments, a simple but practical modeling process of viscoelastic beam vibration is provided in Chapter 3.2, and then the effects of the support lines and the signal acquisition process will be discussed in Chapters 3.3 and 3.4. The models discussed in this chapter are the basics of the following experimental investigations.

3.2 Vibrations of a viscoelastic beam with free–free end boundary conditions

One can start the analysis from a general solution of the viscoelastic beam vibration problem based on the dynamic stress–strain relation, given as an integral type

$$\sigma(t) = E_0 \varepsilon_0 R(t) + E_0 \int_0^t R(t-\zeta) \frac{d\varepsilon(\zeta)}{d\zeta} d\zeta, \quad (3.4)$$

or a differential type

$$P\sigma = Q\varepsilon. \quad (3.5)$$

Here, σ and ε are the time-dependent normal stress and strain along the axial direction

of the beam; $R(t)$ is the relaxation (or memory) function of time t ; $p = \sum_{j=0} p_j \frac{d^j}{dt^j}$ and

$Q = \sum_{j=0} q_j \frac{d^j}{dt^j}$ are the differential operators; and $j = 1, 2, 3, \dots$. Based on the Euler–

Bernoulli beam theory, the bending moment is

$$M = \int_A \sigma y dA, \quad (3.6)$$

where A is the area of the beam cross section and y is the coordinate of a point at the cross section from the neutral axis and along the deflection direction (see Fig. 3.1(a)).

Let $w(x, t)$ be the beam deflection at the axial coordinate x and time t , and the governing vibrational equation of the Euler–Bernoulli beam is

$$\frac{\partial^2 M}{\partial x^2} + \rho \frac{d^2 w}{dt^2} = F(x, t), \quad (3.7)$$

where $F(x, t)$ is the external force. Using the relationship $\varepsilon = y(\partial^2 w / \partial x^2)$ based on the plane section assumption, Laplace transforms of Eqs. (3.4–3.7) are given as follows:

$$\begin{cases} \hat{\sigma} = H(s) \hat{\varepsilon} + f \\ \hat{M} = \frac{\partial^2 \hat{w}}{\partial x^2} H(s) I_z + g \\ \frac{\partial^2 \hat{M}}{\partial x^2} + \rho s^2 \hat{w} = \rho h + \hat{F}(x, s) \end{cases}, \quad (3.8-3.10)$$

where the overhead ‘^’ represents the corresponding variable after the Laplace transformation, $H(s)$ is the generalized Young’s modulus in the Laplace domain, s is the Laplace variable, $f = sE_0 \hat{R}(s) \cdot \varepsilon|_{t=0}$, $g = \int_A y f dA$, and $h = s w|_{t=0} + \dot{w}|_{t=0}$ are all due to

the initial beam deflection and deflection velocity. Further, $H(s) = sE_0\hat{R}(s)$ for the integral-type viscoelastic model, and $H(s) = \sum_{j=0} q_j s^j / \sum_{k=0} p_k s^k$ for the differential-type viscoelastic model with steady initial conditions.

Considering the case in which the initial deflection and velocity are both zero and the beam is excited by an external impulse force $F(x, t) = I_p \delta(x - L/2) \delta(t)$ at the middle span, the initial conditions can be expressed as

$$\begin{cases} \varepsilon|_{t=0} = w|_{t=0} = \dot{w}|_{t=0} = 0 \\ \hat{F}(x, s) = I_p \delta(x - L/2) \end{cases} \quad (3.11)$$

Therefore, $f = g = h = 0$ and Eq. (3.12) is recast, after substituting Eq. (3.11) into Eqs. (3.8–3.10).

$$H(s)I_z \frac{\partial^4 \hat{w}}{\partial x^4} + \rho s^2 \frac{\partial^2 \hat{w}}{\partial x^2} = I_p \delta(x - L/2) \quad (3.12)$$

Now, let us consider the modal response and assume that

$$\hat{w}(x, s) = \sum_{m=1}^{\infty} X_m(x) \Gamma_m(s), \quad (3.13)$$

where $X_m(x) = C_m \{ \cos(\lambda_m x/L) + \text{ch}(\lambda_m x/L) - p [\sin(\lambda_m x/L) + \text{sh}(\lambda_m x/L)] \}$ is the orthogonal modal function of the free-free beam at mode m , $p = \frac{\cosh \lambda_m - \cos \lambda_m}{\sin \lambda_m - \sinh \lambda_m}$, C_n

is the normalization factor when $\int_0^L X_n^2(x) dx = 1$, and $\Gamma_m(s)$ be the undetermined response function. Substituting Eq. (3.13) into Eq. (3.12) leads to

$$\sum_{m=1}^{\infty} \left[\frac{\partial^4 X_m(x)}{\partial x^4} \Gamma_m(s) + \frac{\rho s^2 L^4}{H(s)I_z} X_m(x) \Gamma_m(s) \right] = \frac{I_p \delta(x - L/2)}{H(s)I_z}. \quad (3.14)$$

Using the orthogonality and normality of $X_m(x)$, one can multiply $X_n(x)$ to both sides of Eq. (3.14) and integrating them with respect to x , resulting in

$$\Gamma_n(s) = \frac{I_p X_n(L/2)}{H(s) I_z (\lambda_n/L)^4 + \rho s^2}. \quad (3.15)$$

Note that the denominator of the right-hand side of Eq. (3.15) is the characteristic function of the dynamic system. Among the roots of the equation,

$$H(s) I_z (\lambda_n/L)^4 + \rho s^2 = 0, \quad (3.16)$$

and those with negative real parts expressed as $s = -\beta \pm \omega_d$, govern the damped vibration, as illustrated in Eq. (3.1).

In using IET to determine Young's modulus of the material, the standardized practice [152] is that the peak of the sound spectrum, denoted by ω_c , is directly substituted into Eq. (3.3) with the assumption that $\omega_c = \omega_E$. This method is valid for the pure elastic scenario. However, when this method is applied to measure Young's modulus of glassy materials at temperatures close to or even higher than T_g , the influence of viscosities should be scrutinized. To analytically unveil the influence of viscosity on the Young's modulus measurements, I consider the energy spectrum (ES) based on the Laplace domain response function (Eq. (3.15)) under the fundamental mode ($n = 1$).

$$F(\omega) = |\Gamma_1(i\omega)|^2 = \left| \frac{I'_p}{H(i\omega) I_z (\lambda_1/L)^4 - \rho \omega^2} \right|^2, \quad (3.17)$$

where $I'_p = I_p X_1(L/2)$. Then, the peak center of $F(\omega)$ can be calculated from

$$\left. \frac{\partial F(\omega)}{\partial \omega} \right|_{\omega=\omega_c} = 0. \quad (3.18)$$

For a certain viscoelastic model, its formula of $H(s)$ in the Laplace domain is the same regardless of whether it is derived from integral or differential types; therefore, the above derivations are available for any linear viscoelastic models that have proper Laplace transform $H(s)$. Moreover, the derivations are easy to extend to the beam with

other different boundary conditions by replacing $X_m(x)$. Eq. (3.16) has no information on boundary conditions except λ_m ; thus, it is available for different boundary conditions by replacing the value of λ_m .

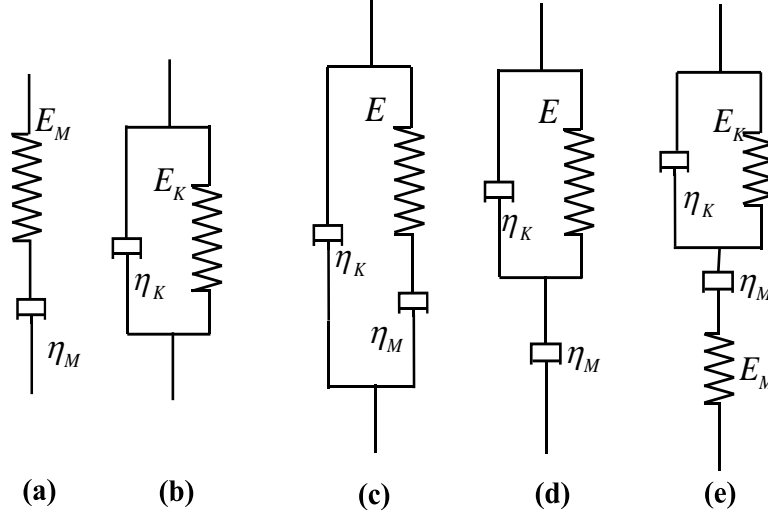


Fig. 3.2 Representations of viscoelastic models: (a) Maxwell model, (b) Kelvin model, (c) Zener model [166], (d) Jeffery model [167] and (e) Burgers model.

Table 3.1 Comparison of different viscoelastic models. ($\tau_i = \eta_i / E_i, i = K, M$)

Type	$H(s)$	β	ω_0
Maxwell	$E / (1 + (s\tau_M)^{-1})$	$1/(2\tau_M)$	ω_E
Kelvin	$(1 + \tau_K s)E$	$\omega_E^2 \tau_K / 2$	ω_E
Zener	$\frac{E}{1 + (s\tau_M)^{-1}} + \tau_K sE$	$\frac{1/\tau_M + \omega_E^2 \tau_K}{2}$	$\omega_E (1 + \tau_K / \tau_M)^{1/2}$
Jeffery	$\frac{E(\tau_K s + \tau_M \tau_K s^2)}{1 + (\tau_M + \tau_K)s}$	$\frac{\tau_M^{-1} + \tau_K \omega^2}{2(1 + \tau_K / \tau_M)}$	$\omega_E (1 + \tau_K / \tau_M)^{-1/2}$
Burgers	$\frac{E_M(\tau_M s + \tau_M \tau_K s^2)}{1 + (\tau_M + \tau_K + \chi_E \tau_M)s + \tau_K \tau_M s^2}$	$\frac{1}{3\eta_K} \left(E_M + E_K - \frac{P}{U} - \frac{U}{4} \right)^\dagger$	$\frac{\sqrt{3}}{3\eta_K} \left(\frac{P}{U} - \frac{U}{4} \right)^\dagger$

†NOTE: $P = (E_M + E_K)^2 - 3M\eta_K^2 E_M$, $Q = 2(E_M + E_K)^3 + 9\eta_K^2 M(2E_K - E_M)E_M$, $M = \left(\frac{\lambda}{L}\right)^4 \frac{I_z}{\rho}$.

The schematics of several classical viscoelastic models are drawn with a spring-dashpot system in Fig. 3.2, for which the constitutive stress–strain relations, derived decay rates, and vibration frequencies for free–free beams are listed in Table 3.1. The

spring represents the elastic relation $\sigma = E\varepsilon$, and the dashpot represents the Newtonian viscous relation $\sigma = \eta(d\varepsilon/dt)$, where E and η are the elastic and viscous constants, respectively. It is well known that the basic viscoelastic models are Kelvin–Voigt (using Kelvin only for the sake of simplification in the following) and Maxwell types, as shown in Figs. 3.1(a) and (b). The viscosity of the dashpot connected in parallel with a spring is denoted as η_K , which represents the Kelvin solid damping effect. Furthermore, η_M denotes the viscosity of the dashpot in series with a spring, which is the flow (or Maxwell) viscosity generally referred to in the glass research community. The elasticity represented by Young’s modulus has similar denotations. Based on the theory of Fourier transform, ω_c is closer to ω_0 than ω_d for most engineering cases. Therefore, the obtained frequency from the energy spectrum is treated as ω_0 in the following. It can be found from Table 3.1 that only in the simplest cases, that is, the Maxwell and Kelvin models, the obtained ω_0 strictly equals to ω_E .

3.3 Damping effects of support lines

The above theoretical investigations only consider the ideal case of a free–free beam. However, making a beam completely free is impossible. This leads to some difficulties in quantitatively understanding the damping behaviors of the sample [150]. The two nodes on the beam have no displacement in the first-order vibration, and both deviate from the corresponding end with $0.22L$. In the experiment, thin metal wires were used as two-point support to reduce the extra interactions in the first order. Moreover, high-order vibration modes can be effectively mitigated. Therefore, the supports exert a damping force on the beam, which can be described as

$$F(x, t) = I_p \delta(x - L/2) - c\dot{w}(N_1, t)\delta(x - N_1) - c\dot{w}(N_2, t)\delta(x - N_2), \quad (3.19)$$

where c is the damping coefficient of the support wires and N_1 and N_2 are the support

positions. Thus, Eq. (3.12) can be rewritten as

$$\begin{aligned} & H(s)I_z \frac{\partial^4 \hat{w}}{\partial x^4} + \rho s^2 \hat{w} \\ & = I_p \delta(x-L/2) - cs\hat{w}(N_1, s)\delta(x-N_1) - cs\hat{w}(N_2, s)\delta(x-N_2) \end{aligned} \quad (3.20)$$

Then, the response function is recast as

$$\Gamma_m(s) = \frac{I_p X_m(L/2) / \varphi_m}{H(s)I_z (\lambda_m/L)^4 + \rho s^2 + sQ}, \quad (3.21)$$

where $Q = \frac{c}{\varphi_m} \left[X_m(N_1) \sum_{n=1}^{\infty} X_n(N_1) + X_m(N_2) \sum_{n=1}^{\infty} X_n(N_2) \right]$. It learns from Eq. (3.21)

that when N_1 and N_2 are located exactly on the two fixed points, $X_1(N_1) = X_2(N_2) = 0$, resulting in $Q=0$, the supporting points have no effect on the first-order vibration as needed. However, placing the supporting wires exactly at the two nodes is nearly impossible; therefore, the effects of the support wires are involved. Based on the models involving the Kelvin part, which has the term $s\tau_K$ in $H(s)$, the effect of the supports given by sQ will be indistinguishable from the contribution of the term $s\tau_K I_z (\lambda/L)^4$, which represents internal Kelvin-type damping.

3.4 Shoulder peak phenomenon

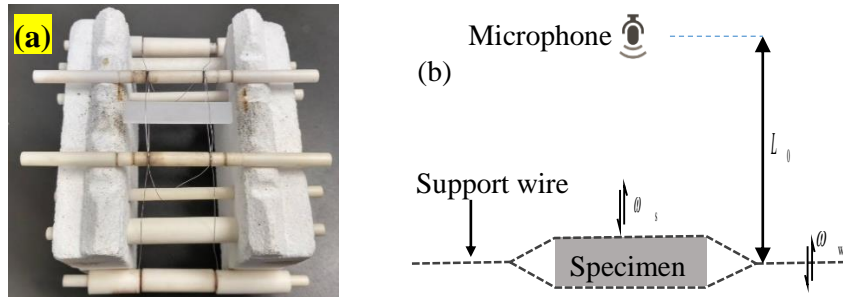


Fig. 3.3 Vibrations of the detected system. (a) Image of setup and (b) diagram of setup.

Fig. 3.3 shows how a beam specimen is tied using metal wires in our experiment

(Fig. 3.3(a)) and the schematic of the testing system in a side view (Fig. 3.3(b)), respectively. After the beam specimen was excited by a tapper, the supporting wires also vibrated, causing the beam to move up and down and changing the distance between the beam and the microphone. The sound intensity signal collected by the microphone can be expressed as

$$\Omega_s = \chi \cdot S_s, \quad (3.22)$$

where $S_s = A_s \exp(-\beta_s t) \cos(\omega_s t)$ represents the vibration of a point in the beam sample, Ω_s is the sound intensity, and χ is the conversion coefficient from the beam displacement to the sound intensity. Considering that, in Eq. (3.22), χ is related to the distance L_0 between the beam and the microphone, the vibration of wires, $S_w = A_w \exp(-\beta_w t) \cos(\omega_w t)$, will slightly change the distance; thus, we write χ as a function of $(S_w + L_0)$. The parameters S , A , β , and ω used above represent the displacement, amplitude, decay rate, and angular frequency of the specified vibration, respectively, with subscripts 's' and 'w' pertaining to specimen and wire, respectively. Since $S_w \ll L_0$, expressed $\chi(S_w + L_0)$ by Taylor's series at L_0 , leads to

$$\chi(S_w + L_0) = \chi_0 [1 + \alpha S_w + \dots], \quad (3.23)$$

where $\chi_0 = \chi(L_0)$ and $\alpha = \chi'(L_0)/\chi(L_0)$. Substituting Eq. (3.23) into Eq. (3.22) and neglecting higher-order items, we have

$$\begin{aligned} \Omega_s &\approx \chi_0 S_s (1 + \alpha S_w) \\ &= A_s^* \exp(-\beta_s t) \cos(\omega_s t) \\ &\quad + A_w^* \exp[-(\beta_s + \beta_w) t] \cos[(\omega_s + \omega_w) t] \\ &\quad + A_w^* \exp[-(\beta_s + \beta_w) t] \cos[(\omega_s - \omega_w) t] \end{aligned} \quad (3.24)$$

where $A_s^* = \chi_0 A_s$ and $A_w^* = \frac{1}{2} \chi_0 \alpha A_s A_w$ are the amplitudes of the sound signal at frequencies ω_s and $\omega_s \pm \omega_w$, respectively.

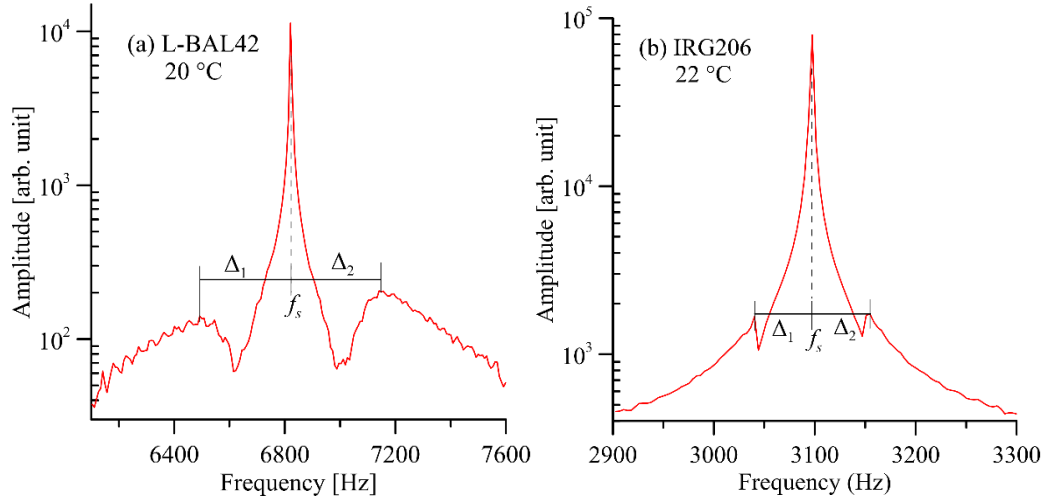


Fig. 3.4 Fourier spectrum of the specimen at room temperature. In plot (a), $f_s = 6820.68$ Hz and $\Delta_1 = \Delta_2 = 320.44$ Hz; the Fourier frequency resolution is 7.63 Hz. (b) $f_s = 3097.50$ Hz and $\Delta_1 = \Delta_2 = 57.22$ Hz; the frequency resolution is 3.815 Hz.

Eq. (3.24) indicates the two accompanying peaks at $\omega_{1,2} = \omega_s \pm \omega_w$ located on both sides of the main peak at ω_s . Fig. 3.4 exemplifies the Fourier spectra of some glass samples at room temperature (~ 20 °C). They are on the ‘shoulder’ of the main peak, thus called the shoulder peaks. These glasses were borosilicate (L-BAL42, $40.08 \times 7.98 \times 1.97$ mm³, 1.9471 g, obtained from OHARA Inc., Japan) and chalcogenide glass (IRG206, $40.03 \times 8.04 \times 2.45$ mm³, 3.6396 g, obtained from Hubei New Hua-Guang Information Materials Co., Ltd, China). Using the logarithmic scale in the ordinate, the shoulder peaks are clearly observed, although they are almost two orders lower than the main peak. At high temperature, the strength of shoulder peaks may be comparable with the primary peak, as shown in Fig. 3.5, where the shoulder peaks have a similar height

to the primary peak for a stainless steel specimen (type 430, 70% cool-rolled, $45.79 \times 9.56 \times 1.42 \text{ mm}^3$, 4.7819 g, self-prepared). With the effects of noise, the left shoulder peak is even higher than that of the primary peak. This causes confusion in the real peak contributed by the sample vibration if the shoulder peak phenomenon was not understood in advance.

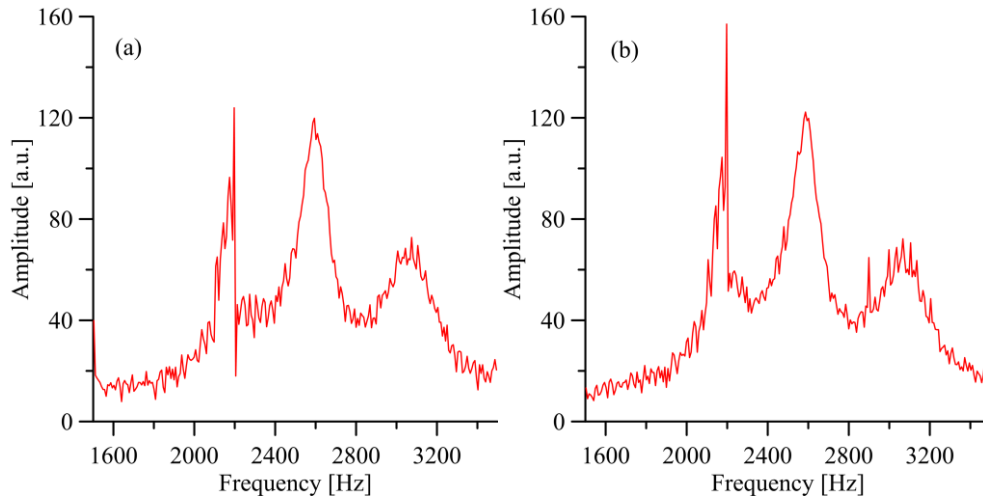


Fig. 3.5 Fourier spectrum of the 70% cool-rolled stainless steel specimen at the high temperatures of (a) 839 °C and (b) 847 °C.

Table 3.2 Cases of the supports

	Sampling rate (s ⁻¹)	Duration (s)	f_s (Hz)	β_s (s ⁻¹)	β_w (s ⁻¹)	A_s^*/A_w^*
Case A: Before T_g	250 000	3	6500	150	100	10
Case B: After T_g	25 000	1	6200	300	150	1

The frequency of the supporting wire $f_w = 0.5\omega_w/\pi$ could be tens or hundreds of Hz in practice, which varies with temperature, sample weight, and the wire tension. Owing to the symmetry of the shoulder peaks, they do not change ω_s . However, they may significantly affect the determination of the obtained decay rate. Corresponding to

the HT1600 system and the experiment on L-BAL42, two cases in Table 3.2 are investigated, and the effects of the support line are plotted in Fig. 3.6. Case A has a relatively higher frequency while lower decay rates, thus corresponds to low temperature conditions; Case B has a relatively lower frequency while higher decay rates, thus corresponds to high temperature conditions. In Fig. 3.6(a) corresponding to Case A, the main peak is much higher than the shoulder peaks. When the wire frequency is small (lower than 50 Hz in Case A), the main peak and the shoulder peaks mix and cannot be distinguished. With increasing frequency, the shoulder peaks gradually separate from the main peak. A similar situation can be found when the temperature is high, as shown in Fig. 3.6(b). At high temperatures, the heights of the shoulder peaks are comparable to the main peak, which may disturb the measurement. Because the shoulder peaks are systematically located beside the main peak, the measured frequency from the peak center does not change. However, the decay rate, which is from the HWHM, may be overestimated if the line frequency is low. At low temperatures, the effects are not significant, while at high temperatures, as shown in Fig. 3.6(b), the measured HWHM is almost twice that of the pure main peak when the line frequency is 50 Hz. That is, when the frequency of the support line is low, an illusory increase in the decay rate can be found with temperature growth, which may lead to some disastrous conclusions. Finally, the shoulder peaks may have complex behaviors during the experiment because the support lines may not be stable after heating and continuous striking. Therefore, very careful consideration should be applied related to this issue. However, it should be noted that the height ratio between the main and the shoulder

peaks is largely dependent on the fixed system and the sample itself. Therefore, the above conclusion is qualitative rather than quantitative for different experimental systems and samples.

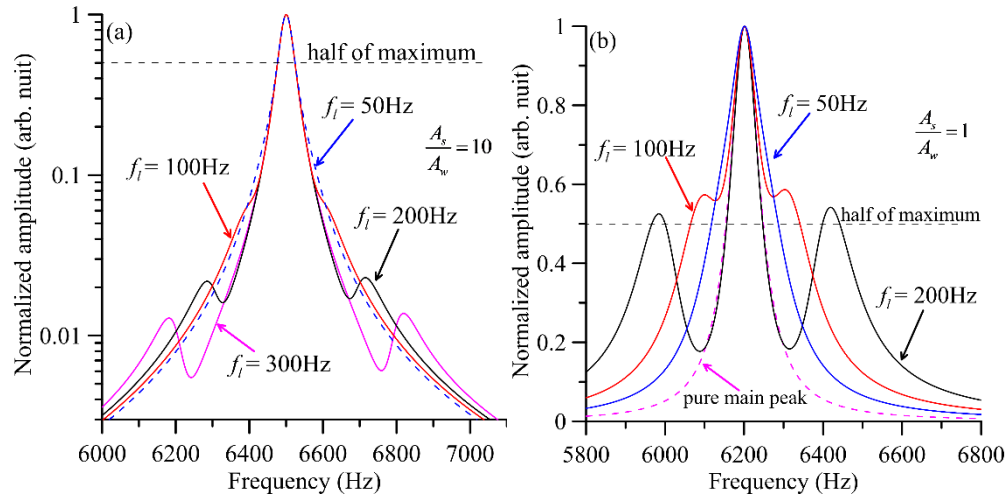


Fig. 3.6 Fourier spectrum affected by different line frequencies for (a) Case 1 and (b) Case 2.

To reduce the effects of shoulder peaks in the measurement, some possible methods can be found in Eq. (3.24). Firstly, one can enlarge the line frequency to make the shoulder peaks further from the main peak. Secondly, one can reduce the height of shoulder peaks by reducing the line amplitude A_w and increasing the line decay rate β_w . The vibration of the sample-wire system can be simplified as the free vibration of a string with a mass point. Thus, the line frequency is proportional to the square root of the tension force, which suggests that increasing the tension force is a practical way to increase the line frequency. Increasing the tension force also can reduce the amplitude of A_l because the same displacement requires more energy. Furthermore, because A_s and A_w are all related to the striking power, an elaborate striking power design may be useful.

3.5 Summary

In this chapter, a general theory of viscoelastic vibrations of a free–free end beam is derived. By applying viscoelastic models, the natural frequency and decay rate of free–free beam vibration are provided. Theoretically, the effects of support are discussed. The decay rate of support wires can be considered as an enhancement of the Kelvin-type viscosity. Moreover, the vibration of the support wires may bring some extraneous information to the obtained Fourier spectrum, including additional damping and shoulder peaks.

Chapter 4 Glass transition and primary (α) relaxations revealed by Young's modulus and decay rate in *in situ* experiments

4.1 Introduction

Though numerous theories have been proposed to understand the nature of glass [34], the experimental characterization of glass transition is mainly based on the remarkable difference between the solid-like and liquid-like behaviors and their markedly different temperature dependence. Glass transition has been investigated by monitoring the temperature dependences of volume [65], enthalpy [66], refractive index [67], viscosity [28, 29], elastic modulus [68, 69] or other macroscopic properties [70]. It is not always possible to measure a physical property *in situ* in a continuous heating or cooling process. For example, the measurement of the refractive index, which is crucial for optical glasses, can only be carried out at room temperature based on quenched specimens [67]; for viscosity measurement, different technologies must be employed in varying ranges: the rotation viscometer is used for low-viscosity measurement ($\eta < 10^8$ Pa s), the beam bending, fiber elongation, bar torsion, and penetration methods are applied for the high-viscosity range ($\eta > 10^8$ Pa s) [168], and the parallel plate method [169] is used for the intermediate viscosity range ($10^4 \sim 10^{10}$ Pa s). Kostal et al. [27] summarized 11 methods for measuring glass viscosity that are all for isothermal measurement; that is, they are unsuitable for capturing the transient viscosity change during the heating/cooling process. Mauro et al. [170] modified the beam bending method to measure non-equilibrium viscosity which may probe the time dependence of viscosity at a constant temperature. Sellier et al. [171] proposed that the shear relaxation modulus and structural relaxation function could be measured by *in*

situ monitoring variation of the glass plate thickness, which however has not been experimentally validated. In the past, differential scanning calorimetry (DSC) and dilatometry have been the most frequently adopted *in situ* methods for characterizing glass transition, and monitor changes in enthalpy and volume, respectively, during a continuous heating/cooling process [172]. Recently, the measurement of elastic modulus becomes another *in situ* method, which has been applied in studying different kinds of glasses [68, 69, 173].

Using the change in elastic modulus with temperature may be advantageous for studying glass transition, because: (i) the elastic modulus changes far more significantly than enthalpy and volume at a temperature near T_g , and (ii) the elastic modulus can be determined almost instantaneously (at very high frequency) using photoacoustic techniques [174] or more cost-effectively IET [150]. The elastic modulus obtained from an IET experiment is very weakly dependent on the vibration frequency, which can be considered as the instantaneous modulus, and therefore has been used to determine the glass transition point of various glasses [173]. In 2014, Liu et al. [68] have further used IET to characterize the time-temperature dependence of the Young's modulus and parameterize the Tool-Narayanaswamy-Moynihan parameters.

In addition to the elastic modulus, the exponential decay rate of the flexural vibration, hereafter called decay rate for shorthand, can also be determined in IET experiments. The decay rate, generally determined after Fourier analysis of the high frequency IET data ($10^3 \sim 10^4$ Hz), is equivalent to the logarithmic decrement of amplitude determined in the conventional low-frequency torsion pendulum method [84] and can also be used to understand the dynamic behavior of materials [175]. The temperature dependence of the decay rate may peak at some temperatures, which renders some structural information [158] or indicates phase transformation [159]. It

was also shown that after glass transition occurs, the decay rate will surge owing to the quick reduction of viscosity [69]. However, the quantitative relation between decay rate and stress relaxation is still not clear, owing partly to the rather large scattering of decay rate data in their work and, more fundamentally, the lack of a proper viscoelastic model.

In this Chapter, the temperature dependence of Young's modulus and decay rate will be examined experimentally and theoretically based on the various linear viscoelastic models, and the physics behind viscoelastic models will be discussed. In Section 4.2, the measurement results of glasses of four different types will be reported, and the viscosity obtained from the decay rate will be discussed in Sections 4.3 and 4.4. All the results will be concluded in Section 4.5.

4.2 Experimental results of time-dependent Young's modulus and decay rate

Table 4.1 Dimensions and T_g of used glasses

Glass	Size / mm ³ (±0.01mm)	Mass / g (±0.1mg)	T_g (Viscosity)	T_g (Dilatometry)	T_g (Young's modulus)
L-BSL7	40.1×10.1×1.52	1.4644	488 °C(AP)	498 °C	484 °C (±1 °C)
L-BAL42	40.08×7.98×1.97	1.9471	494 °C(AP)	506 °C	497 °C (±1 °C)
IRG202	40.03×8.02×2.44	3.4572	288°C[69]	282°C	280°C (±1 °C)
IRG206	40.07×8.02×2.45	3.6610	182°C[26]	180°C	177°C (±1 °C)

Four types of glasses listed in Table 4.1 are measured. Two are borosilicate glasses, L-BSL7 (SiO₂(69.13)-B₂O₃(10.75)-Na₂O(10.40)-K₂O(6.29), wt.%) [176] and L-BAL42 (SiO₂(40-50)- BaO(20-30)-B₂O₃(2-10)-Al₂O₃(2-10)-ZnO(2-10)-Others, wt.%) [177] from OHARA Corporation; and the other two are chalcogenide glasses, IRG202(Ge₂₂Se₅₈As₂₀, mol%) and IRG206(Se₆₀As₄₀, mol%) from Hubei New Hua-Guang Information Materials Co., Ltd. In the measurement, nitrogen gas is purged into the furnace to protect the sample from oxidation (especially for the chalcogenides). The

experimental errors could arise from dimensional (± 0.01 mm) and weight (± 0.1 mg) measurements as well as the temperature measurement (± 0.5 °C). Considering these effects, the Young's modulus determined from Eq. (3.3) could deviate from the actual magnitude within about ± 2 %. Besides, the measurement of decay rate is affected by the condition of support, which will be discussed later in the last of Section 3.1.

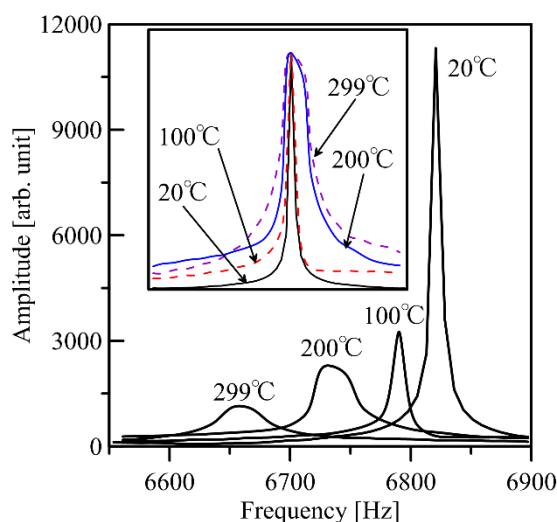


Fig. 4.1 Energy spectrums of the acoustic signal at different temperatures for L-BAL42

Fig. 4.1 displays the energy spectra of the acoustic signal at different temperatures from the L-BAL42 measurements, which illustrates that the peak position shifts to the left with increasing temperature, indicating that the modulus decreases with increasing temperature. The height of the peak reduces with temperature increase, which is owing to the increase of the decay rate. In the inset of Fig. 4.1, the spectra are normalized by the height and frequency of the respective maxima, indicating that the peak becomes more obtuse and the HWHM increases with the temperate rise, thereby further demonstrating the increase in decay rate. Using these clear-cut signals, we can obtain high-quality modulus and decay rate data for a glass specimen.

The variations in the Young's modulus E and decay rate β of glass L-BSL7 are illustrated in Fig. 4.2(a). Along with the Young's modulus decline with temperature, a distinct change in the decreasing rate can be identified at approximately 484°C. This temperature can be regarded as the glass transition point determined from the modulus variation. It should be noted that this temperature is approximately 14°C lower than the T_g determined by dilatometry (498°C), according to data provided by the manufacturer. Although the glass transition point T_g can be measured by various methods, it should be noted that the consensus on the definition of T_g is based on the particular magnitude of viscosity. Angell et al. [28, 29, 91] suggested that the flow viscosity η is 10^{12} Pa s at T_g , which hereafter is referred as $T_{g,v}$. In the glass industry, the Annealing Point (AP) is generally measured, at which the viscosity could be slightly larger than 10^{12} Pa s (typical magnitude is $10^{12.2}$ Pa s). Since AP is very close to $T_{g,v}$, it is directly used here to compare with other T_g measurement. The AP of L-BSL7 is 488°C, only 4 °C higher than the T_g determined based on modulus variation. This result demonstrates that measuring the modulus change is also an effective approach to investigating glass transition. Fig. 4.2(b) illustrates the variations in Young's modulus and decay rate of the optical glass L-BAL42. The T_g determined from the modulus variation is 497°C, which also agrees strongly with the $T_{g,v}$ of L-BAL42 (494°C, AP).

Table 4.2 The parameters of decay rate in Eq. (4.1)

Eq. (4)	p_1 / s^{-1}	$p_2 / ^\circ\text{C}$	p_3 / s^{-1}	$p_4 / (s^\circ\text{C})^{-1}$
L-BSL7	1.0E-25	8.8	18	0.2
L-BAL42	5.0E-32	7	-13	0.36
IRG202	7.4E-5	24.05	2.07	0.0484
IRG206	1.58E-7	10.26	-0.55	0.1194

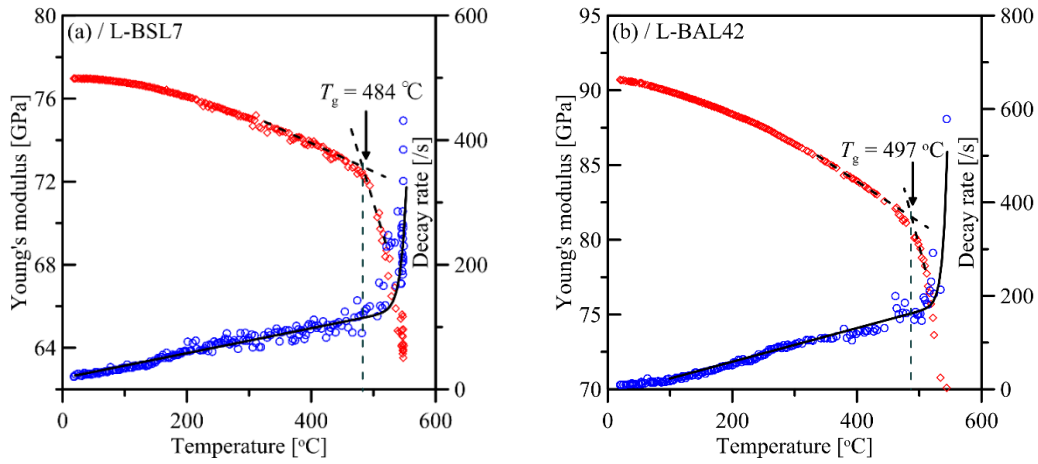


Fig. 4.2 Variations in Young's modulus and decay rate with temperature for borosilicate glasses: (a) L-BSL7 and (b) L-BAL42. The red rhombuses and blue circles indicate Young's modulus and decay rate respectively. The relative error in determining Young's is $\pm 2.14\%$.

The decay rate data fluctuate far more significantly than the modulus data. Therefore, I fit these with the equation:

$$\beta = p_1 \exp(T/p_2) + p_3 + p_4 T \quad (4.1)$$

where $p_1 \sim p_4$ are fitting parameters that are listed in Table 4.2. This equation consists of the linear and exponential functions of temperature. It is noted that the low-temperature (below T_g) variation of decay rate is essentially linear, as shown in Fig. 4.2. Therefore, it is expected that the exponential term in Eq. (4.1) should be caused by the swift decrease of flow viscosity when the temperature is higher than T_g . In Fig. 4.2, a sharp increase in the decay rate can be observed. Intuitively, it would be expected that such a drastic change in decay rate occurs near T_g ; however, this is not the case, as indicated in Fig. 3(a) and (b) by the vertical dashed line. In Fig. 4.2, the apparent sharp increase in decay rate occurs at a temperature that is at least 10°C higher than the T_g determined from the modulus variation. This deviation can be understood based on the Maxwell model provided in Section 3.2. Consider the Maxwell flow viscosity in the range of

$10^{10} \sim 10^{12}$ Pa s. The decay rate contributed by it, given by $\beta = E/2\eta_M$ (where η_M is the flow viscosity), is within the range of $0.01 - 1 \text{ s}^{-1}$, which remains very small compared to other damping effects (for example, Kelvin damping of the material and damping due to suspension wires).

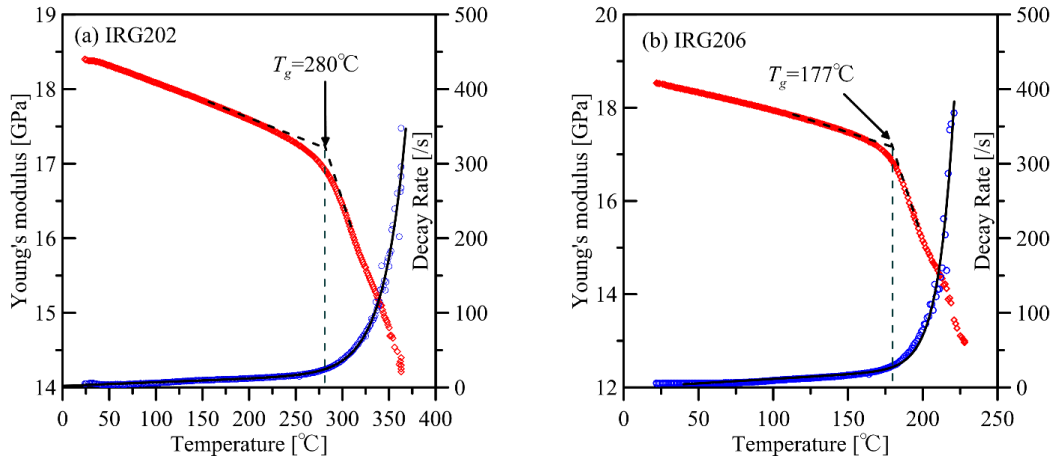


Fig. 4.3 Variations of Young's modulus and decay rate with temperature for chalcogenide glass: a) IRG202 and b) IRG206. The red rhombuses and blue circles indicate Young's modulus and decay rate respectively. The relative error in determining Young's is $\pm 1.46\%$.

The measured results for chalcogenide glasses are plotted in Fig. 4.3. The variations in Young's modulus of the chalcogenide glass resemble those of borosilicate glass, and the glass transition points are determined as 280°C and 177°C for IRG202 and IRG206, respectively. As opposed to the borosilicate glass cases, these two temperatures are very close to the T_g measured by dilatometry, namely 282°C and 180°C for IRG202 and IRG206, respectively. The same experiment on IRG202 was conducted by Bourhis et al. [69], who demonstrated that the T_g measured by Young's modulus was between $270\sim 280^\circ\text{C}$, consistently with our measurement. It should be noted that Bourhis et al. [69] used silver paint to protect the sample from oxidation (whereas we simply purge nitrogen), which may affect the modulus measurement,

leading to a slightly different T_g . The glass transition temperatures of the four glasses determined from the variations in modulus, viscosity, and volume expansion are summarized in Table 4.1. For borosilicate glasses, the T_g determined from the modulus variation is consistent with $T_{g,v}$. In contrast, the $T_{g,v}$ of either chalcogenide is higher than the T_g measured by IET and dilatometry.

The decay rate variations of the two chalcogenide glasses also differ from those of the two borosilicate glasses. Surprisingly, the fluctuations in the decay rate data of chalcogenide glasses are significantly smaller than those of borosilicate glasses, as illustrated in both Figs. 4.3(a) and (b), the transition from the slow and linear increase to the precipitous decay rate rise is far less abrupt than that of borosilicate glasses, and the transition occurs almost exactly at the T_g , as indicated by the vertical dashed lines in Figs. 4.3(a) and (b). The decay rate is also fitted by Eq. (4.1) and the parameters are listed in Table 4. 2.

4.3 Discussion (I): The viscoelastic relaxations of phenomenological models

4.3.1 Finding viscosity from the results of IET experiments

It is well known that the decay rate results from the external and internal dissipation mechanisms [69], which can be modeled as a viscous effect. However, the conversion from the measured decay rate to the flow viscosity of glassy materials is rarely reported in the available literature. A possible reason for this is that the fundamental models, namely the Maxwell (Fig. 3.2(a)) and Kelvin (Fig. 3.2(b)) models, cannot be directly applied to describe the full range of temperature and time dependence, and those complex models are difficult to use owing to some undetermined fitting

parameters. Scherer [178] suggested that the simplest viscoelastic model for glass is the Burgers model, namely a series combination of a Maxwell and Kelvin unit, as illustrated in Fig. 3.2(c). Note that I denote the viscosity of the dashpot parallelly connected with a spring as η_K , which represents the damping effect of the Kelvin solid. And η_M denotes the viscosity of the dashpot in series with a spring, which is the flow (or Maxwell) viscosity usually referred to in the glass research community. For the case of beam vibration, the extensional viscosity is used, which can be converted to the shear viscosity by dividing three [179] for comparing with other viscosity measurements.

In studies on the stress relaxation or creep behavior of borosilicate glasses, the Burgers model provides an effective description of experimental results [180-182]. However, four undetermined parameters exist in the Burgers model, while we have only two measured variables, namely frequency and decay rate, in the IET experiment. Thus, additional assumptions are necessary so that the glass flow viscosity can be assessed from the IET measurements. Fortunately, certain characteristics of the Burgers model can aid in determining the flow viscosity η_M from the decay rate β .

When the Maxwell viscosity $\eta_M \rightarrow \infty$ and the Kelvin viscosity $\eta_K \rightarrow 0$, Burgers model degenerates to pure elastic cases and the effective modulus is:

$$E_B = \frac{E_M E_K}{E_M + E_K}. \quad (4.2)$$

where E_M and E_K are the modulus of Maxwell and Kelvin units, respectively. When the damping or viscous effect is negligible, the modulus measured by IET should be the effective modulus E_B .

When the temperature is low, $\eta_M \rightarrow \infty$ and the effect of Maxwell viscosity vanishes. Thus, the decay rate β is only contributed by Kelvin viscosity, i.e.,

$$\beta_K = \beta(\eta_M \rightarrow \infty). \quad (4.3)$$

It is determined that β_K is the function of the modulus ratio $\chi_E = E_M/E_K$, but is not dependent on the magnitude of either modulus, as exemplified in Fig. 4.4(a). Moreover, from Fig. 4.4(b), it can be determined that β_K is proportional to the magnitude of η_K if χ_E is fixed.

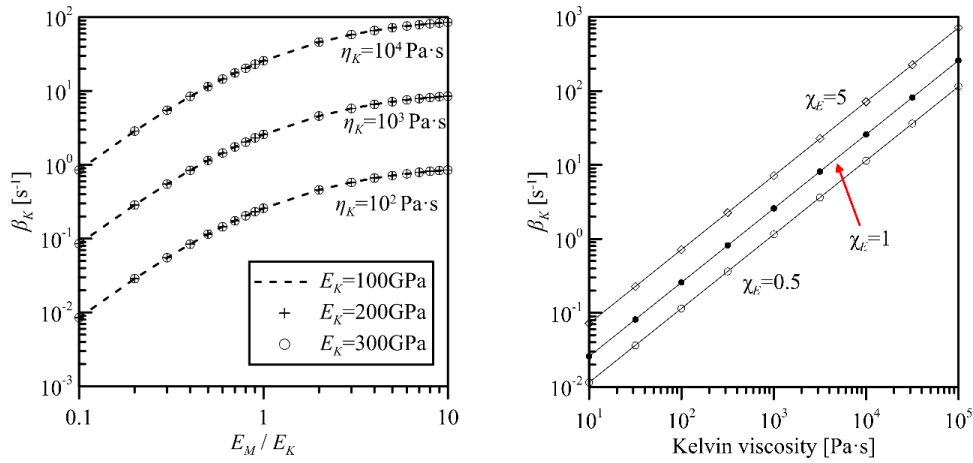


Fig. 4.4 Variations of decay rate on (a) modulus ratio and (b) Kelvin viscosity using specimen L-BAL42.

In the case of finite η_M , $(\beta - \beta_K)$ represents the contributions from the Maxwell viscosity and the coupled effect of the Maxwell and Kelvin units. The Burgers model degenerates to the Maxwell model when $\eta_K \rightarrow 0$. Therefore, the Maxwell viscosity contribution (refer to the decay rate derived from the Maxwell model, as shown in Table 3.2) can be defined as:

$$\beta_M = \beta(\eta_K \rightarrow 0) = 0.5E_B / \eta_M \quad (4.4)$$

I then define the variable $\alpha = (\beta - \beta_K) / \beta_M$ to determine the coupling effect. Fig. 4.5 illustrates the variation of $|\alpha - 1|$ with η_M . It is found that the value of α is very

close to 1 (error less than 1%) for varied with η_K and η_M , and when χ_E is within the range of 10^{-2} and 10^2 (note: in the fitting of experiments, for example, Refs. [180, 181], χ_E is in the range of $0.1 \sim 10$). Because of this weak coupling effect, the decay rate can be expressed as $\beta \cong \beta_K + \beta_M$. Furthermore, the flow viscosity can be determined as $\eta_M = 0.5E_B/\beta_M = 0.5E_B/(\beta - \beta_K)$ if the Kelvin contribution β_K is known.

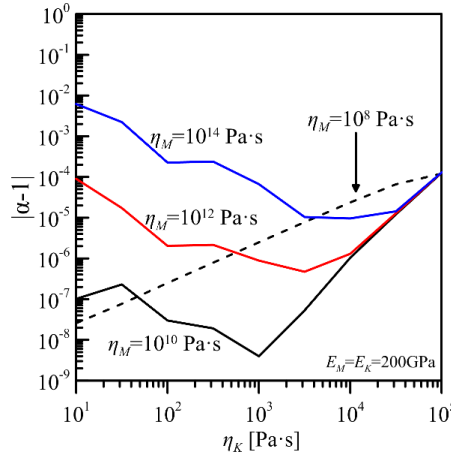


Fig. 4.5 $|\alpha - 1|$ with varying Kelvin viscosity for L-BAL42 when η_M is near 10^{12} Pa s.

Then an approach can be conceived to determine the Kelvin viscosity variation with temperature. At a low temperature, the atomic system vibrates in the potential well, while at a high temperature, the system can jump out of the well to a new configuration [178]. The former situation corresponds to the Kelvin model, and the latter should at least be modeled by the Maxwell model. I assume that the relation between η_K and temperature can be extrapolated to a temperature higher than T_g . Furthermore, the difference between the actual decay rate and that extrapolated from the Kelvin model should lead to the Maxwell viscosity. As the decay rate results can be fitted effectively by Eq. (4.1), in which the linear terms pertain to the low-temperature variation and the exponential describes the precipitous rise at a high temperature, the exponential term

$p_1 \exp(T/p_2)$ in Eq. (4.1) can be directly used to calculate the Maxwell viscosity η_M . It should be noted that Young's modulus is involved in the viscosity calculation, for which the experimental results are used directly.

4.3.2 The temperature-dependent viscosity determined from IET

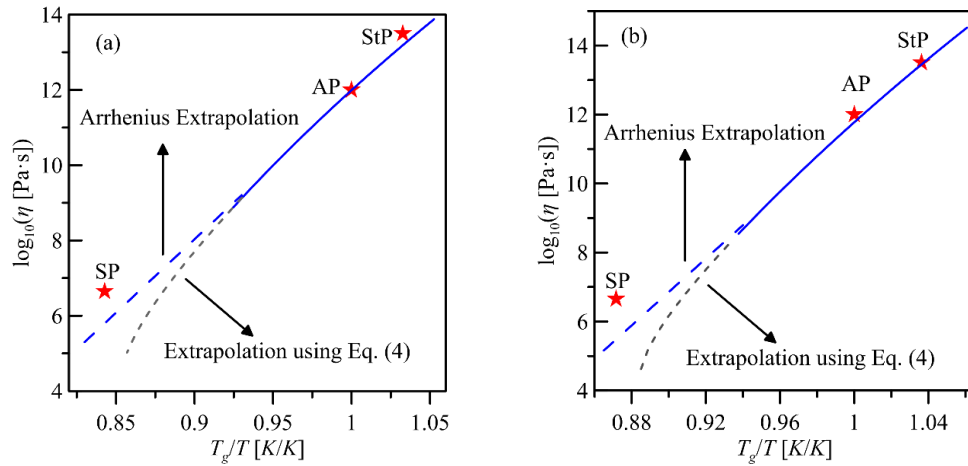


Fig. 4.6 Shear viscosities determined using the Burgers model and plotted using the Angell plot[29] for glass (a) L-BSL7 and (b) L-BAL42, in which the solid blue lines are calculated from decay rate based on the Burgers model.

The calculated shear viscosity is exhibited using the Angell plot, as shown in Fig. 4.6(a) and (b) for L-BSL7 and L-BAL42 respectively. The strain Point (StP), annealing point (AP), softening point (SP), are defined at viscosities of $10^{13.5}$, 10^{12} and $10^{6.65}$ Pa s, which are measured using viscometer and provided by the manufacturer. The obtained viscosity curves are almost linear and well match the low-temperature (AP and StP) viscosity data provided. It is noted that the IET data is only available at about 550 °C ($T_g/T \sim 0.93$ K/K) for both glasses, at which the viscosity is about 10^9 Pa s. When the viscosity is lower than this value, the acoustic signal has been too weak to obtain a clear

energy spectrum peak. Therefore, I extrapolate the viscosity-temperature curve to a higher temperature. If the fitting equation of decay rate is still used, the extrapolation leads to a quick reduction of viscosity and a very large deviation from the SP. However, consider the well-known fact that borosilicate glass is a strong glass, of which the temperature dependence of viscosity flows Arrhenius law, I thus linearly extrapolate the viscosity curves. At the SP temperature, the difference between extrapolated viscosity and the measured value is well below a decimal order for both glasses. Therefore, based on this observation, we claim that the decay rate obtained from IET experiments can effectively be used to calculate the flow viscosity of borosilicate glass based on the Burgers model.

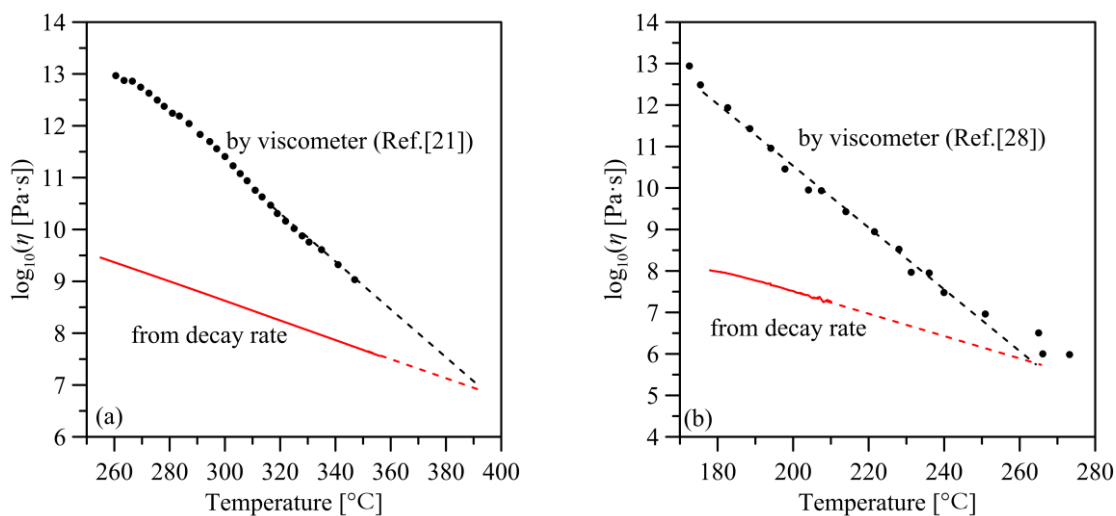


Fig. 4.7 The contribution of shear viscosity on decay rate of chalcogenide glass

The successful application of the Burgers model to the borosilicate glasses inspires us to conduct a similar treatment on the decay rate data of chalcogenide glasses. The obtained viscosity is plotted in Fig. 4.7, in which the viscosities measured by a

viscometer [26, 69] are also displayed. However, the comparison is disappointing because the viscosities obtained from the decay rates based on the Burgers model are significantly smaller than those from the viscometer, although the difference reduces with temperature. There may be two reasons for this disagreement: firstly, the linear extrapolation of the relation between the Kelvin viscosity η_k and temperature to a temperature higher than T_g may be incorrect for chalcogenide glasses; and secondly, the Burgers model may be inapplicable for describing chalcogenide glasses. In a recent study [183], it was proposed that chalcogenide glass may be non-flowing under small stress, even when the temperature is higher than the SP, indicating that the Burgers model may be invalid. A study by Bernard et al. [180] in 2007 demonstrated that, although the stress relaxation of the Te–As–Se system can be fitted by the Burgers model, the obtained parameters fail to describe the strain-recovery process. Furthermore, later work [184] illustrated that the Burgers model cannot model the relaxation in both short and long periods of Te–As–Se and Ge–Se glasses. These studies suggest that the viscoelastic behaviors of chalcogenide glass are fundamentally different from those of borosilicate glass, which needs further discussion.

4.4 Discussions (II): The physics picture under the phenomenological models

4.4.1 Simplified model for transition from solid-like to liquid-like behaviors

The above analysis raises the more fundamental question of how to select a viscoelastic model for describing viscoelastic behavior in the glass transition

temperature range, and what the physical picture is if a viscoelastic model is selected. Without a clear physical picture, the fundamental difference between the borosilicate and the chalcogenide glasses is still vague. To answer these questions, I first establish a minimal model to describe the effects of glass transition on the stress-strain relation of glassy material in integral forms, expressed as Eq. (3.4).

It begins with a mosaic picture of glass transition [185], whereby a glass may be simplified into many small patches (that is, the atomic subsystem), which can spontaneously change their configuration when the temperature is elevated to the glass transition range. Under a constant strain, the stress of a viscoelastic reduces with time, which could approach a non-zero magnitude (damping or solid-like behavior) or zero (decaying or liquid-like behavior). Damping could be attributed to thermal fluctuations, which may not be related to structural relaxation. However, decaying (to zero) must have a structural origin as rearrangements of atoms (either locally or globally) are necessary to accommodate the applied strain. Therefore, stress relaxation and structural relaxation should be closely related, even though they could refer to different length and time scales. Assume that such a configuration change occurs within the infinitesimal time span $[\tau, \tau+d\tau]$ with a probability $Jd\tau$, where J is the transition rate, and that such a transition leads to a total loss of memory and zero stress at the transition instant τ . I then follow the behavior of a single patch, which may or may not change its configuration over time $[0, t]$. The details of these two scenarios are described as follows.

(1) The patch does not change its configuration during the time $[0, t]$ with a probability $P(t)$. As the configuration does not change, I assume that the mechanical behavior should be solid-like, represented by the relaxation function $R_0(t)$.

(2) The patch does not change its configuration during the time $[0, \tau]$, and then changes at the instant τ . The joint probability is then $P(\tau)Jd\tau$, and the total probability of this behavior, when the instant τ runs from 0 to t , is $\int_0^t P(\tau)Jd\tau$. It should be noted that the patch changes its configuration at τ and can change further multiple times, during the time span $[\tau, t]$, which depicts structural relaxation and liquid-like behavior [90]. Therefore, a new relaxation function, different from the above solid-like function $R_0(t)$, must be assumed. I assume that this relaxation function is identical to that of the entire system $R(t)$, based on the rationale that the response of a single patch over a sufficiently lengthy period (time average) should be identical to the average response of many patches (ensemble average).

The summation of the above two scenarios leads to the average stress at time t , which reads:

$$\begin{aligned} \sigma(t) &= \int_0^t E_0 R(t-\xi) \frac{d\varepsilon}{d\xi} d\xi \\ &= P(t) \int_0^t E_0 R_0(t-\xi) \frac{d\varepsilon}{d\xi} d\xi + \int_0^t P(\tau) \left\{ \int_\tau^t E_0 R(t-\xi) \frac{d\varepsilon}{d\xi} d\xi \right\} Jd\tau, \end{aligned} \quad (4.5)$$

The summation rule of probability requires $P(t) + \int_0^t P(\tau)Jd\tau = 1$, for which the solution is

$$P(t) = \exp(-Jt). \quad (4.6)$$

By substituting Eq. (4.6) into (4.5) and changing the integration order of ξ and τ ,

we obtain:

$$\begin{aligned} \int_0^t R(t-\xi) \frac{d\varepsilon}{d\xi} d\xi &= e^{-Jt} \int_0^t R_0(t-\xi) \frac{d\varepsilon}{d\xi} d\xi + \int_0^t \left\{ \int_0^\xi R(t-t') \frac{d\varepsilon}{d\xi} J e^{-J\tau} d\tau \right\} d\xi, \\ &= \int_0^t R_0(t-\xi) e^{-Jt} \frac{d\varepsilon}{d\xi} d\xi - \int_0^t R(t-\xi) (e^{-J\xi} - 1) \frac{d\varepsilon}{d\xi} d\xi \end{aligned} \quad (4.7)$$

which can be further simplified as:

$$\int_0^t R_0(t-\xi) e^{-Jt} \frac{d\varepsilon}{d\xi} d\xi = \int_0^t R(t-\xi) e^{-J\xi} \frac{d\varepsilon}{d\xi} d\xi. \quad (4.8)$$

I then apply Laplace transformation to Eq.(4.8), rendering:

$$\hat{R}(s) = \hat{R}_0(s+J). \quad (4.9)$$

If the material is purely elastic before glass transition (no viscous effects), one has

$R_0(t)=1$ leading to $\hat{R}_0(s) = \hat{R}_E(s) = 1/s$. With a non-zero transition rate J , the

relaxation function becomes

$$\hat{R}(s) = \hat{R}_E(s+J) = 1/(s+J), \quad (4.10)$$

which represents the Maxwell model. If the material is the Kelvin solid prior to glass

transition, described by $\hat{R}_0(s) = \hat{R}_K(s) = 1/(s + \tau_K)$, the memory function following

glass transition is:

$$\hat{R}(s) = \hat{R}_K(s+J) = 1/(s+J) + \tau_K, \quad (4.11)$$

which is the Zener model, as illustrated in Fig. 3.2(d). The solution in Table 3.1

demonstrates that the decay rate derived from the Zener model is the sum of those provided by the Kelvin and Maxwell models, which is identical to the above calculation

derived from the Burgers model. It should be noted that no coupling term of η_K and

η_M exists in the decay rate expression from the Zener model. However, with the

Burgers model, these two viscous units are weakly coupled when the ratio of two elastic constants is within the range of $[10^{-2}, 10^2]$. Moreover, the Kelvin damping assumed in the model, manifested as the non-vanishing decay rate at a low temperature, may not arise from the material response alone. The hanging wire causes the same damping effect, which cannot be distinguished from the Kelvin damping of the materials, as analyzed in section 3.1. However, as the coupling between the Kelvin damping and flow viscosity is very weak (or vanishing based on the Zener model), the flow viscosity determined from the decay rate data is therefore sensible for borosilicate glasses.

Before closing this discussion, a brief discussion on the Jeffery model (Fig. 3.2(e)) which is also widely used to study slow relaxation is needed. The Jeffery model is very similar to the Zener model, containing three parameters, which can also be derived from the Burgers model when χ_E is very large. Based on the decay rate formulae provided in Table 3.1, the Jeffery model renders $\tau_M^{Jeffery} = (1 - 2\beta\tau_K) / (2\beta - \omega^2\tau_K)$, which is smaller than that based on the Zener model with the same β and τ_K , $\tau_M^{Zener} = 1 / (2\beta - \omega^2\tau_K)$. When τ_K is small (in most cases of glass it is), the two types of relaxation time are almost the same.

4.4.2 Effect of non-exponential relaxation

For the chalcogenide glasses, greater consideration is required, as their relaxation behaviors are apparently more complex than those of borosilicate glasses. In the Burgers model, the Maxwell unit, which describes an exponential relaxation, maybe too simplistic to capture the relaxation behavior in chalcogenide glass, leading to the apparent disparity as illustrated in Fig. 4.7. Therefore, the non-exponential relaxation should be considered.

The most important feature of a non-exponential relaxation is that the loss spectrum of the corresponding linear response, expressed as $\chi(is) = 1 - s\hat{R}(s)$ [186, 187], becomes broader than that of exponential decay. This is known as the stretching phenomenon, which may be fitted by various expressions [187]. The most widely adopted time-domain relaxation function is probably the Kohlrausch-Williams-Watts (KWW) function $R(t) = \exp\left[-(t/\tau)^{B_{KWW}}\right]$ [83], where τ is the relaxation time and B_{KWW} is the stretched exponent, which is generally smaller than one. The Laplace transform of the KWW function is nontrivial; therefore, other Laplace domain expressions of the linear response function $\chi(is)$ were proposed, which is more convenient for fitting the stretched loss spectrum. These expressions are also more convenient for studying the beam vibration in this work, as the response function Eq. (3.15) is also expressed in the Laplace domain. In the following, I proceed to use the Cole-Davidson (CD) [188] expression: $\chi_{CD}(is) = (1 + s\tau)^{-B_{CD}}$, where B_{CD} is also a stretched exponent. Using the least-squares method, Lindsey and Patterson [189] provided the relation between B_{CD} and B_{KWW} :

$$B_{KWW} = \begin{cases} 0.970B_{CD} + 0.144, & 0.2 \leq B_{CD} \leq 0.6 \\ 0.683B_{CD} + 0.316, & 0.6 \leq B_{CD} \leq 1.0 \end{cases}, \quad (4.12)$$

which can then be used to convert B_{CD} into B_{KWW} .

The CD expression leads to the relaxation function [187]:

$$\hat{R}(s) = \frac{1}{s} \left(1 - \frac{1}{(1 + s\tau)^{B_{CD}}} \right). \quad (4.13)$$

The viscosity measurement; for example, using the beam bending method for the viscosity range in this work, is conducted in the time domain. This is the process of

obtaining the strain rate under constant stress σ_0 , which is expressed as

$$\frac{d\varepsilon}{dt} = \frac{\sigma_0}{\eta(t)}. \quad (4.14)$$

The strain rate is usually not a constant in a short time but levels off after a sufficient time, and a steady viscosity value is then obtained. Using the Laplace transform of the linear viscoelastic constitutive relation: $\hat{\sigma}(s) = E_0 s R(s) \hat{\varepsilon}(s)$, this measurement process is expressed as:

$$\lim_{t \rightarrow \infty} \frac{d\varepsilon}{dt} = \frac{\sigma_0}{\eta} = \frac{\sigma_0}{E_0} \lim_{t \rightarrow \infty} \mathcal{L}^{-1} \left(\frac{1}{s \hat{R}(s)} \right) = \frac{\sigma_0}{E_0 \hat{R}(s \rightarrow 0)} \quad (4.15)$$

where \mathcal{L}^{-1} indicates the inverse Laplace transform. The proof of the final equality is based on the identity $\lim_{t \rightarrow \infty} F(t) = \lim_{t \rightarrow \infty} \int_0^t dF/dt dt = \lim_{s \rightarrow 0} s \hat{F}(s)$. The viscosity based on the CD expression Eq. (4.13) can then be obtained as follows:

$$\eta_{\text{vis}} = E_0 \hat{R}(s \rightarrow 0) = E_0 \tau B_{CD}. \quad (4.16)$$

Obviously, when $B_{CD} = 1$, the Maxwell expression $\eta = E_0 \tau$ is recovered.

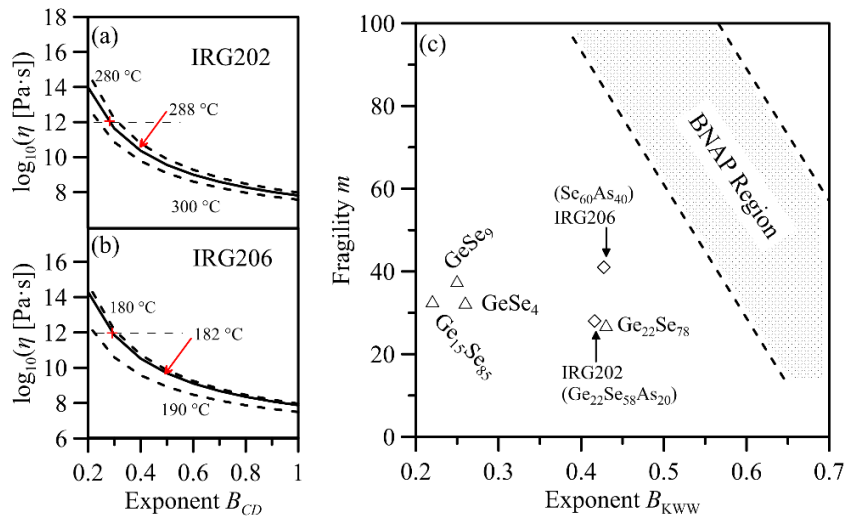


Fig. 4.8 The effect of stretching exponent on the calculated viscosity for (a) IRG202 and (b) IRG206

and (c) the correlation between the fragility versus stretching exponent. The data points of some chalcogenide glasses (including this work) are outside the BNAP region [82].

Eq. (4.16) represents the viscosity measured by a viscometer of a non-exponential relaxation glass. A comparison between the IET and viscometer measurement can finally be established based on Eqs. (4.13) and (4.16). We firstly substitute Eq. (4.13) into Eq. (3.15) to obtain the response function induced by the non-exponential relaxation. For any given B_{CD} within the range of $[0, 1]$, E_0 and τ are adjusted to match the peak center and HWHM with the experimental results. After E_0 and τ are determined, η_{vis} is calculated using Eq. (4.16). If the calculated η_{vis} is the same as the value from the viscometer experiment, the corresponding B_{CD} is selected. Then, using Eq. (4.12), B_{CD} is converted into B_{KWW} .

Fig. 4.8(a) and (b) illustrate the calculated viscosity variation with varying B_{CD} for IRG202 and IRG206, respectively. The calculated viscosity decreases monotonously with an increase in B_{CD} . Therefore, the viscosity measured by the viscometer will only correspond to one B_{CD} at a specific temperature. It is finally determined that the stretched exponent B_{KWW} at $T_{g,v}$ is ~ 0.42 for IRG202 and ~ 0.43 for IRG206, both being markedly smaller than one. It is noted that the fragility m is 28 for IRG202 and 41 for IRG206, based on the viscosity-temperature curves (measured by viscometer) shown in Fig. 4.7. With such a small magnitude of m , B_{KWW} is markedly smaller than that expected from the correlation map between the fragility and stretched exponent proposed by Böhmer et al. [82], which is labeled as “BNAP region” in Fig. 4.8(c). This deviation may be attributed to the short-time (much less than one second) dynamics

probed by IET, which may not be captured by a stress relaxation experiment based on tensile tests [190], or to the specific chemical structures of these two chalcogenide glasses. Furthermore, we note that other studies have reported similar small B_{KWW} values for certain chalcogenide glasses, as plotted in Fig. 4.8(c). For example, Gueguen et al. [184] conducted stress relaxation experiments on several chalcogenide glasses $\text{Ge}_x\text{Se}_{1-x}$, and found that B_{KWW} is within the range of [0.22, 0.26], while the fragilities range from 32 to 37 [191]. Li et al. [192] found that $\text{Ge}_{22}\text{Se}_{78}$ has a fragility of 27 and also a very small $B_{KWW} = 0.43$, which is identical to our result. They suggested that the cause of small B_{KWW} could be the mixing effect of basic structural motifs.

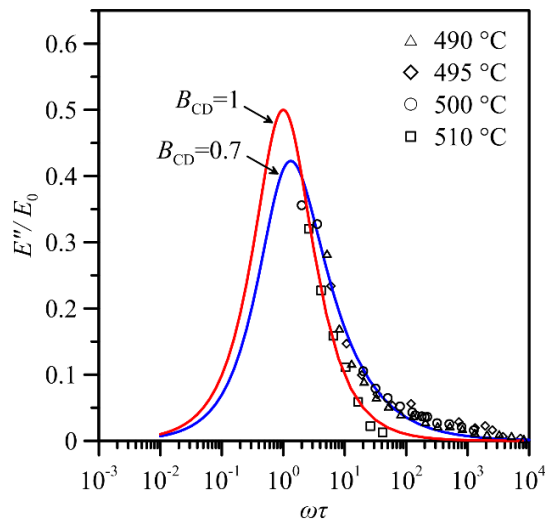


Fig. 4.9 Loss spectrum of L-BAL42 at the temperature of 490, 495, 500, and 510 °C. DMA data are normalized using $E_0 = 82, 81, 80, 78$ GPa and $\tau = 130, 60, 20$ and 10.4 s, for the four temperatures respectively.

For borosilicate glasses, it is expected that non-exponential relaxation is insignificant, which is the reason for the agreement of viscosities calculated from decay rate and measured by viscometer as shown in Fig. 4.6. To verify this point, DMA

experiments are conducted (using DMA1 from Mettler Toledo, Switzerland) to obtain the loss spectrum of the dynamic modulus which can be fitted with the expression of loss modulus E'' derived from the CD expression, as:

$$\frac{E''}{E_0} = \left[1 + (\omega\tau)^2\right]^{-B_{CD}/2} \sin\left[B_{CD} \arctan(\omega\tau)\right], \quad (4.17)$$

where ω is the stimulated frequency. Fig.4.9 shows DMA results of E''/E_0 against $\omega\tau$, in which E_0 and τ are obtained based on the IET results (i.e., from Figs. 3(b) and 8(b) respectively). The data points collapse onto the narrow region bounded by the curves of Eq. (4.17) with $B_{CD} = 0.7$ and 1. It is noted that the curve of Eq. (4.17) with $B_{CD} = 0.7$ (i.e., $B_{KWW}=0.8$) well fits the loss spectrum at the temperatures near T_g (490~500°C) and that the loss spectrum at the higher temperature of 510°C becomes almost unstretched ($B_{CD} = 1$). These results corroborate the large (close to unity) stretching exponent of the examined borosilicate glass and also indicate the consistency of IET and DMA measurements.

4.5 Summary

This work examines the validity of applying the IET to studying structural relaxation in the glass. It is demonstrated that the temperature dependence of Young's modulus can be utilized to study the glass transition phenomenon for both borosilicate and chalcogenide glass. Furthermore, the flow viscosity of borosilicate glass can be determined from the decay rate data, based on the Burgers or Zener model; however, a more elaborate model is required for chalcogenide glass. Based on the theoretical and experimental investigations, the following remarks are made:

- (1) The glass transition point determined from the modulus variation with temperature

is very close to $T_{g,v}$ for the examined borosilicate glasses. However, this is not the case for the chalcogenide glasses.

(2) The flow viscosity of borosilicate glass determined from the decay rate data agrees well with the measurements using a viscometer, indicating that the Burgers or Zener model can be used and that our approach of linear extrapolation of the Kelvin damping contribution is sensible. However, the same approach does not work for chalcogenide glasses.

(3) A minimal model describing the transition from solid-like to liquid-like behavior is proposed, which can aid in choosing a viscoelastic model. For the borosilicate glasses, the low-temperature behavior may be purely elastic or Kelvin-Voigt, leading to a single structural relaxation time following glass transition. This is the fundamental reason that the viscosity determined from the decay rate data can match that measured by the viscometer.

(4) For chalcogenide glass, the large discrepancy in viscosities, as estimated from the decay rate of the IET tests and measured by the viscometer, is resulted from the Burgers model. This indicates a striking non-exponential relaxation, which cannot be described by the single Maxwell unit in the Burgers model. The CD expression is then used to evaluate the effect of non-exponentiality and to estimate the stretched exponent in a KWW expression. The stretching exponent at $T_{g,v}$ is about 0.4 for both chalcogenide glasses, which is consistent with some investigations.

Chapter 5 The secondary (β) mechanical relaxation in glass and its performance in IET experiments

5.1. Introduction

After the pioneering finding of Johari and Goldstein [193, 194] in 1970, the secondary relaxation, or β relaxation, of glass has drawn lots of attention [43, 44, 109, 195-200] because it not only helps to disclose the nature of glass transition [43] but also helps on practical applications, for example, adjust the properties of metallic glass [42, 161, 201]. To reveal β relaxation, many experimental methods [44, 109, 195-198] have been applied. Among others, dielectric spectroscopy (DS) is the most effective because of the wide frequency range [196, 197] that a DS can swap. Successively, β relaxation has been found in the dielectric spectra of polymers [202] and other molecular glass [203]. Based on the measurements of DS, β relaxation could further be categorized into two types [204]: a separated secondary relaxation peak or an excess wing of the α -relaxation peak. The temperature scaling law of the two manifestations of β relaxation seems disparate below T_g , that is the average relaxation time of a separated β peak strictly follows an Arrhenius behavior [204], whereas that of an excess wing follows a super-Arrhenius law (for example, a Vogel–Fulcher–Tammann (VFT) law) that is strongly coupled to the corresponding α -relaxation. When the temperature is close to or higher than T_g , the characteristic time of β relaxation of some glass formers increases with temperature, which disagrees with the intuition that higher temperature leads to shorter relaxation time [196, 205-207]. This counterintuitive relation has also been

found in a water-absorbed porous glass [200], suggesting an intricate mechanism [205] that is still unclear.

The mechanical response of glass has also been employed to study β relaxation in it, especially in the cases that DS is unsuitable, for example, metallic glasses [43]. Moreover, mechanical measurements could reveal more internal dynamics than DS because the stress relaxation of a glassy material is related to all diffusion modes, whereas the dielectric response was only related to the reorientation of dipoles [198]. For example, the rotational diffusion about the C_{2v} axis in poly(methyl methacrylate) (PMMA) does not induce the change of dielectric properties; therefore, the only mechanical approach can reveal the corresponding relaxation process [198]. For metallic glasses, the internal friction associated with β relaxation can only be observed through mechanical means [199] because there is no re-orientation of atomic dipoles. Johari [208] suggested that a mechanical β relaxation is essentially due to the translational motion of atoms in metallic and other glasses, which is consistent with the conception of “islands of mobility” proposed by Johari and Goldstein [193].

However, the mechanical approach is much less used to detect the characteristic frequency of β relaxation because of the difficulties to achieve a measurement with a wide frequency range. When the test frequency is lower than 10^3 Hz, some forced vibration methods, for example, dynamic thermomechanical analysis (DMA), can be employed. When the test frequency is larger than 10^9 Hz, some scattering methods, for example, inelastic light scattering, can be adopted [209]. But for the frequency between these two regimes, there is no standard approaches or commercialized facilities. To

expand the frequency range in mechanical tests, Hecksher et al. [174] fused seven different methods with their self-developed facilities. In these frequency dependent tests, β relaxation generally corresponds to a secondary hump lower than T_g in the loss spectrum of temperature scan. In addition, the decayed free vibration based on the impulse excitation technique (IET) [150] can also be used to study the relaxation behaviors of glassy materials [68, 161, 163]. It should be noted that IET is based on the free vibration of samples, whereas DMA and the approach adopted by Hecksher et al. [174] are based on forced vibration. Comparing with forced-vibration approaches, IET cannot achieve a frequency scan because the natural frequencies of a sample are a series of discrete values. However, the simple and standardized [152, 153] setup of IET, the extended frequency into the ultrasound range ($10^3 - 10^6$ Hz), and the applicability at a temperature as high as 1750 °C [157] makes it a useful alternative to study relaxation behavior of glasses at the frequency outside the assessable range of DMA. Recently, Liu and Zhang [210] found two adjacent peaks in the acoustic spectrum of a PMMA beam excited by IET, which was ascribed to β relaxation. Their experimental results indicate that the Fourier spectrum of an excited beam also contains the information of β relaxation.

The dynamic response of a structure subjected to an impulse may reflect the relaxation kinetics inside the material. However, this relation is implicit, which requires a constitutive model to bridge them. Therefore, in the following, I firstly used a phenomenological model with the differential form to examine the possibility of modeling. Then I describe a physical model of β relaxation based on the conceptual

picture of the potential energy landscape (PEL) and then establish a simplified viscoelastic model based on it. Experimentally, we obtained the double-peaked acoustic spectra of a fluorosilicate glass that validates the β relaxation phenomenon predicted by the theoretical model.

5.2. Phenomenological modeling in the differential form

5.2.1 Mathematical derivations

Without much insight into the cause, let us suppose that it is incurred by the nontrivial viscoelastic property, which may be described by a generalized differential viscoelastic (GDVE) model:

$$P\sigma = Q\varepsilon \quad (4.18)$$

where $P = \sum_{k=0}^{\sigma} p_k \frac{d^k}{dt^k}$ and $Q = \sum_{k=0}^{\sigma} q_k \frac{d^k}{dt^k}$ are the differential operator; $k=1, 2, 3, \dots, \sigma$

and ε are the uniaxial stress and strain, respectively, and t is time. To minimize the number of parameters yet keep a sufficient complexity for arriving at a double-peak spectrum, we keep the first three order differentials:

$$\sigma + p_1 \frac{d\sigma}{dt} + p_2 \frac{d^2\sigma}{dt^2} + p_3 \frac{d^3\sigma}{dt^3} = q_0\varepsilon + q_1 \frac{d\varepsilon}{dt} + q_2 \frac{d^2\varepsilon}{dt^2} + q_3 \frac{d^3\varepsilon}{dt^3}. \quad (4.19)$$

The dynamic modulus in the Laplacian domain is then expressed as:

$$H(s) = \frac{\hat{\sigma}}{\hat{\varepsilon}} = \frac{q_0 + q_1s + q_2s^2 + q_3s^3}{1 + p_1s + p_2s^2 + p_3s^3}, \quad (4.20)$$

where s is the Laplace variable and the overhead “ $\hat{}$ ” represents the corresponding variable after Laplace transformation. Later one will see, the double-peak phenomenon

found in my samples occurs at the temperatures higher than T_g , where the stresses in the material can be fully relaxed and the viscosity can be measured. Therefore, the viscosity η must be finite:

$$\eta = \lim_{s \rightarrow 0} \frac{H(s)}{s} = q_1, \quad (4.21)$$

with $q_0 = 0$. On the other hand, the instantaneous Young's modulus E is obtained at $s \rightarrow \infty$:

$$E_\infty = \lim_{s \rightarrow \infty} H(s) = q_3 / p_3 \quad (4.22)$$

Noted that the Young's moduli determined from IET based on the ASTM [152] or ISO [153] standard should be regarded as the instantaneous Young's modulus. Therefore, we shall determine the condition for the occurrence of double peaks based on the constitutive relation of Eq. (4.19) and how to retrieve the instantaneous modulus E_∞ if the double-peak phenomenon occurs.

Recall the response function of a free-free beam used in IET experiment based on the Euler-Bernoulli beam theory:

$$\Gamma_n(s) = \frac{A}{H(s)I_z(\lambda_n/L)^4 + \rho s^2} \quad (4.23)$$

where A is a variable scale with the impulse, I_z is the second moment of inertia of the beam's cross section, λ_n is the modal constant for the n th flexural vibration mode, L is the length of the beam, and ρ is the linear density. Eq. (4.23) can be recast in the form of Laurent series:

$$\Gamma_n(s) = \sum_{j=1}^m \frac{A_j}{s - s_j} \quad (4.24)$$

where A_j is partition constants, s_j is the pole of Eq. (4.23), and can be solved from the equation:

$$H(s)I_z(\lambda_n/L)^4 + \rho s^2 = 0, \quad (4.25)$$

and m is the number of poles. $\frac{1}{s-s_j}$ corresponds to $\exp(s_j t)$ in the time domain.

Therefore, if s_j is a complex number with a negative real part, it corresponds to a damped vibration. Besides, the Fourier spectrum of a beam vibration described by Eq. (4.23) can be formulated as:

$$F(\omega) = |\Gamma_n(s)|_{s=i\omega}^2 = \left| \sum_{j=1}^N \frac{A_j}{s-s_j} \right|_{s=i\omega}^2 \quad (4.26)$$

where $|\cdot|$ gives the modulus of a complex number. In general, multivariate regression is needed for determining p_i and q_i that brings about the best fit of experimental results with Eq. (4.26), which could be costly due to the complexity and strong nonlinearity of Eq. (4.26) and the unbounded orders of magnitude of the parameters. We herein propose an approximate but sufficiently-accurate approach which can lead to a very good estimate of the instantaneous Young's modulus in comparison with multivariate regression.

Substituting Eq. (4.20) into Eq. (4.25) leads to

$$s^4 + \frac{p_2}{p_3} s^3 + \left(\omega_0^2 + \frac{p_1}{p_3} \right) s^2 + \left(\frac{q_2}{q_3} \omega_0^2 + \frac{1}{p_3} \right) s + \frac{q_1}{q_3} \omega_0^2 = 0 \quad (4.27)$$

where

$$\omega_0 = \sqrt{\frac{E_\infty I_z \lambda_n^4}{\rho L^4}} \quad (4.28)$$

is the natural frequency of the n th mode. To achieve double peaks, Eq. (4.27) must

have two sets of the conjugated roots, given as:

$$\begin{cases} s_{1,2} = -\beta_1 \pm \omega_{d1} \\ s_{3,4} = -\beta_2 \pm \omega_{d2} \end{cases}, \quad (4.29)$$

which leads the following parametric equations after substituting Eq. (4.29) into Eq.

(4.27):

$$\begin{cases} p_1 = p_3 (\omega_1^2 + \omega_2^2 + 4\beta_1\beta_2 - \omega_0^2) \\ p_2 = 2p_3 (\beta_1 + \beta_2) \\ q_2 = -\frac{E_\infty}{\omega_0^2} + 2\left(\frac{\beta_1}{\omega_1^2} + \frac{\beta_2}{\omega_2^2}\right)\eta, \\ p_3 = \frac{\eta\omega_0^2}{E_\infty\omega_1^2\omega_2^2} \end{cases}, \quad (4.30)$$

where $\omega_1 = \sqrt{\omega_{d1}^2 + k_1^2}$ and $\omega_2 = \sqrt{\omega_{d2}^2 + k_2^2}$. Therefore, Eq. (4.30) builds the relation between double-peak phenomenon and the viscoelastic parameters of glass.

5.2.2 Primary experimental examination

The IET setup was employed to examine a fluoride-borosilicate glass S-FSL5 (SiO₂(60-70)-B₂O₃(10-20)-F₂(2-10)-Al₂O₃(0-2)-Sb₂O₃(0-2), wt.%) procured from OHARA Inc., Japan. The sample exhibited double peaks has the dimensions of 40.08×7.95×1.98 mm³ with a mass of 1.5477 g, with the measurement errors <0.01mm and <0.0001g, respectively. S-FSL5 glass has the room-temperature Young's modulus of 62.3 GPa and T_g of 500 °C based on dilatometry measurement. The sample was heated from room temperature to $T_g+50^\circ\text{C}$ with the prescribed heating rate of 2 °C/min.

In Fig. 5.1(a) and (b), I show the comparison of the fitting results based on the multivariant regression for the cases of S-FSL5 at 531 °C and 549 °C, respectively.

Note that shoulder peaks are associated with the main peak with a constant offset frequency due to the vibration of wires. Accompanying the double peaks, there could be shoulder peaks as indicated by arrows “A” and “B”. The determined parameters p_i and q_i for these two temperatures are listed in Table 5.1.

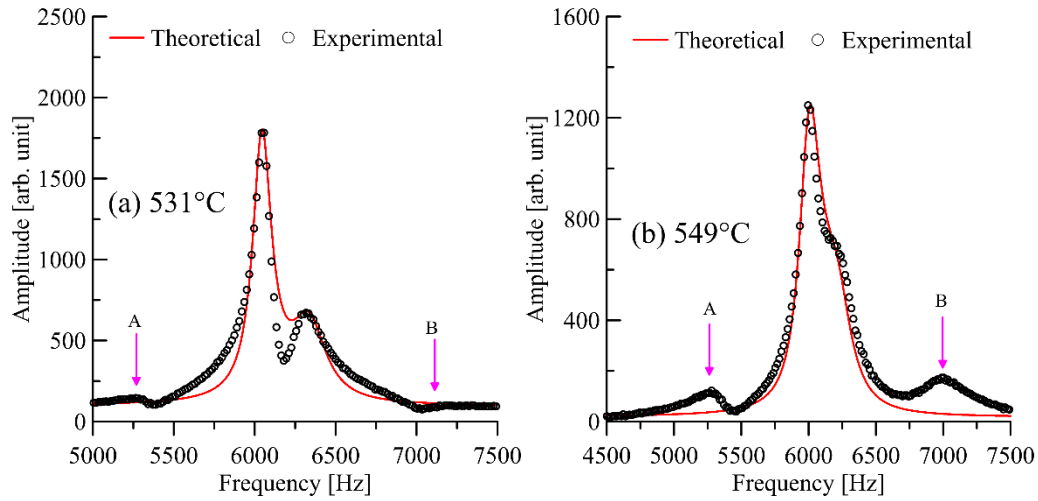


Fig. 5.1 The Fourier spectrum of S-FSL5 and the fit by the obtained viscoelastic parameters. The positions of shoulder peaks are labeled by A and B.

Table 5.1 The parameters of the proposed model of Eq. (4.19)

Temperature	p_1 (s)	p_2 (10^{-7} s^2)	p_3 (10^{-10} s^3)	$q_1(\eta)$ (Pa s)	q_2 (10^4 Pa s^2)	q_3 (Pa s^3)
531 °C	0.657026	9.076644	4.340310	$10^{10.59}$	5.2517578	25.4982823
549 °C	0.167860	3.581489	1.136309	$10^{9.98}$	2.0331319	6.55984500

5.2.3 Beta relaxation revealed by the model

After modeling the double-peak phenomenon by the proposed viscoelastic model phenomenologically, I examine the mechanical relaxation processes. The loss

spectrums expressed as $E''(\omega) = \text{Im}[H(s)]|_{s=i\omega}$ are plotted in Fig. 5.2(a), and the stress relaxation functions $R(t) = \mathcal{L}^{-1}[H(s)/s]$ are plotted in Fig. 5.2(b), based on the obtained viscoelastic parameters given in Table 5.1. Herein $\text{Im}[z]$ gives the imaginary part of the complex number z , and $\mathcal{L}^{-1}[F(s)]$ denotes the inverse Laplace transform of $F(s)$.

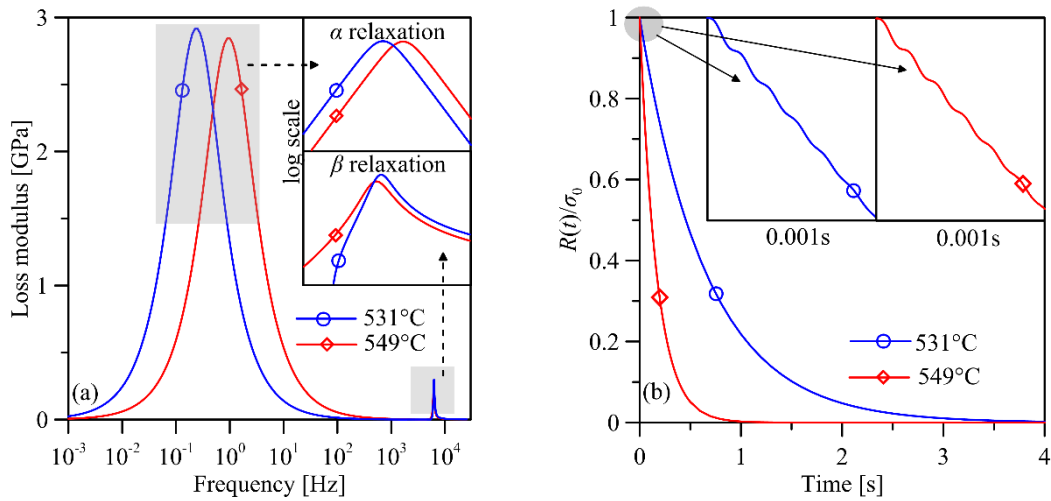


Fig. 5.2 β relaxation revealed by IET experiments of S-FSL5 at 531°C and 549°C: (a) the mechanical loss spectrum and (b) the stress relaxation process. In the two insets of Fig. 5.2(a), the axes are both logarithmic.

Following the usual notation of the two peaks found in a loss spectrum, the two peaks shown in Fig. 5.2(a) correspond to a slow “ α process” with a low frequency f_α and a faster “ β process” with a high frequency f_β [187]. It can be found that the α process is nothing more than an exponential decay due to the shape of an isosceles triangle, therefore $2\pi f_\alpha = \tau_\alpha^{-1}$ with τ_α being the relaxation time, which reduces from 4.2s to 1.1s when the temperature increases from 531 °C to 549 °C. However, the α process cannot lead to the double peaks in the IET experiment, which can be easily determined

from the analytical solution of the free-free beam of a Maxwell material [163]. The double peak is indeed associated with the β process with $f_\beta \cong 6.1$ kHz. The stress relaxations in Fig. 5.2(b) seems merely an exponential decay corresponding the α process. However, at the very beginning, as shown in the inset of Fig. 5.2(b), multiple relaxation steps are vanishing very quickly within 10^{-3} s. Subtracting the exponential decay correspond to the slow α process results in oscillations with a quickly diminishing amplitude. The frequencies of these oscillations are consistent with the corresponding β relaxation peak frequency determined in Fig. 5.2(a).

5.3. Modeling mechanical β relaxation using PEL

Motivated by the frequency consistency between the β relaxation peak and the stress oscillations, normal mode analysis(NMA) is one potential approach because α - β relaxations studied by NMA have shown similar oscillation processes [121], though the similar comparison between the two frequencies has never been conducted previously. In NMA, α process is caused by the spontaneous hopping among local minima, also called inherent structures (ISs), of the potential energy landscape of glassy material, and β process originates from the interaction of atomic oscillations in the basins associated with different ISs. To simplify the analysis, harmonic oscillation is assumed, which can be treated as a combination of the instantaneous normal modes (INM). Both processes lead to the relaxation of physical quantities. For example, Keyes [211] has applied NMA to model the α - β relaxation of polarizability dynamics in CS₂ and achieved a good fit for his atomic simulation. In the present work, we extend the model

to describe mechanical α - β relaxation.

Formally, let us recall the constitutive relation of a linear viscoelastic material which can be written in the form of hereditary integral:

$$\sigma(t) = E_{\infty} \varepsilon_0 C(t) + E_{\infty} \int_0^t C(t-\zeta) \frac{d\varepsilon(\zeta)}{d\zeta} d\zeta, \quad (5.1)$$

where $\sigma(t)$ and $\varepsilon(t)$ are the stress and strain at time t ; $C(t)$ is the relaxation function; ε_0 is the instantaneous strain at $t = 0$. This constitutive relation describes a microscale representative volume element (RVE), which can be divided into many atomic subsystems that can be treated as isolated atomic groups with different ISs. Based on the Green-Kubo relation, the relaxation function is proportional to the stress autocorrelation function (SAF):

$$C(t) \propto \langle \tilde{\sigma}(t) \tilde{\sigma}(0) \rangle, \quad (5.2)$$

where $\tilde{\sigma}(t)$ is the instantaneous stress of a subsystem, and “ $\langle \rangle$ ” means the average of all atomic subsystems. Following the NMA [211], the fluctuation within a PEL basin is assumed to be harmonic and the stress variation associated with a basin is given as:

$$\tilde{\sigma}(t) \cong \tilde{\sigma}_{IS} + \sum_i \left(\frac{\partial \tilde{\sigma}}{\partial q_i} \right)_{IS} q_i(t), \quad (5.3)$$

where $\tilde{\sigma}_{IS}$ is the stress contributed by an IS, q_i is the mass-weighted normal coordinate of the i th vibration mode. The SAF can then be expressed as the average of different ISs [211]:

$$\langle \tilde{\sigma}(t) \tilde{\sigma}(0) \rangle = \langle \tilde{\sigma}_{IS}^2 \rangle + k_B T \int \frac{\langle \rho_{IS}(\omega) \rangle}{\omega^2} \cos(\omega t) d\omega, \quad (5.4)$$

On the right-hand side of Eq. (5.4), the first term is the average contribution of ISs, and

the second term is the contribution of the average harmonic fluctuations in different ISs.

Note that $\rho_{IS}(\omega) = \sum_i \left[\left(\partial \tilde{\sigma} / \partial q_i \right)_{IS}^2 \delta(\omega - \omega_i) \right]$ and $\int_0^{2\pi/\omega_i} (q_i(t))^2 dt = k_B T / \omega_i^2$

have been employed [211, 212].

In Eq. (5.4), the effect of hopping among ISs is not considered; therefore, $\langle \tilde{\sigma}_{IS}^2 \rangle$ is not a function of time [211] and represents a pure elastic effect. The involvement of structural relaxation brings about memory loss of previous stresses, which can be described by a relaxation function [163, 213]. For simplification, we assume the barrier crossing is an Arrhenius process with a constant barrier height, then an exponential decay can be obtained [36]. Therefore, $\langle \tilde{\sigma}_{IS}^2 \rangle$ should be multiplied by $\exp(-t/\tau_\alpha)$ with τ_α being the structural relaxation time. This is also because the stress relaxation induced by α relaxation in silicate glass is nearly exponential at the temperature higher than T_g [163]. The second term on the right-hand side of Eq. (5.4) represents the relaxation induced by harmonic fluctuations, i.e., the relaxation owing to the dephasing induced by the broad distribution of INM frequencies [211]. Though the harmonic term in Eq. (5.4) is affected by barrier crossing, Cho *et al.* [214] suggested that the additional effect of barrier crossing is not necessary because the dephasing suffices to lead to a reasonable decaying time correlation function. Therefore, the modified SAF involving basin hopping is expressed as:

$$\langle \tilde{\sigma}(t) \tilde{\sigma}(0) \rangle = \langle \tilde{\sigma}_{IS}^2 \rangle \exp(-t/\tau_\alpha) + \int_0^\infty G(\omega) \cos(\omega t) d\omega \quad (5.5)$$

where $G(\omega) = k_B T \omega^{-2} \langle \rho_{IS}(\omega) \rangle$ is a weighted density of states (WDOS). In principle, $G(\omega)$ can be determined from the eigenvalues of the Hessian matrix of a well-defined

atomic model. For example, in the study of the polarity fluctuation of CS₂ [211], $\langle \rho_\alpha(\omega) \rangle$ was found to possess several peaks and $G(\omega) \propto \langle \rho_\alpha(\omega) \rangle / \omega^2$ should enhance the contribution of lower-frequency peaks. Following Moore and Space [215], one may assume that $G(\omega)$ describes a bell-shaped distribution, approximated by a Gaussian or Lorentzian function, at a certain frequency range of concern. Assuming that $G(\omega)$ is a Lorentzian function:

$$G(\omega) = \frac{a}{(\omega - \mu)^2 + \gamma^2}, \quad (5.6)$$

and submitting it into Eq. (5.5), the relaxation function is recast as:

$$C(t) = (1-x)\exp(-t/\tau_\alpha) + x\exp(-\gamma t)\cos(\mu t) \quad (5.7)$$

where μ is the central angular frequency of the Lorentzian distribution, γ is the half-width at half maximum (HWHM) of a peak corresponding the structural heterogeneity, $x = \pi a / (\langle \tilde{\sigma}_{IS}^2 \rangle \gamma + \pi a)$, and a is a constant. Naturally, x can be considered as the proportion of the relaxation contributed by β process. It is noted that if $\mu = 0$, Eq. (5.5) reduces to the scenario of two-step exponential relaxation. In addition, it can be further modified to involve a distribution of relaxation time so that the non-exponential relaxations can also be involved. It is noted that the two-step relaxation function has been used to fit the experimental results of mechanical α - β relaxation [216, 217]. However, in the following, I shall focus on the case that μ is nonzero. This makes the relaxation process more complex than a two-step scenario and is indeed necessary to explain our experimental results.

To exemplify the α - β processes revealed by Eq. (5.7), I plot the relaxation

function in Fig. 5.3 (a) with $x = 0.0002$, $\mu\tau_\alpha = 38000$, and amplify the relaxation in initial $0.001\tau_\alpha$ in the insets of Fig. 5.3(a) with different γ . With the timescale of τ_α , the relaxation function is seemingly a straightforward exponential decay. However, at the very beginning, the stress relaxation could exhibit a plateau if the distribution $G(\omega)$ is very broad ($\gamma\tau_\alpha = 15000$) or oscillate if $G(\omega)$ is sharp ($\gamma\tau_\alpha = 200\sim 6000$). It is noted that the initial oscillations are captured in molecular dynamics simulations. For example, based on a bead-spring polymer model, Vladkov and Barrat [218] showed that the short time SAF oscillated and could be fitted with a function identical to the form of Eq. (5.7). Agrawal *et al.* [219] conducted full-atom molecular dynamics simulations of a polyurea system and clearly showed the transition from initial fast decayed oscillation to long-time decay.

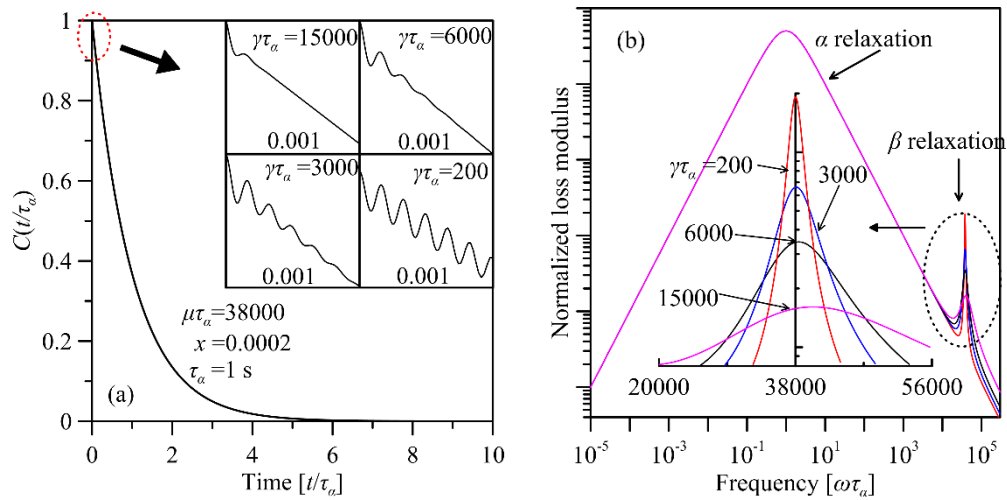


Fig. 5.3 Examples of stress relaxation (a) and loss spectrum (b) calculated from NMA with Cauchy distribution of $G(\omega)$.

In Fig. 5.3(b), I convert the stress relaxation into the normalized loss modulus spectrum $E''(\omega)/E_\infty = \text{Im}[i\omega\tilde{C}(i\omega)]$, where $\tilde{C}(s)$ is the Laplace transform of $C(t)$

with s being the Laplace variable. It is noted that β peaks appear right at the frequency $\omega = \sqrt{\mu^2 + \gamma^2} \approx \mu$ with the width determined by $\sim 2\gamma$. In the scenario of two-step relaxation ($\mu=0$), the frequency of β relaxation peaks at γ [216, 217]. This is the same as what we have found by the phenomenological model.

After substituting the constitutive equations of Eqs. (5.1) into (4.23) with the consideration of (5.7), the Fourier spectrum of the beam vibration can be obtained as:

$$F(\omega) = A \left| \frac{N(s)}{M(s)} \right|_{s=i\omega}^2 \quad (5.8)$$

with

$$N(s) = (s + \tau_\alpha^{-1})(s + \gamma + i\mu)(s + \gamma - i\mu), \text{ and}$$

$$M(s) = s(s^2 + s\tau_\alpha^{-1} + \omega_0^2 - x\omega_0^2) \left[(s + \gamma)^2 + \mu^2 \right] + xs(s + \gamma)(s + \tau_\alpha^{-1})\omega_0^2,$$

where

$$\omega_0 = \sqrt{\frac{\lambda_n^4 E_\infty I_z}{\rho L^4}} \quad (5.9)$$

is the natural frequency. $M(s)$ is a quartic function with four roots. If these roots are all complex, i.e.,

$$\begin{cases} s_{1,2} = -\beta_1 \pm \omega_{d1} \\ s_{3,4} = -\beta_2 \pm \omega_{d2} \end{cases} \quad (5.10)$$

the Fourier spectrum $F(\omega)$ have double peaks near ω_j with $\omega_j = \sqrt{\omega_{dj}^2 + \beta_j^2}$ ($j=1, 2$). To demonstrate, Fig. 5.4 shows the theoretical double-peaked spectra based on the material parameters used in Fig. 5.3 and the natural frequency ω_0 in the range of 0.98μ to 1.02μ .

When ω_0 is very close to μ , double peaks are observed and both peak maxima deviate from ω_0 . For example, for the cases of $\omega_0 = 0.998\mu$, μ and 1.002μ . It is interesting to

note that μ corresponds to the minimum point between the two peaks. This observation can be confirmed based on poles of the reciprocal response function $\Gamma_n^{-1}(s)=M(s)/N(s)$ at $-\gamma \pm i\mu$, which indicates that one of the minima of $F(\omega)$ should be found at $\sqrt{\mu^2 + \gamma^2}$ if double peaks are found. Therefore, the frequency at the minimum point between double peaks can be considered as the frequency of β process when $\gamma \ll \mu$. When ω_0 is not so close to μ , as exhibited by the cases of $\omega_0=0.98\mu$ and 1.02μ , only one peak can be discerned. It should be noted that even for a single peak case, the frequency at the maximum of the peak could still depart from the natural frequency ω_0 because of the influence of β relaxation. This deviation is demonstrated to be about 2% for the cases of $\omega_0=0.98\mu$ and 1.02μ . When ω_0 is further deviated from μ , e.g., by changing the dimensions of a sample, the determination of ω_0 using the peak maximum becomes more accurate.

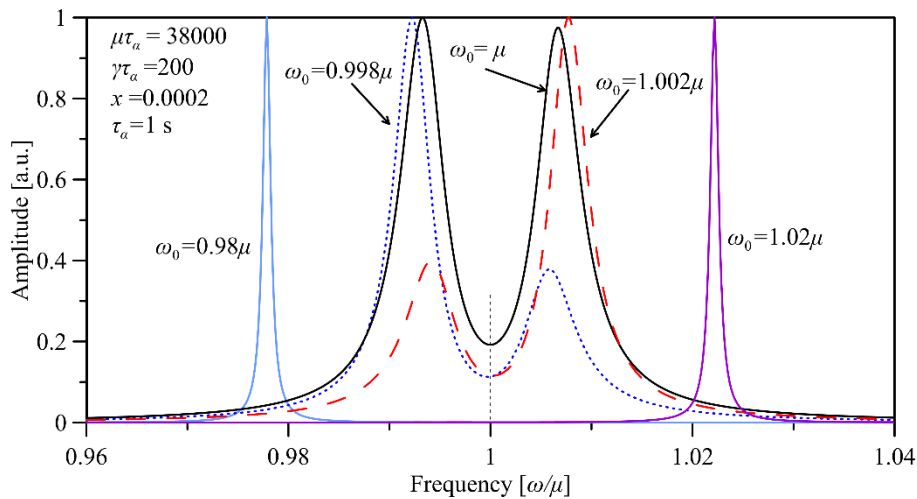
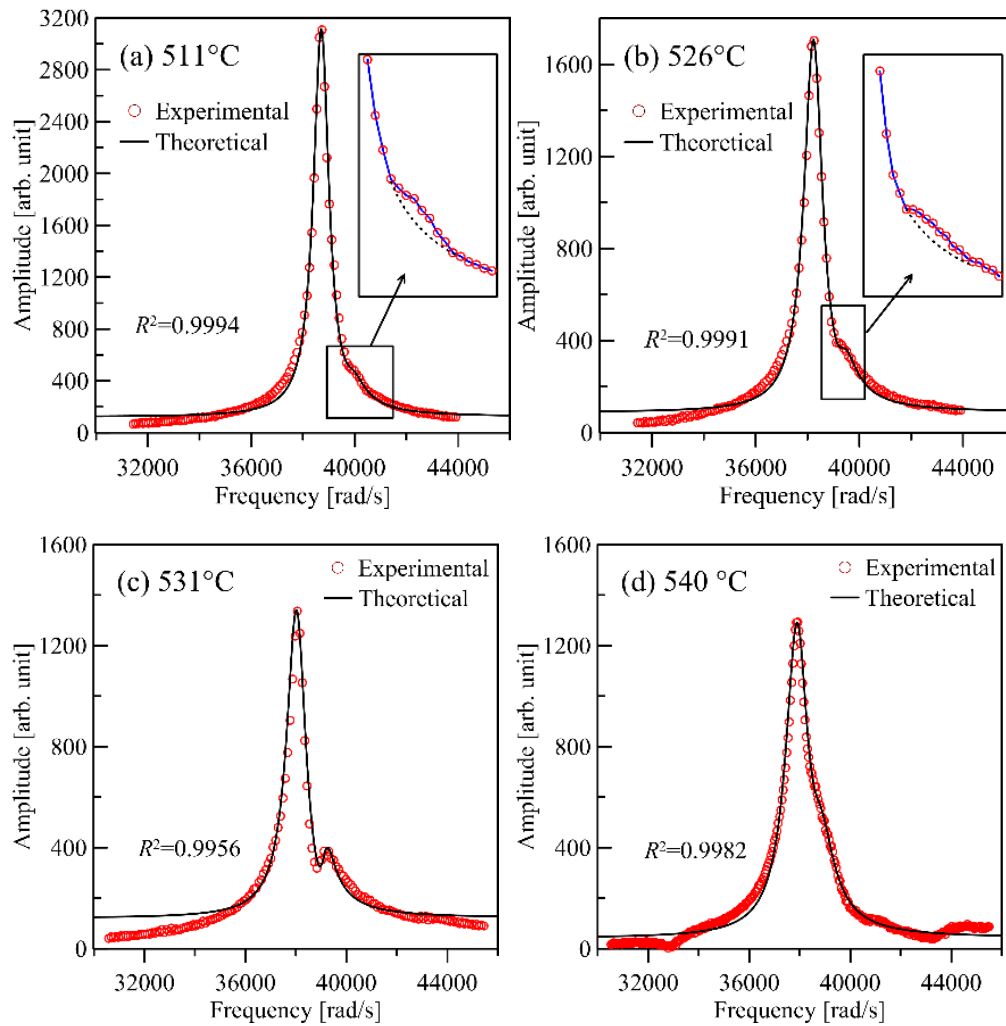


Fig. 5.4 Examples of double peaks predicted by the viscoelastic model from NMA.

The results shown in Fig. 5.4 indicate that the excited vibration of a free-standing

glassy beam can amplify the β process even though it is very subtle in a stress relaxation curve or a loss spectrum, as shown in Fig. 5.3. However, to capture the double-peaked Fourier spectrum, ω_0 must be very close to μ . This condition is difficult to meet if μ is not known *a priori* to a glassy material. In the following, we present a series of clear double-peaked spectra obtained in examining a fluorosilicate glass.

5.4. Experimental results of double peaks



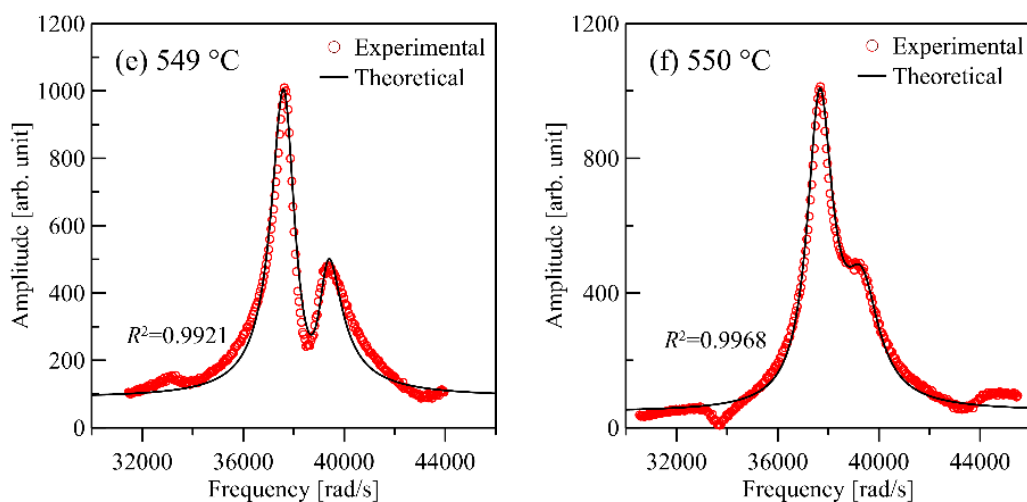


Fig. 5.5 The double-peak phenomena in Fourier spectra of the free vibration signal of S-FSL5 at different temperatures. In the insets of (a) and (b), the solid lines are used to connect the experimental points, while the dashed curves are used to show the tendency of the left peak without humps. In the main plot of all figures, the circles are experimental data, and the solid curves are theoretical predictions. R^2 is the adjusted determination coefficient representing fitting quality.

Fig. 5.5 shows some typical Fourier spectra from 511 °C to 550°C, together with the prediction curve based on NMA with the parameters from the best fit. In the tests, only one peak was found when the temperature was lower than T_g+10 °C. But after that, a small bump associated with the peak gradually grew to a remarkable secondary peak with the temperature increased, leading the double-peak phenomenon. Figs. 5.3(a) and (b) show the cases with a small hump at 511°C and 526°C, respectively, which can be observed after zooming in, as shown in the insets. With the temperature increase, two clear peaks are observed at 531 °C, as shown in Fig. 5.3(c), whereas only an excess wing associated with the main peak can be found at 540 °C, as shown in Fig. 5.3(d). In the experiment, these two manifestations appear alternately after 530 °C, which are further exhibited in 5.3(e) and 5.3(f) for $T = 549$ °C to 550 °C, respectively. It is noted

that the difference between the spectra at 549 °C and 550 °C is substantial, although the temperature difference is only one degree. This could be attributed to the long aging time between the two temperatures, because the actual heating rate after 547 °C decreased automatically due to the limited controllability of the heating system, *i.e.*, the temperature controller must slowly approach the target temperature for high accuracy and small fluctuations. Consequently, from 549 °C to 550 °C it took 7.5 minutes instead of the predefined 0.5 minute. The experimental results shown in Fig. 5.5 has all been well fitted by Eq. (5.8) using Levenberg-Marquardt arithmetic (The fitting parameters will be discussed later). The adjusted determine coefficients (R^2) are also shown in the plots. One may notice that there are still some small humps at both sides of the double peaks as shown in Fig. 5.3. They are the so-called “shoulder peaks” mentioned in Section 3.4.

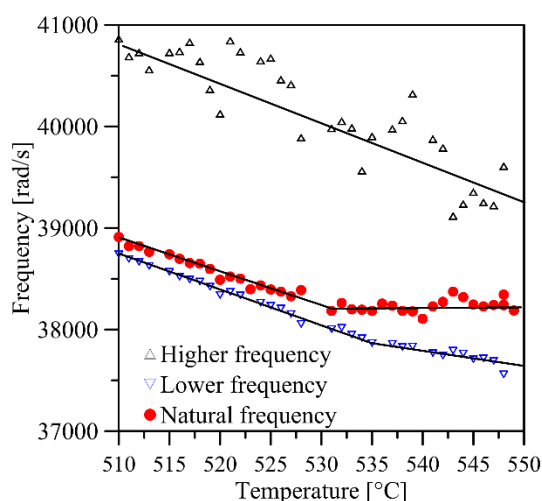


Fig. 5.6 The temperature dependence of higher/lower frequency from the spectrum, and the calculated natural frequency and relaxation frequency. The lines are artificial trendlines.

In Fig. 5.6, the two frequencies pertaining to the two peak maxima are collected.

The lower frequency corresponds to the left peak maximum and the higher one corresponds to the right one. All the spectra have been fitted using Eq. (5.8), which leads to the determination of the natural frequency ω_0 which is also shown in the figure. The actual natural frequency ω_0 , determined from the instantaneous Young's modulus and dimensions of the beam (Eq. (5.9)), differs from two apparent frequencies obtained from the two peak maxima. It is noted that the natural frequency is close to the lower frequency, suggesting that $\omega_0 < \mu$. When the temperature is higher than 530°C, the natural frequency has a weaker temperature dependence and departure more from the lower frequency. This slop change of natural frequency around 530 °C suggests there may be some complex structural change in the glass, which needs more investigations.

5.5. Physical understanding of the temperature dependence of the mechanical β relaxation in the fluorosilicate glass

Based on the proposed model, the temperature dependence of β relaxation in the fluorosilicate glass is exhibited in Fig. 5.7. The central frequency μ and the HWHM γ are plotted in Fig. 5.7(a) and (b), respectively, and the proportion x is plotted in Fig. 5.7(c). Owing to the experimental noise and also because the proposed model could be still simplistic to describe real physics, all the obtained parameters fluctuate with temperature. However, the general trends of these parameters are clear. It is noted that the frequency associated with the β relaxation decreases with temperature, as shown in Fig. 5.7(a), and that γ is weakly dependent on (or slightly decreases with) temperature

when $T < 540^\circ\text{C}$ and then increase with temperature when $T > 540^\circ\text{C}$, as shown in Fig. 5.7(b). This indicates the distribution of INM frequencies becomes broader after 540°C , which could be ascribed to the increase of the disorderliness of the atomic system. The fraction of β relaxation x is smaller than 0.0025, which agrees with previous investigations on the strength of β relaxations [193, 194, 220]. In addition, x increases with temperature, especially when the temperature is larger than 530°C , as shown in Fig. 5.7(c).

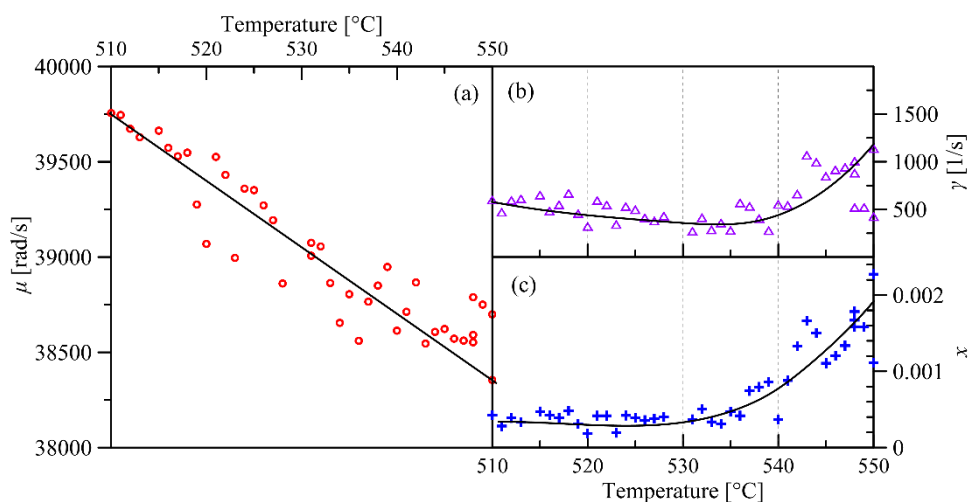


Fig. 5.7 The temperature dependence of central frequency μ , the HWHM γ , and proportion x . The points are from the theoretical calculation based on experimental data, and the curves are artificial trendlines.

The frequency μ does not follow Arrhenius or super-Arrhenius law. Such a result is seemingly consistent with the recent experimental work of Hecksher *et. al* [217] who used their self-developed device to reveal that the mechanical β peak frequency may also decrease with temperature in squalane. The positive temperature dependence of β frequency may be comprehensible [204] if the reciprocal of β frequency is considered

to be a relaxation time, but the negative temperature dependence of β frequency is anomalous. However, the latter is not unusual and also found in DS measurements of various glass formers [196, 200, 205-207]. The existing explanation is phenomenological based on a minimal model (MM) of asymmetric double-well potential [196] or a nonmonotonic relaxation kinetic model (NRKM) [200]. In MM, the two energy wells have different temperature dependence, thus the relaxation time may show anomalous temperature dependence. In NRKM, a rather counterintuitive physical picture is proposed. That is, with temperature increase the total volume of the system changes at a rate smaller than the rate of defect increase. Therefore, the average free volume associated with every defect becomes smaller and then reduces the space of β relaxation, leading to the negative temperature dependence of β relaxation frequency.

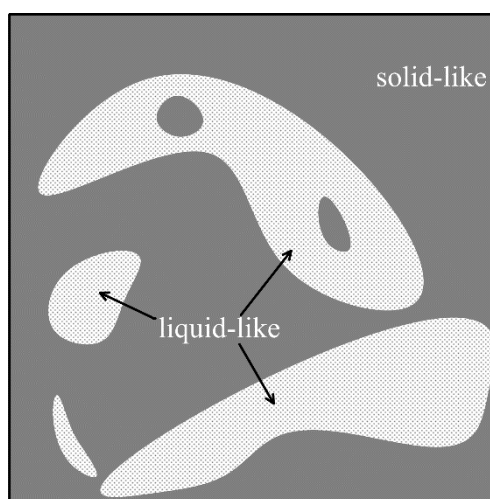


Fig. 5.8 The sketch of the solid-like and liquid-like region of glass near the glass transition. The grey regions are solid-like and the white regions are liquid-like.

Based on the NMA used in the present work, another view may be provided for comprehending the negative temperature dependence of the β frequency. Based on our

model, the oscillation frequency of β process is because the WDOS $G(\omega)$ has a peak at the corresponding frequency range. This requires very weak interactions and large atomic clusters. It is presumed that only in weakly bonded regions β relaxation could take place [221], thus the negative temperature dependence of β relaxation is owing naturally to the weaker interactions when temperature increases and volume expands. In S-FSL5, the atoms are bonded by ionic-covalent interaction in structural polyhedron and connected by the long-range interactions (for example, Coulombic interactions [222]) between polyhedrons. Moreover, the introduction of the network modifier fluorine increases the possibility of isolated polyhedrons. The β relaxation is found in the experiment at the temperature higher than T_g but much lower than the melting point. In this temperature regime, the materials experience a transition from a solid-like to liquid-like state, which can be described by the picture of Orowan [223], as illustrated in Fig. 5.8. When the temperature is low, the material must have local mobile regions surrounded by a rigid matrix that did not permit viscous flow. With temperature increase, the sizes and numbers of such regions grow until they are connected, and viscous flow becomes possible. These liquid-like regions are reminiscent of Johari and Goldstein's picture of "islands of mobility" (or "loosely packed isolated regions") [193, 208] which has also been employed by Nemilov [222] to explain β relaxation in silicate-based glasses. When the temperature is lower than T_g , they provide room for β relaxation of some small atomic clusters. When the temperature is higher than T_g , the mobility and size of liquid-like regions increase significantly, and some bigger atomic clusters (mainly oxide-network patches in S-FSL5) fall off from the matrix and take

part in the activities of β relaxation. Besides, the long-range interactions become also weaker with temperature increase. Therefore, the β relaxation can be found at a relatively low frequency which decreases with temperature, as shown in Fig. 5.7(a). In addition, the fraction of β relaxation, namely x , should increase with temperature, which is also corroborated by Fig. 5.7(c).

5.6. Conclusions

I established a viscoelastic model based on the normal mode analysis of the potential energy landscape to describe mechanical α and β relaxations in a glassy material. Based on the model, it is predicted that an apparent double-peak phenomenon in the Fourier spectrum of a free beam vibration can be generated by a very weak β process when the frequency of β relaxation peak is close to the natural frequency of the specimen. This result has been validated by the acoustic spectrum of a fluorosilicate glass (S-FSL5) beam excited by a mid-span impulse. By analyzing the experimental results with the proposed model, it is found that there is a negative temperature-dependence of the β frequency in the fluorosilicate glass, which can be explained based on the picture of fragmented oxide-network patches in liquid-like regions.

Chapter 6 Ergodicity breaking of an inorganic glass in aging near T_g probed by elasticity relaxation

6.1 Introduction

When a glass is aged at a temperature for which the decay of a physical variable is measurable, one intuitively expects that the dependence on the initial state, or the memory, should decay to zero based on the ansatz that the equilibrium state of supercooled liquid is approachable and unique [35]. That is, a glassy system is still ergodic over sufficiently long times even below the glass transition point, T_g , as the latter is merely an inflection point of a continuous cooling/heating curve, which does not indicate any critical feature of symmetry breaking. The ultimate fate of being ergodic is the cornerstone of the constitutive theories of glass [40], *e.g.*, the Tool-Narayanaswamy-Moynihan (TNM) [107-109] and the Kovacs-Aklonis-Hutchinson-Ramos (KAHR) models [110], where a fictive temperature evolving towards the bath temperature is hypothesized to account for the fading memory. However, this ansatz was challenged by Kovacs' experimental study on the volume relaxation of a polymeric glass below T_g in 1964 [38], showing that the effective relaxation time (τ_{eff}) after long-time aging was still affected by the initial state especially in the experiments of temperature up-jump. Because of the presumed uniqueness of an equilibrium (ergodic) state (note that the equilibrated volume was not provided by Kovacs [38]), the observed divergence of τ_{eff} was termed as "expansion-gap paradox" or " τ_{eff} paradox" [40, 224], questioning how a *quasi*-equilibrated system can exhibit disparate dynamics. Owing to

the fundamentality in understanding glass relaxation, Kovacs' experiment was later re-examined by McKenna *et al.* [40] and repeated by Koll and Simon [224], which confirmed the gap in the *quasi*-equilibrium τ_{eff} .

In other glassy systems such as a charge-density glass [62] and more extensively studied spin glasses [225], aging experiments also revealed a non-vanishing dependence on historic disturbance especially when the latter was applied with a long waiting time. This was manifested by not only the varied spectrum of relaxation time [225], corresponding to Kovacs' finding, but also the non-converged physical quantity in an experimentally accessible duration [226]. Such observations together with the similar results of numerical simulations [61, 102] have led to the concept of ergodicity breaking (EB) described by a phenomenological model based on a rugged free-energy surface [102], or more analytically, replica symmetry breaking (RSB), revealed in the mean-field solutions of spin systems [227, 228]. Therefrom, to our understanding, a spin-glass transition, occurring at a critical temperature T_C , can be precisely defined (*i.e.*, weakly dependent on cooling rate [102]), as it manifests EB. In aging, it signifies a phenomenon that the long-term memory of historical disturbance persists below T_C , and *vice versa* vanishes when $T > T_C$ [102, 225]. While it is generally believed that the results of spin-glass models can be extended to structural glasses, it is still arguable on the possibility of finding any EB phenomenon in the latter, considering that the built-in randomness of spin-spin interactions differs fundamentally from the self-generated position randomness of structural glasses.

Kovacs' finding of the expansion gap seemingly hints at this possibility. However,

his results were criticized especially by the inorganic glass community [229-231] as the dilatometry experiments with inorganic glasses [232, 233] after Kovacs did not render a convincing trend of persistent history dependence near T_g . For example, Goldstein and Nakonecznyj [232] speculated that τ_{eff} paradox might not be found in inorganic glasses because they had a narrower relaxation-time spectrum than a polymeric glass did. Struik [41] criticized that the τ_{eff} paradox might merely be a manifestation of the divergence of τ_{eff} when a stretched exponential process approached equilibrium. These criticisms might have discouraged the effort following the route of Kovacs to unveil an EB phenomenon or the nature of glass transition in structural glasses through monitoring volume (V) change.

In this work, the attention is switched to the variation of Young's modulus of a structural glass because it is a two-time quantity (*i.e.*, the autocorrelation function of stress or strain [234, 235]) that can be analogous to the magnetic susceptibility of a spin glass and must be more sensitive to the heterogeneous dynamics in a glass [236]. Also, in experiments with structural glasses, E changes much more significantly in the temperature range of glass transition. Roughly speaking, $-\lg(dE/dT/E)$ is 2 – 3 [68, 163] and $-\lg(dV/dT/V)$ is 5 – 6 [68] for an inorganic glass, *i.e.*, the variation in Young's modulus is at least two orders of magnitude more significant than that in volume at temperatures near T_g . Hence, it is more plausible to probe an EB phenomenon, if any, based on $E(t)$ than that based on $V(t)$. On the other hand, the relaxation of elasticity is essential to the practical applications, and almost all the manufactory processes of glass devices are related to the elasticity. For example, during precision molding simulations,

real-time Young's moduli are needed [237].

Therefore, a series of aging experiments will be conducted in this Chapter to investigate the temperature-time dependencies of Young's modulus. The experimental results are reported in Section 6.2, the results are analyzed in Section 6.3. In Section 6.4, a novel understanding of the relaxation of elasticity is proposed. All the results are summarized in Section 6.5.

6.2 Temperature jump experiments

The instantaneous Young's modulus was measured. In the experiment, the sample was first heated to and annealed at an initial temperature T_1 for a sufficiently long time to reach a *quasi*-equilibrium state (no apparent trend of modulus change) and then quickly (about 0.5 °C/s) heated or cooled to the final temperature T_2 . I chose¹ the commercial chalcogenide glass As_2Se_3 (Hubei New Hua-Guang Information Materials Co., Ltd, China) with the dilatometry $T_g = 180$ °C, at which the viscosity is approximately 10^{12} Pa s [26]. As_2Se_3 glass is a representative of chalcogenide glasses which has been widely used in infrared imaging [22] and optical switches [238]. It has excellent thermal stability against crystallization [28] with the lowest crystallization temperature of 200 °C, as extrapolated in the plot of isothermal crystallization rate [239]. The results presented in this letter were obtained from a sample of $40.025 \times 8.035 \times 2.45$ mm³ and 3.6396 g, measured using an IET station HT1600 (IMCE, Belgium). During

¹ Several oxide glasses were attempted. But the results were much more contaminated by experimental fluctuations, causing ambiguity to make any judgement. A plausible cause could be the noise in high-temperature measurements because of the higher T_g (~ 500 °C). The IET system we employed is to record the sound generated by sample vibration. At a higher temperature, the environmental noise more deteriorates the weak acoustic signal.

heating, argon gas was purged to protect the sample from oxidation and Young's moduli were measured and recorded every 20 seconds. Fig. 6.1 shows the results of aging at $T_2 = 175\text{ }^\circ\text{C}$ after the temperature jumps from $T_1 = T_2 \pm \Delta T$ with $\Delta T = 5, 10, \text{ and } 15\text{ }^\circ\text{C}$. An example temperature profile of the two-step aging is shown in the above-left inset, which illustrates the temperature overshoot and slow variations in a jump from $T_1 = 160\text{ }^\circ\text{C}$ to $T_2 = 175\text{ }^\circ\text{C}$. Though this transition took hundreds of seconds, it is regarded to be a short transient process in comparison with the long aging time at T_1 and T_2 ($\sim 10^4$ s). Also, the relaxation at T_2 starting from $t = 0$ as defined in this inset is clear-cut, which warrants the determinations of quasi-equilibrium relaxation time and Young's modulus.

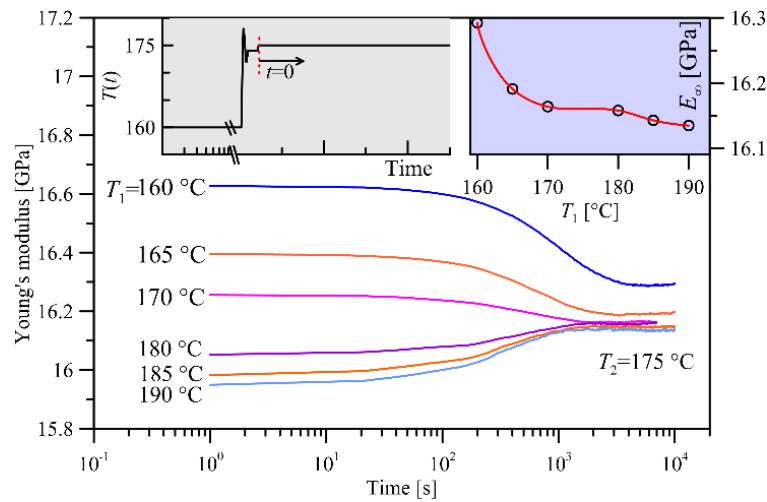


Fig. 6.1 Two-step aging results of As_2Se_3 glass with $T_2 = 175\text{ }^\circ\text{C}$ and $T_1 = T_2 \pm 5, 10, \text{ and } 15\text{ }^\circ\text{C}$. Main plot: relaxation and *quasi*-equilibrated Young's modulus at T_2 , showing that the divergence of Young's modulus relaxation time process, illustrating a T_1 -dependence. The above-left inset: a temperature profile from 160 to 175 $^\circ\text{C}$; the above-right inset: plot of quasi-equilibrium Young's modulus E_∞ against T_1 ,

As shown in the main plot of Fig. 6.1, when $\Delta T = 5\text{ }^\circ\text{C}$, the relaxation processes

after up and down jumps are almost symmetric and the Young's modulus after a long relaxation seemingly merges. With the increase in ΔT , the relaxations after up and down jumps become asymmetric, and more surprisingly, the quasi-equilibrium Young's moduli are also different. I averaged the final leveled segment of the Young's modulus data, containing over 400 data points collected in hours, to quantify the *quasi-equilibrium* magnitude of Young's modulus E_∞ , as plotted in the above-right inset of Fig. 6.1 against T_1 . Though the difference of E_∞ is small ($< 1.5\%$), it is noteworthy that the divergence of E_∞ at T_2 is systematic, *i.e.*, E_∞ decreases with T_1 and up-jump experiments render more deviation than down-jump ones when ΔT is the same.

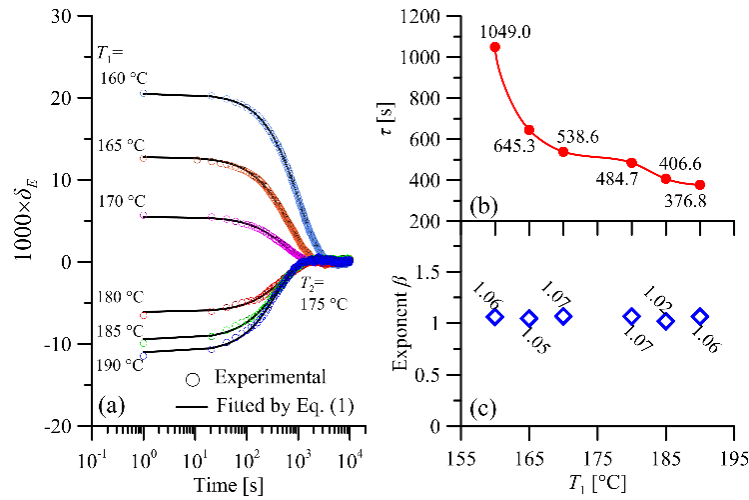


Fig. 6.2 (a) Plots of the relative change of Young's modulus $\delta E(t)$ with fitting results using Eq. (6.1), and plots of (b) relaxation time τ and (c) exponent β against T_1 , indicating exponential relaxations

Using Kovacs's definition [38], we study the normalized modulus change $\delta_E(t) = (E(t) - E_\infty)/E_\infty$, as shown in Fig. 6.2(a) with the fitting curves using a stretched/compressed exponential function:

$$\delta_E(t) = \delta_0 \exp\left[-(t/\tau)^\beta\right], \quad (6.1)$$

where τ is the relaxation time, β the stretching/compressing exponent, and δ_0 a scaling constant. As shown in Fig. 6.2(a), all the relaxation curves are well fitted, and the fitting parameters of τ and β are plotted in Figs. 6.2(b) and (c) against the initial temperature T_1 . We notice that β is almost unity with a maximum deviation of 0.07. Therefore, it is safe for us to claim that the relaxation $E(t)$ in the chalcogenide glass As_2Se_3 is exponential with negligible stretching and that Kovacs' finding of the non-converged relaxation time has been explicitly shown in Fig. 6.2(b); more specifically, τ decreases with the increase of T_1 .

While various models have been proposed to reconcile the conflict between equilibrium dynamics and the history dependence indicated by Kovacs' τ_{eff} paradox, such as the rational thermodynamics [240], stochastic relaxation model [241], or coupling model [242], a loophole in the paradox is indeed the experimental inability to probe the slowest relaxation in a non-exponential process [41, 224]. In our experiments, however, the relaxations are exponential, the loophole vanishes, and the history dependence of the relaxation time stands. Furthermore, we have supplemented the observation that the long-term relaxation may not bring the system to equilibrium because E_∞ does not converge, *i.e.*, the ergodicity is broken and the glassy system can only explore a T_1 -dependent subregion of the configurational space. This finding echoes the extensive computational and experimental findings that the aging of a spin glass system, at temperatures below T_g , does not bring the system asymptotically to an equilibrium state [61, 102, 226]. Note that we cannot exclude the possibility that an ultra-long relaxation may bring the system to equilibrium because of the constraint of

the experimental system (in our case it is due to the limit of inert gas supply). However, because all the $E-t$ curves clearly leveled off as shown in Fig. 6.1 with durations of the flat segments over 10τ , it is reasonable to claim that the further relaxation, if exists, needs a timescale well beyond experimentally accessible range.

6.3 The relation between relaxation time and elasticity

6.3.1 Global elastic model

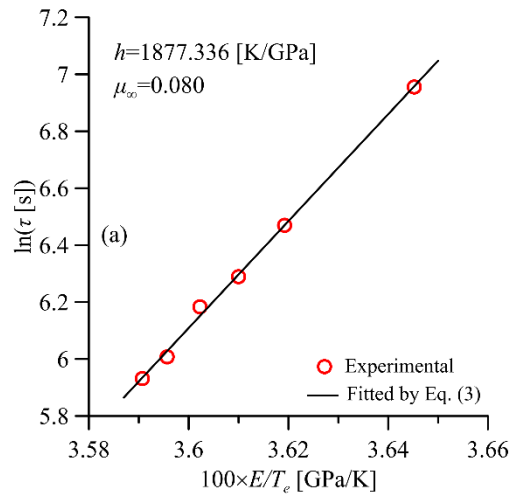


Fig. 6.3 Analysis of T_1 dependence of (a) relaxation time τ based on the elastic model

We anticipate further a correlation between the dynamics, manifested by τ , and the statics, manifested by E_∞ , because the temperature dependences of them display similar features. Based on the elastic model proposed by Mooney [105] which was derived based on Eyring's picture of local molecular movements [243], a relaxation comes about when thermal fluctuations generate a local expansion exceeding a certain critical value. Mooney [105] estimated the probability of these relaxation events interfered by

the thermal longitudinal sound waves and proposed that:

$$\tau = \tau_0 \exp\left[\frac{Q}{k_B T}\right], \quad (6.2)$$

where τ_0 is a pre-factor, k_B is the Boltzmann constant, $Q \propto c_\infty^2 \propto E$ is the activation energy, and c_∞ is the speed of longitudinal sound waves. Note that the temperature T in Eq. (6.2) is a phonon temperature which does not account for the effect of the non-equilibrium dynamics associated with an unrelaxed atomic configuration [244]. We follow Tools [107] and other researchers [45, 245] to involve the effect of structural temperature by introducing an equivalent temperature $T_e \in [T_1, T_2]$ to replace T in Eq. (6.2), because the glass is sufficiently equilibrated at T_1 and then aged at T_2 . For simplicity, letting $T_e = \mu T_1 + (1-\mu)T_2$ with $\mu = \mu(t) \in [0, 1]$ being time-dependent, Eq. (6.2) is then recast as

$$\ln \tau = \ln \tau_0 + h \frac{E}{T_e}, \quad (6.3)$$

where $h = Q/(k_B E)$. At a *quasi*-equilibrium state, E_∞ and $\mu_\infty = \mu(t \rightarrow \infty)$ are constant. Replacing E with E_∞ in Eq. (6.3), and fitting the results of τ , it is obtained that $\mu_\infty = 0.080$, as shown in Fig. 6.3, wherein the data points collapse to a straight line given by Eq. (6.3). The obtained slope $h = 1877.3$ K/GPa, together with $E_\infty = 16.2 \pm 0.1$ GPa (see the above-right inset of Fig. 6.1), leads to the activation energy of $Q = h E k_B = 60.4 \pm 0.4$ kcal/mol, agreeing reasonably well with the activation energy of 68 kcal/mol of As_2Se_3 near T_g [246] determined based on the temperature dependence of shear viscosity.

6.3.2 Mori-Tanaka (MT) analysis of glass after aging

The small value of μ_∞ indicates the non-vanishing structural memory in an aged glass, corresponding to the unmerged E_∞ as shown in the right-above inset of Fig. 6.1. I now draw a simplified picture for the aged glass to be a composite, wherein the matrix is a fully equilibrated (no memory) system at T_2 and inclusions are the persistent structure of T_1 , as sketched in the inset of Fig. 6.4. Denoted by E_i and E_m the Young's moduli of the initial state and the fully relaxed state, respectively, the ratio $y=E_\infty/E_i$ can be expressed as a function of $x = E_i/E_m$, i.e., $y=f(x)$. Due to small μ_∞ , it is imaginable that the inclusions have tiny fractions, thus (1) the interactions between inclusions can be neglected, and (2) every inclusion can be considered in an infinite element. Therefore, the above composite question can be considered with the assumption of spherical inclusion, and the effective shear and bulk modulus can be derived based on the Mori-Tanaka (MT) method [247]:

$$\begin{cases} G_\infty = G_m + \frac{G_i - G_m}{1 + 4(1 - V_f)G_p(G_i - G_m)} V_f \\ K_\infty = K_m + \frac{K_i - K_m}{1 + 9(1 - V_f)K_p(K_i - K_m)} V_f \end{cases} \quad (6.4)$$

where

G_∞ : effective shear modulus;

G_i : shear modulus of initial structures;

G_m : shear modulus of relaxed structures;

K_∞ : effective bulk modulus;

K_i : bulk modulus of initial structures;

K_m : bulk modulus of relaxed structures.

and

$$\begin{cases} G_p = \frac{3(2G_m + K_m)}{10G_m(4G_m + 3K_m)} \\ K_p = \frac{1}{3(4G_m + 3K_m)} \end{cases} \quad (6.5)$$

Considering the relation

$$\begin{cases} G_g = \frac{E_g}{2(1+\nu_g)} \\ K_g = \frac{E_g}{3(1-2\nu_g)} \end{cases}, \quad (6.6)$$

where E_g , and ν_g are Young's modulus and Poisson's ratio, respectively; $g = i$ and m . Then the effective Young's modulus can be written as

$$E_\infty = \frac{9K_\infty G_\infty}{3K_\infty + G_\infty} = g(E_i, E_m) \Big|_{(\nu_i, \nu_m, \nu_f)} \quad (6.7)$$

That is, E_∞ can be considered as a function of E_i and E_m with parameters of (ν_i, ν_m, ν_f) .

Normalizing Eq. (6.7) with E_i leads to

$$E_\infty / E_i = f(1, E_r / E_i) \Big|_{(\nu_i, \nu_r, \nu_f)} = y(x) \Big|_{(\nu_i, \nu_r, \nu_f)}. \quad (6.8)$$

Interestingly, $f(y)$ is found to be very weakly dependent on ν_i and ν_r , which leads to possibility of calculation of ν_f . Let E_r be the average of E_∞ when $\Delta T = \pm 5$ °C and E_i the Young's modulus of the relaxed structure of T_1 when it is kept at T_2 (*i.e.*, corrected by the Debye-Grüneisen coefficient). Plotted in Fig. 6.4 is the experimental results of $f(y)$ together with the theoretical curve passing through experimental points when $\nu_i = \nu_r = 0.3$ and $\nu_f = 0.08095$ (if ν_i and ν_r vary between [0.1, 0.4], ν_f varies between

[0.08094, 0.08101]). It is intriguing that V_f is identical to μ_∞ though they are determined in completely different ways, a demonstration that the quasi-equilibrium dynamics and atomic arrangement are closely related.

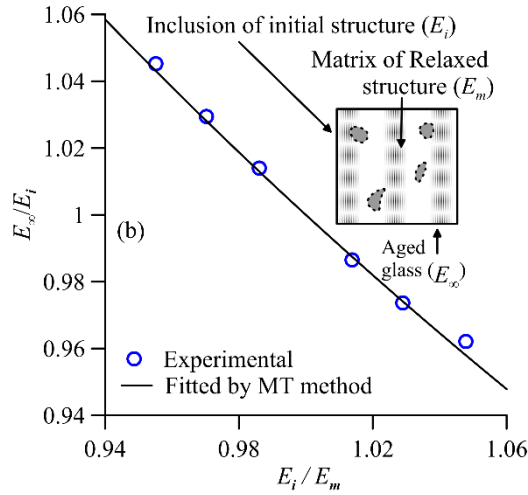


Fig. 6.4 Analysis of the microstructures of aged glass based on the Mori–Tanaka approach; the inset illustrates the simplification of the T_2 -aged glass to be a composite.

Noting that $[df(x)/dx]_{(x=1, v_i=v_m)} + 1 = V_f$, *i.e.*, the slope in the plot of Fig. 6.4 near $x = 1$ can be used to estimate V_f . The aging experiments are repeated with $T_2 = 170, 173, 177, \text{ and } 180^\circ\text{C}$, and $T_1 = T_2 \pm 10^\circ\text{C}$ to obtain the relation between V_f and T_2 , *i.e.*, the temperature dependence of memory persistence. The results are plotted in Fig. 6.5. To exemplify, the relaxation curves of $T_2 = 170^\circ\text{C}$ and 180°C are shown in the insets of Fig. 6.5. We notice that at 180°C the two curves merge after a long-time aging and the exponential relaxation times after up and down jumps are almost identical (~ 300 s). Therefore, $V_f = 0$ at 180°C . Noteworthy, when $T_2 = 177^\circ\text{C}$, V_f is 0.005 determined from the separate values of E_∞ after up and down jumps. Besides, $\tau = 394.0$ s and 320.2 s based on exponential fits for up and down jumps at this temperature, respectively, with

the expected difference that the up-jump case relaxed slower. Fig. 6.5 suggests there is a critical temperature $T_p \in (177^\circ\text{C}, 180^\circ\text{C})$ that can be analogous to T_C of a spin glass. Below T_p , the structural memory persists, *i.e.*, ergodicity is broken; above it, the memory can fade completely, *i.e.*, the system restores ergodicity. For As_2Se_3 , T_g is not a uniquely determined temperature but varies in the range of $175 - 180^\circ\text{C}$ [248] due to the variety of characterization techniques. It is hence argued that the critical temperature T_p is within the empirical range of T_g , at least for As_2Se_3 , signifying that structural glass transition is not just a slowing-down process. Also, we emphasize that our work has paved the way to uniquely determine T_p through measuring E_∞ after two-step aging with $\Delta T \sim 10^\circ\text{C}$. The measurement of the exact T_p for As_2Se_3 would only depend on the accuracy and resolution of temperature control and modulus measurement.

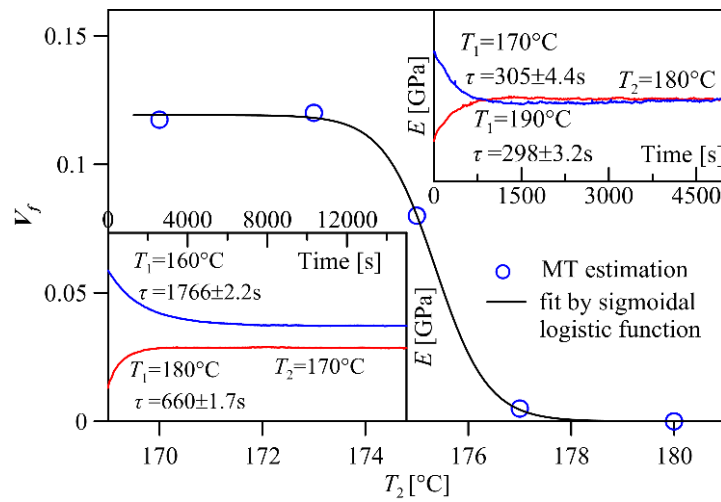


Fig. 6.5 Plot of the measure of memory persistence V_f against the aging temperature T_2 , indicating a clear transition at a critical temperature $T_C \in (177^\circ\text{C}, 180^\circ\text{C})$ with bottom-left and upright insets showing the aging curves $E(t)$ at $T_2 = 170$ and 180°C , respectively, after equilibrated at $T_1 = T_2 \pm 10^\circ\text{C}$.

6.4 Ergodicity breaking origin to dynamic heterogeneity

Phenomenologically, the persistent memory can be explained based on a rugged free energy landscape [102], namely, a glassy system may be trapped in deep energy basins during aging at T_1 , constraining the exploration of the full energy landscape at T_2 within an experimentally accessible time that is already much longer than the relaxation time estimated from viscosity. This picture is also reminiscent of the “mosaic” transition delineated by the random first-order transition theory [122], that is, a glassy system transforms into a patchwork consisting of distinguishable atomic arrangements below T_g . In the two-step aging experiments, some patches at T_1 persists at T_2 during the long aging.

However, the mean-field picture based on a free-energy landscape does not explain how a persistent memory forms from the random variations of atomic configurations, especially when $T_p \sim T_g > T_K$ (T_K , the Kauzmann temperature). Therefore, a real-space picture is needed. Trying to establish it, at least with a clue, we note several recent attempts in establishing the connection between static structures and long-time dynamics based on molecular dynamics (MD) simulations. In a very recent investigation of structural-property relation in a binary Lennard–Jones glass, a machine learning algorithm [148] was established, which, after training, can predict long-time dynamics based on the static initial structures. This result is a triumph in decoding the nature of glass state, as it unveils that the information of initial structures is not “forgotten” in the subsequent relaxation process [149], similar to our results on the initial-state dependence of relaxation time. More transparently, Wang *et al.* [249]

conducted MD simulations of $\text{Cu}_{50}\text{Zr}_{50}$ and found that the activation energy had a strong correlation with the vibrational mean squared displacement (VMSSD) instead of the short-range structural indices. As VMSSD describes the long-range elastic interactions, Wang *et al.* [249] argued that the effect of elastic constraint could be the rate-limiting mechanism of structural relaxation in a glass, which is also the reason we employed the elastic model to analyze relaxation time.

Interestingly, Wang *et al.* [249] found that the glass could be more heterogeneous during relaxation because the soft spots, those substructures with higher flexibility (higher free energy), tended to flock together, leading the heterogeneity in both structure and dynamics. Parallely, Zhang and Lam [250] established a distinguishable-particle lattice model (DPLM), which can be regarded as an abstraction of soft-spot dynamics. It simplifies position randomness in a structural glass to be a random force field between site particles and introduces voids to mimic the motion of soft spots. Such a setup leads to *spatially constrained dynamics* (SCD), *i.e.*, only agminated voids bring about significant relaxation events while isolated voids are trapped. The DPLM simulations successfully reproduced the separation of *quasi-equilibrium* τ_{eff} [251] even though the void concentration and thus the equilibrium state were predefined. Encouraged by the DPLM result and MD simulations, I anticipate that a simplified real-space glass model revealing SCD may involve additionally the generation and depletion of soft spots (or voids) that is dependent on the bath as well as structural temperatures, local stress state, and global energy penalty, following the free-volume picture [252]. Thus, the initial-state dependence, in terms of both relaxation time and quasi-

equilibrium state, may be revealed as a consequence of SCD and the associated evolution of the distribution of soft spots.

6.5 Conclusions

In conclusion, I performed two-step aging experiments with an inorganic glass As_2Se_3 and revealed for the first time the clear phenomena of ergodicity breaking based on the measurements of instantaneous Young's modulus. Both the dynamics and the *quasi*-equilibrium structures are found to be dependent on the thermal history. A critical ergodicity-breaking temperature was identified in As_2Se_3 in terms of the volume fraction of the persistent memory, which was within the empirical glass transition range.

Chapter 7 Birth–death model of glass relaxation related to local elastic heterogeneity

7.1 Introduction

Since 1933, Tammann [253] suggested that glass is not formed homogeneously. With the accumulation of experiments [47, 254-256] and MD simulations [199, 257-259], local structural heterogeneity can be stated more explicitly. Due to thermal fluctuation and structural heterogeneity, some regions in the glass act as a ‘solid-like site’, which is rigid, while other regions act as ‘flow unit’ [48] or ‘liquid-like site’ [260] which is very soft. In 2010, Dmowski *et al.* [47] experimentally found that the volume fraction of soft regions that can flow at a constant temperature in Vit-105 metallic glasses ($\text{Zr}_{52.5}\text{Cu}_{17.9}\text{Ni}_{14.6}\text{Al}_{10}\text{Ti}_5$) is as high as 25%. Using atomic force acoustic microscopy, Wagner *et al.* [261] and Liu *et al.* [254] detected elastic heterogeneity at the nanoscale. More intuitive and intellectual pictures were found in the MD simulations. Yoshimoto *et al.* [257] conducted MD simulations of polymer glass and found that the distribution of shear modulus on a scale is Gaussian. A similar work was proposed by Tsamados *et al.* [262] who studied a model Lennard–Jones (LJ) glass (molecular glass) and found that both bulk and shear moduli exhibit Gaussian distributions.

As long-range structures are not found in glass, the structural heterogeneity is inescapably caused by the slowed relaxation of cooling liquids. Alternatively, heterogeneity has a significant influence on glass relaxation, as mentioned in the

previous chapters. That is, the relaxation and local heterogeneity are coupled in the glass. To explain the relaxation affected by the heterogeneity, many theories have been proposed, including the coupling model [119, 120] and stochastic models controlled by energy [121, 124, 125, 131] or volume [65, 135, 137, 138]. In addition, the spatial heterogeneity resulting from relaxation was studied by Lam *et al.* [250, 251] using an energy-based lattice gas model.

Except for energy and local volume heterogeneity, the most intuitive understanding, elastic property, has not been well understood theoretically. An attempt was proposed by Sun *et al.* [259] who used an empirical relation to describe the local elastic relaxation. However, this is far from a comprehensive understanding of coupled relaxation. Conversely, the demands for the principles of elastic relaxation from industrial communities are very strong. For example, in PGM, the real-time Young's modulus affected by thermal history is needed for technology simulations [237].

These critical issues inspired me to consider the modeling of elastic relaxation influenced by local heterogeneity. Based on the MD simulations of Refs. [257, 262], the elastic modulus distribution seems a continuous Gaussian function, thus an institutive reaction is to consider the transitions between different elastic 'phase'. This idea is similar to that of Medvedev *et al.* [65] on a specified volume. However, the mathematical processes of Medvedev *et al.* [65] are very complex and may not be preferred (especially by the industry). In this chapter, a birth–death (BD) model, which is relatively simple but practical, is proposed to consider the coupled relation between local elastic heterogeneity and macro relaxation. In the model, the global system is

controlled by two different states that can jump to each other. Later, I will show that such a simplification is available to describe the elastic relaxation and that the Gaussian distribution found in MD simulations [257, 262] is misleading to some degree.

In this chapter, mathematical modeling is proposed in Section 7.2. The time–temperature-dependent survival ratio will be derived in rigid mathematics. Then, the expression of Young’s modulus and its variance related to scale will be discussed based on the model. In Section 7.3, I will conduct a real statistical simulation to confirm the formulas derived in Section 7.2. In 7.4, applications of the BD model and some associated issues are discussed. All results are summarized in Section 7.5.

7.2 Mathematical modeling

7.2.1 Birth–death process at a constant temperature

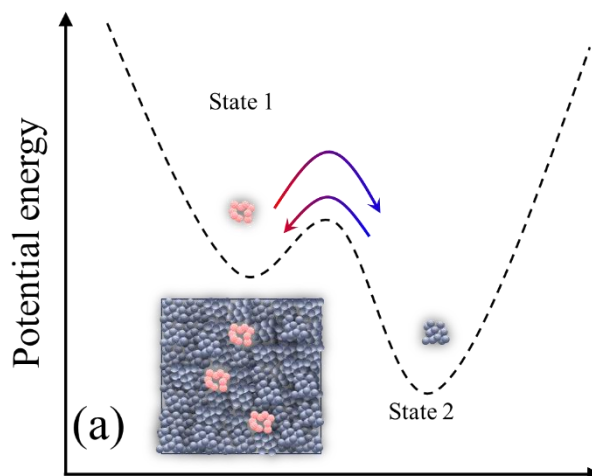


Fig. 7.1 Sketch of a birth–death process. The states can jump to each other with a specified jump rate.

As shown in Fig. 7.1, the representative volume element has been separated into N small patches, which may occur in two different states S_1 and S_2 that can jump to each

other:

$$S_1 \xrightleftharpoons[J_2]{J_1} S_2, \quad (7.1)$$

where J_1 is the jump rate from S_1 to S_2 , J_2 is the jump rate from S_2 to S_1 , and $J_1\Delta t$ and $J_2\Delta t$ are the corresponding jump probabilities in a short time interval Δt , respectively.

Let n_1 be the number of S_1 , while $n_2 = N - n_1$ is the number of S_2 . Without loss of generality, one can choose state S_1 as the observed target whose probability is $P(n, t)$, where n is the number of S_1 patches and t is the time. Then, the master equation of the birth–death processes is given by

$$\begin{aligned} \frac{\partial P(n, t)}{\partial t} = & (n+1)J_1P(n+1, t) + (N-n+1)J_2P(n-1, t) \\ & - [nJ_1 + (N-n)J_2]P(n, t) \end{aligned} \quad (7.2)$$

When n varies from 1 to N , one can obtain a set of equations with N equations and N unknown $P(n, t)$. With the boundary condition $P(N+1, t) = 0$ and initial state $P(n, t = 0)$, the equation set can be solved numerically or analytically, and can be solved through the moment-generating function, which is defined as

$$G(s, t) = \sum_{n=-\infty}^{\infty} s^n P(n, t). \quad (7.3)$$

It is noted that $n \in [0, N]$; thus, $P(n, t) = 0$ for $n \notin [0, N]$ to make the above equation useful. Summing both sides of Eq. (7.2) for n from $-\infty$ to $+\infty$ after timing s^n , one has

$$\frac{\partial G(s, t)}{\partial t} = (1-s) \left[(J_1 + J_2 s) \frac{\partial G(s, t)}{\partial s} - J_2 N G(s, t) \right]. \quad (7.4)$$

Eqs. (7.2) and (7.4) are equal. That is, the multidimensional equations have been transformed into a one-dimensional equation. Eq. (7.4) can be solved by the method of characteristics.

Firstly, I rewrite the equation as

$$(s-1)J_2NG(s,t) = \frac{\partial G(s,t)}{\partial t} + (s-1)(J_1 + J_2s) \frac{\partial G(s,t)}{\partial s}. \quad (7.5)$$

Using the substitution $G(s,t) = G(s(x), t(x)) = G(x)$, we have the following deferential chain:

$$\frac{dG}{dx} = \frac{\partial G}{\partial s} \frac{ds}{dx} + \frac{\partial G}{\partial t} \frac{dt}{dx}. \quad (7.6)$$

The consistency of Eqs. (7.5) and (7.6) provides

$$\frac{dt}{dx} = 1, \quad (7.7)$$

$$\frac{ds}{dx} = (s-1)(J_1 + J_2s), \quad (7.8)$$

$$\frac{dG}{dx} = (s-1)J_2NG. \quad (7.9)$$

Eq. (7.7) implies $x = t$ (It sets $t_0 = 0$ without loss of generality); therefore, the solution of Eq. (7.8) is

$$s(t) = \frac{1 + J_1 e^{(J_1+J_2)(t+C_1)}}{1 - J_2 e^{(J_1+J_2)(t+C_1)}} = \frac{1 + C_1 J_1 e^{(J_1+J_2)t}}{1 - C_1 J_2 e^{(J_1+J_2)t}}. \quad (7.10)$$

Eq. (7.9) can be rewritten as

$$\frac{d \ln G}{dt} = \frac{1}{G} \frac{dG}{dt} = (s-1)J_2N, \quad (7.11)$$

whose integration is

$$\begin{aligned} G &= G_0 \exp \left\{ J_2 N \int_0^t [s(t') - 1] dt' \right\} \\ &= G_0(s) \left[\frac{1 - C_1 J_2}{1 - C_1 J_2 e^{(J_1+J_2)t}} \right]^N, \end{aligned} \quad (7.12)$$

where $G_0(s)$ is an arbitrary function of s .

It can be derived from Eq. (7.10) that

$$C_1 = - \frac{e^{-(J_1+J_2)t} (1-s)}{J_1 + J_2s}. \quad (7.13)$$

Therefore, Eq. (7.12) can be written as a function of s by substituting Eq. (7.13):

$$\begin{aligned}
G &= G_0(s) \left[\frac{J_1 + J_2 s + J_2 e^{-(J_1+J_2)t} (1-s)}{J_1 + J_2} \right]^N, \\
&= G_0(s) \left[1 - \frac{J_2}{J} (1-s) (1 - J_2 e^{-Jt}) \right]^N,
\end{aligned} \tag{7.14}$$

where $J = J_1 + J_2$. Therefore, $G_0(s) = G(s, t = 0)$.

Now, I attempt to derive $P(n, t)$ from Eq. (7.14). Let us consider Case A where there is no target state in the system at the initial state ($t = 0$), one has $P(n, t = 0) = \delta_{n,0}$ and $G_0(s) = 1$. Therefore,

$$G(s) = \left[\frac{J_1 + J_2 e^{-Jt} + J_2 s (1 - e^{-Jt})}{J} \right]^N. \tag{7.15}$$

Based on Newton's binomial theorem, the above equation can be expanded as

$$\begin{aligned}
G(s) &= \sum_0^N C_N^n \left[\frac{J_2 s (1 - e^{-Jt})}{J} \right]^n \left[\frac{J_1 + J_2 e^{-Jt}}{J} \right]^{N-n}, \\
&= \sum_0^N s^n C_N^n \left[\frac{J_2 (1 - e^{-Jt})}{J} \right]^n \left[1 - \frac{J_2 (1 - e^{-Jt})}{J} \right]^{N-n},
\end{aligned} \tag{7.16}$$

where $C_N^n = \frac{n!}{n!(N-n)!}$ is the binomial coefficient and '!' is the factorial symbol.

Comparing Eqs. (7.3) and (7.16), one has a binomial distribution

$$P(n, t) = C_N^n p_A(t)^n [1 - p_A(t)]^{N-n}, \tag{7.17}$$

where

$$p_A(t) = \frac{J_2}{J} (1 - e^{-Jt}), \tag{7.18}$$

is the possibility of finding the target state in Case (A).

Based on the moment-generating function, it is easy to find the expectation

$$\langle n(t) \rangle = \sum_n nP(n,t) = \left. \frac{\partial G(s,t)}{\partial s} \right|_{s=1}, \quad (7.19)$$

where $\langle \rangle$ represents the average among all possibilities at time t . Therefore, the number of target states in the global system is expected as

$$\langle n_A(t) \rangle = \left. \frac{\partial G(s,t)}{\partial s} \right|_{s=1} = N \frac{J_2(1-e^{-Jt})}{J} = Np_A(t). \quad (7.20)$$

Now let us consider the opposite situation, that is, Case B, where the target state fulfils the system in the initial state ($t = 0$); one has $P(n; t = 0) = \delta_{n,N}$ and $G_0(s) = s^N$, and

$$G(s,t) = \left[\frac{J_1 + J_2s - J_1e^{-Jt}(1-s)}{J} \right]^N. \quad (7.21)$$

This leads to a binomial distribution of

$$P(n,t) = C_N^n p_B(t)^n [1-p_B(t)]^{N-n}, \quad (7.22)$$

where

$$p_B(t) = \frac{J_1e^{-Jt} + J_2}{J}, \quad (7.23)$$

is the possibility of finding the target state in Case B) Therefore, the number of target states in the global system is expected as

$$\langle n_B(t) \rangle = \left. \frac{\partial G(s,t)}{\partial s} \right|_{s=1} = N \frac{J_1e^{-Jt} + J_2}{J} = Np_B(t). \quad (7.24)$$

Generally, when the system starts from an arbitrary state $\langle n(0) \rangle$, the evolution of the average number of target states is

$$\begin{aligned} \langle n(t) \rangle &= [N - \langle n(0) \rangle] p_A + \langle n(0) \rangle p_B \\ &= N \frac{J_2}{J} (1 - e^{-Jt}) + \langle n(0) \rangle e^{-Jt}. \end{aligned} \quad (7.25)$$

Moreover, the variance can be derived from $G(s, t)$

$$\langle n^2(t) \rangle = \sum_n n^2 P(n;t) = \frac{\partial}{\partial s} \left[s \frac{\partial G(s,t)}{\partial s} \right] \Bigg|_{s=1}. \quad (7.26)$$

After some derivations, the variance of $n(t)$ can be obtained as

$$\sigma^2 [n(t)] = \sigma^2 [n(0)] e^{-2Jt} + (1 - e^{-Jt}) \left[\langle n(0) \rangle \frac{J_1 - J_2}{J} e^{-Jt} + \frac{J_2}{J^2} N (J_2 e^{-Jt} + J_1) \right]. \quad (7.27)$$

When $t \rightarrow \infty$, the equilibrium state reaches

$$\begin{cases} \langle n \rangle_{\text{eq}} = \langle n(t \rightarrow \infty) \rangle = \frac{J_2}{J} N \\ \sigma^2 [\langle n \rangle]_{\text{eq}} = \sigma^2 [\langle n(t \rightarrow \infty) \rangle] = \frac{J_1 J_2}{J^2} N \end{cases}. \quad (7.28)$$

When N is very large in a macro system, providing a predefined value of N is unnecessary, and the above equation can be normalized by

$$\lambda(t) = \frac{\langle n(t) \rangle}{N}, \quad (7.29)$$

where $\lambda(t)$ is the expected survival ratio of S_1 . Then,

$$\lambda(t) = \frac{J_2}{J} (1 - e^{-Jt}) + \lambda_0 e^{-Jt} \quad (7.30)$$

can be obtained, where $\lambda_0 = \lambda(t=0)$ and

$$\begin{cases} \lambda_{\text{eq}} = \lambda(t \rightarrow \infty) = \frac{J_2}{J} = \frac{J_2}{J_1 + J_2} \\ \sigma^2 [\lambda_{\text{eq}}] \rightarrow 0 \end{cases}. \quad (7.31)$$

Eq. (7.31) suggests that the equilibrium state is determined by the jump rates of both sides.

7.2.2 Variation in survival ratio at varying temperatures

Practically, the jump rate is not constant due to the varying environment, for example, temperature. Therefore, the variation in the survival ratio should be extended

at various temperatures. Let us consider a time-dependent jumping ratio affected by temperature. In a very small time interval from t to $t + dt$ ($dt \rightarrow 0$), the jump rate change can be neglected. Then Eq. (7.30) changes to

$$\lambda(t + dt) = \lambda(t) \exp[-J(t) dt] + \frac{J_2(t)}{J(t)} \{1 - \exp[-J(t) dt]\}. \quad (7.32)$$

Considering the equivalent infinitesimal relation $\exp(\varepsilon) \sim 1 + \varepsilon$, where ε is an infinitesimal, the above equation changes to

$$\lambda(t + dt) = \lambda(t) [1 - J(t) dt] + J_2(t) dt, \quad (7.33)$$

i.e.,

$$\lambda'(t) = \lim_{dt \rightarrow 0} \frac{\lambda(t + dt) - \lambda(t)}{dt} = J_2(t) - J(t) \lambda(t). \quad (7.34)$$

Considering $\lambda(0) = \lambda_0$, the solution of Eq. (7.34) is found by the method of parameter variation

$$\lambda(t) = e^{-\int_0^t J(\xi_1) d\xi_1} \left[\lambda_0 + \int_0^t J_2(\xi_2) e^{\int_0^{\xi_2} J(\xi_1) d\xi_1} d\xi_2 \right]. \quad (7.35)$$

For a complex temperature history, the integration of Eq. (7.35) cannot be calculated directly. Then, one should use the difference method by changing Eq. (7.32) as

$$\lambda(t_{k+1}) = \lambda(t_k) \exp[-J(t_k) dt] + \frac{J_2(t_k)}{J(t_k)} \{1 - \exp[-J(t_k) dt]\}, \quad (7.36)$$

where k is the step number and Δt is the time step. The above explicit scheme is available for any complex case. If a relatively larger Δt is used, the implicit difference scheme is recommended.

$$\begin{aligned}
& \begin{bmatrix} 1 & & & & & \\ -\exp[-J(t_1)\Delta t] & 1 & & & & \\ & -\exp[-J(t_2)\Delta t] & 1 & & & \\ & & \ddots & \ddots & & \\ & & & -\exp[-J(t_{n-1})\Delta t] & 1 & \end{bmatrix} \begin{bmatrix} \lambda_1 \\ \lambda_2 \\ \lambda_3 \\ \vdots \\ \lambda_n \end{bmatrix} \\
& = \begin{bmatrix} J_2(t_0)/J(t_0)\{1-\exp[-J(t_0)\Delta t]\} + \lambda_0 \exp[-J(t_0)\Delta t] \\ J_2(t_1)/J(t_1)\{1-\exp[-J(t_1)\Delta t]\} \\ J_2(t_2)/J(t_2)\{1-\exp[-J(t_2)\Delta t]\} \\ \vdots \\ J_2(t_{n-1})/J(t_{n-1})\{1-\exp[-J(t_{n-1})\Delta t]\} \end{bmatrix} \quad (7.37)
\end{aligned}$$

If the small Δt used in the explicit scheme leads $J(t_k)\Delta t \ll 1$, Eq. (7.36) can be simplified as

$$\lambda(t_{k+1}) = \lambda(t_k)[1 - J(t_k)\Delta t] + J_2(t_k)\Delta t, \quad (7.38)$$

and the corresponding implicit difference scheme is

$$\begin{aligned}
& \begin{bmatrix} 1 & & & & & \\ J(t_1)\Delta t - 1 & 1 & & & & \\ & J(t_2)\Delta t - 1 & 1 & & & \\ & & \ddots & \ddots & & \\ & & & J(t_k)\Delta t - 1 & 1 & \end{bmatrix} \begin{bmatrix} \lambda_1 \\ \lambda_2 \\ \vdots \\ \vdots \\ \lambda_n \end{bmatrix} \\
& = \begin{bmatrix} J_2(t_0)\Delta t + \lambda_0 - \lambda_0 J_2(t_0)\Delta t \\ J_2(t_1)\Delta t \\ J_2(t_2)\Delta t \\ \vdots \\ J_2(t_{n-1})\Delta t \end{bmatrix}. \quad (7.39)
\end{aligned}$$

For the mean-field theory, the derivations in this section decouple the jump rate, which may interact with each other. As Eq. (7.35) is derived with $dt \rightarrow 0$, that is, the higher-order effects of the time dependence of the jump rate are neglected, it is always available if the interaction between different paths can be written into the expression

jump rate. If the integration is difficult to find, the difference methods with the same idea can be used.

7.3 Numeric validation with stochastic simulation

Table 7.1 Jump rate parameters in Eq. (7.40)

f_1	f_2	N	Q_1/k_B	Q_2/k_B	time	Δt
1	0.8	1E4	3800	4000	10000	1

To verify the above derivations, a series of stochastic simulations were performed.

For simplicity, the jump rate is defined in the Arrhenius form.

$$\begin{cases} J_1 = f_1 \exp\left(-\frac{Q_1}{k_B T}\right) \\ J_2 = f_2 \exp\left(-\frac{Q_2}{k_B T}\right) \end{cases}, \quad (7.40)$$

where Q_i is the energy barrier; $f_i = v_0 \times g_i$, where v_0 is the attempt frequency and g_i is the degeneracy (where $i = 1$ and 2). Then, the jumping possibility is defined by

$$\begin{cases} P_1 = J_1 \Delta t \\ P_2 = J_2 \Delta t \end{cases}, \quad (7.41)$$

where $0 < J_i \Delta t < 1$ ($i = 1, 2$). To start the simulation, a system with N patches was considered. The patches are occupied by '1' or '0'. A vector $r(N) \in [0, 1]$ is generated with an N random value. If r is smaller than the jumping possibility, the jumping event occurs; otherwise, the subsystem retains its current state. By repeating the above process step by step, the relaxation process can be simulated. The simulation process is

summarized in Fig. 7.2. To simplify the simulation, dimensionless parameters are used except T , which has a nominal unit of Kelvin. The parameters used are listed in Table 7.1. During the simulation, the jumping judgment was conducted on all the N patches in every time step.

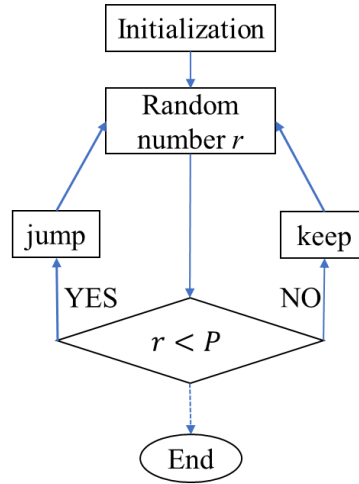


Fig. 7.2 Flow chart for simulating the birth–death process.

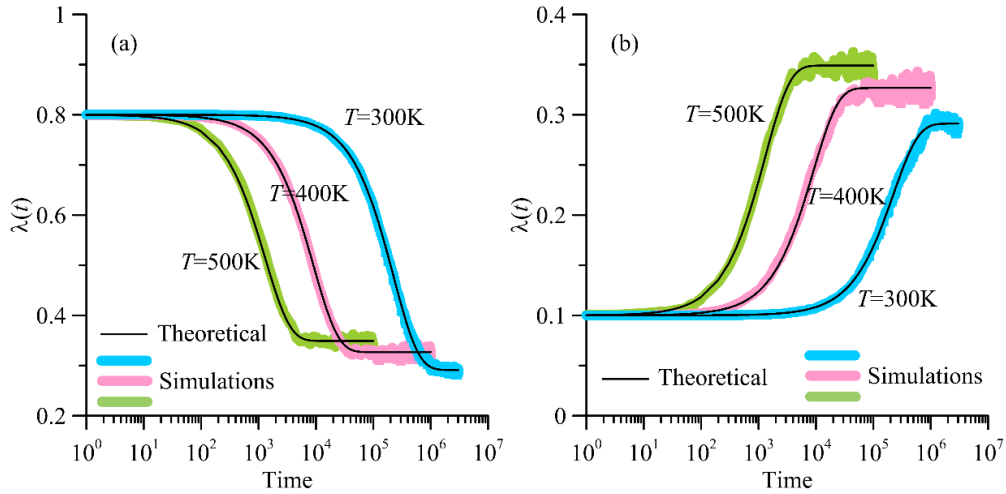


Fig. 7.3 Comparison between stochastic simulation and analytical solution at a constant temperature: (a) starting from $\lambda_0 = 0.8$, and (b) starting from $\lambda_0 = 0.1$. The bold line is the simulation result, and the thin line is the analytical result of Eq. (7.30).

In Fig. 7.3, the relaxation processes at constant temperature are plotted. I consider two cases of (a) $\lambda_0 = 0.8$ and (b) $\lambda_0 = 0.1$, which are larger and smaller than the equilibrium states. The prediction of Eq. (7.30) agrees well with the simulation results.

At a constant temperature, the relaxation processes are exponential, as mentioned by Eq. (2.2). Furthermore, the equilibrium state is also different from the aging temperature, which is due to the difference in the ratio between the jump rates. In Fig. 7.4, similar cases of $\lambda_0 = 0.8$ and $\lambda_0 = 0.1$ are considered, but the temperature changes between 400 K and 500 K with a linear heating and/or cooling process. The prediction of Eq. (7.35) and the simulation are completely consistent, even for cases with complex and non-monotonic relaxation processes (Figs. 7.4(b) and (c)).

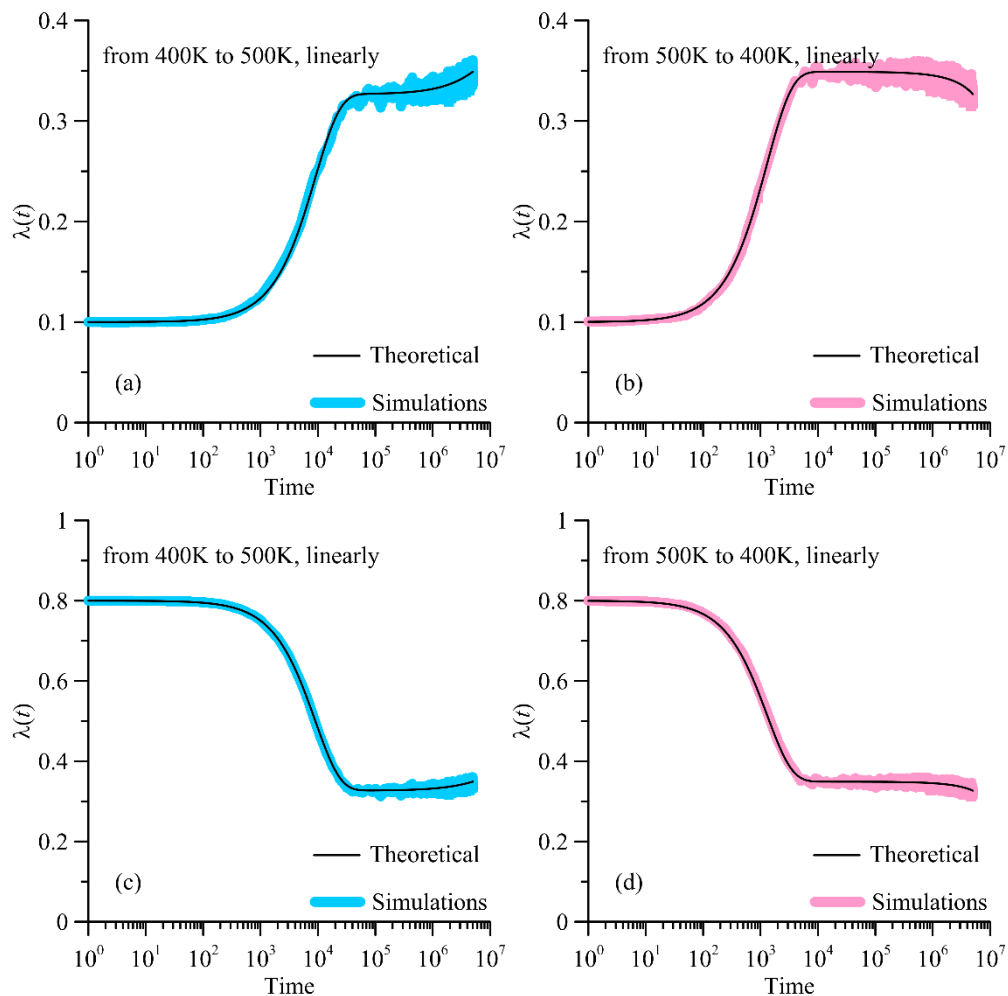


Fig. 7.4 Comparison between stochastic simulation and analytical solutions at various temperatures. The bold line is the simulation result, and the thin line is the analytical result of Eq. (7.35). The temperature varies between 400 K and 500 K with a heating and/or cooling rate of 2×10^{-5} K every time unit.

7.4 Applications of the BD model and discussions

Though the derivations following rigid mathematics are complex, the final equations of survival ratio are elegant, as shown by Eq. (7.30) and (7.35). In this Section, several cases will be addressed to show that this elegant model has powerful potentials on many aspects of glass relaxation.

7.4.1 Prediction on the temperature-dependent Young's modulus

As mentioned above, the variation of Young's modulus during temperature change is critical to the manufacture of glass products [237]. Because glass relaxation is appreciable when the temperature is near T_g , the relaxation of Young's modulus will have memory effects in practical experiments, making it complex to predict the Young's modulus in real-time. The BD model provides a possible approach if the variation of survival ratio of S_1 is known. However, there still needs two conditions, that is, (1) the mixing rule from survival ratio to the macro property, and (2) the two jump rates controlling the relaxation process.

Let us consider the two states in a glass with different Young's moduli $E_1 (S_1)$ and $E_2 (S_2)$. With temperature change, their structures maintain their values only changed with Debye–Grüneisen (DG) relation; that is,

$$\begin{cases} E_1(T) = a_1 + b_1T \\ E_2(T) = a_2 + b_2T \end{cases}, \quad (7.42)$$

where a_1 , b_1 , a_2 , and b_2 are the coefficients. When the two states combined, it is very complex in the mesomechanics to find effective elasticity and has been investigated by many researchers. Based on Hill [263], the arithmetic means of modulus, corresponding Voigt's estimation [264], is the upper bound of the effective modulus, and the harmonic means, corresponding to Reuss' estimation [265], is the lower bound. This is because,

in the direction of applied stress, the arrangement of a composite has two extreme situations, *i.e.*, serial and parallel connections. In cases of calculating the effective bulk modulus, arithmetic means based on Voigt's estimation [264] always works. However, when calculating the effective Young's modulus or shear modulus, the fraction of serial or parallel connections is difficult to determine. For simplification, one can assume that their contributions are almost equal, such as that of Hill's suggestion [263] that an effective modulus is the average of the Voigt and Reuss estimations, which is thus called Voigt–Reuss–Hill (VRH) approximation. Young's modulus is written as follows:

$$E = \frac{1}{2}(E_V + E_H), \quad (7.43)$$

where $E_V = \lambda_1 E_1 + \lambda_2 E_2$ and $E_R = \frac{E_1 E_2}{\lambda_1 E_2 + \lambda_2 E_1}$, λ_i is the composition fraction, and $i = 1, 2$ labels the state. In recent years, some mesomechanic-based methods have been proposed. For example, Sun *et al.* [259] in 2016 derived the effective modulus of glass modeled by a composite of hard/soft patches based on Eshelby's method.

The volume fraction of a single state may vary significantly in a glass. For example, the ratio of liquid-like regions starts from 1 to 1/4 in Vit-105 metallic glass during the manufacturing process [47]; these theoretical predictions should be examined carefully before application. I conduct simulations using the finite element method (FEM) on a 2D composite with 5×5 soft inclusions in a hard matrix. Fig. 7.5 provides a comparison between the predictions of Eshelby's theory, the VRH approximation, and the FEM results. It was found that the VRH approximation provides a very good description of Young's modulus in a broad volume fraction of inclusions. The prediction of Eshelby's theory gradually departs from the FEM results with an increase in the inclusion fraction. This is because the interaction between different inclusions is not considered by Eshelby's theory, but it becomes important when the inclusion fraction is not very small.

During glass transition, the sample changes from solid-like state to liquid-like state, which corresponds to a significant change in the volume fraction of ‘inclusion’. Therefore, the VRH approximation is preferred if one wants to calculate the effective modulus.

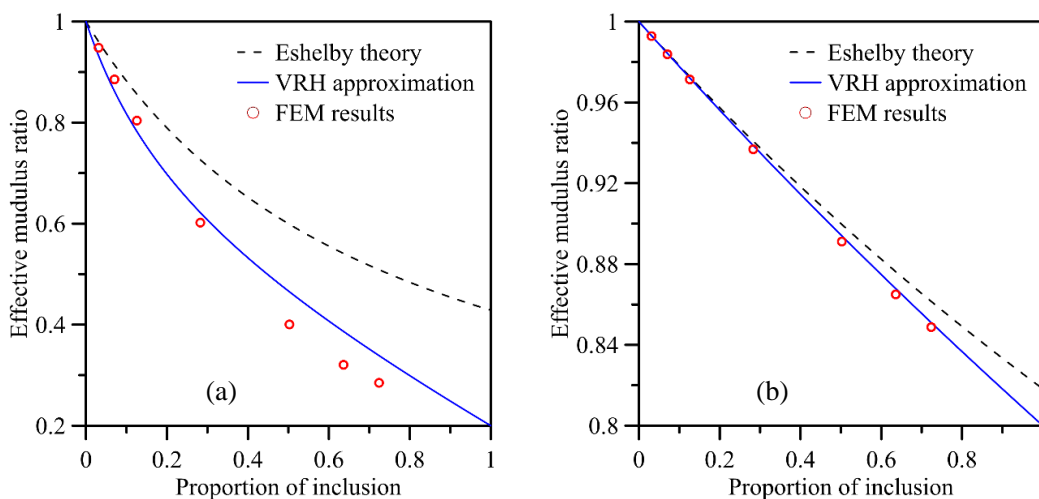


Fig. 7.5 Effective modulus as a function of the fraction of inclusion. The Young's modulus ratio between the inclusion and matrix is (a) 0.2 and (b) 0.8.

As shown in Fig. 7.1, one may consider that the two states have different potential energy states; then, the jump rate between the two states can be defined by the energy barrier, as the definition of the Arrhenius relation of Eq. (7.40). As examples, the temperature dependence of two glasses during heating was examined. The first sample is L-BAL42, which has already been reported in Chapter 4. The second sample was S-FSL5. Different from the sample used in Chapter 5, a new sample ($40.05 \times 7.9 \times 2.02$ mm³, 1.571 g) was used, and the natural frequencies during the entire experimental period were far from the frequency of its β relaxation. This can reduce the effects of β relaxation on the modulus measurements. All the procedures are the same as in Chapter

4, except that the heating rate of S-FSL5 is 5 °C/min.

To predict the experimental results, nine parameters, that is, $\{a_1, b_1, a_2, b_2, f_1, Q_1, f_2, Q_2, \text{ and } \lambda_0\}$, are needed. Herein, λ_0 is the initial proportion of S_1 . To obtain them, the predictions of Young's modulus based on the BD model were fitted to the experimental results. The errors between the predictions and experiments are minimized by the adaptive simulated annealing (ASA) algorithm. Technically, the implicit difference scheme in Eq. (7.37) was used. Since most relaxation events occur at high temperatures, the time interval used in the BD model is not uniform but decreases with increasing temperature. The time interval at the highest temperature is 1% of that at the lowest temperature in the experiments. A total of 10^4 points are used for differences in the prediction of the BD model.

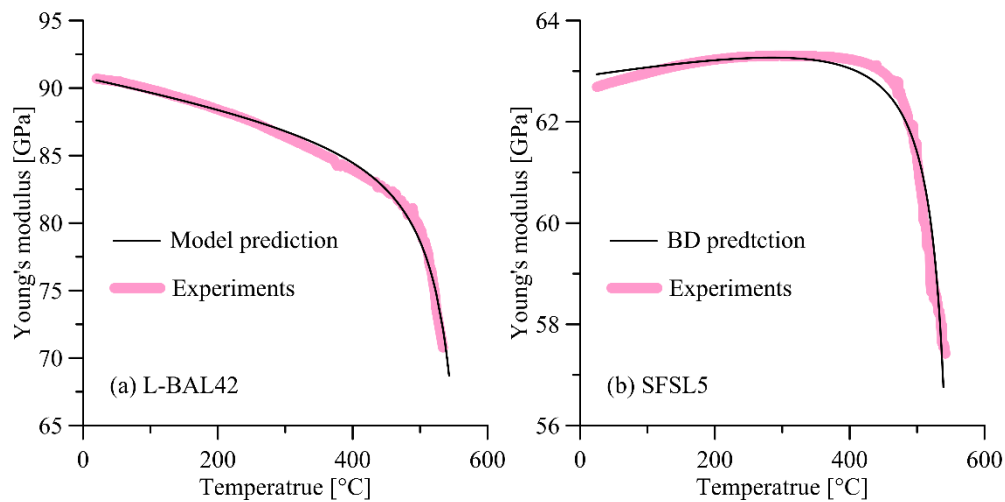


Fig. 7.6 Comparison of temperature-dependent Young's modulus between the experiments and predictions of the BD model.

The comparison between the experiments and the BD model predictions are plotted in Fig. 7.6, and Young's moduli of both L-BAL42 and S-FSL5 were successfully

predicted. For the L-BAL42 glass, the modulus monotonically decreases with temperature and has a sharp transition near T_g . However, for S-FSL5, the temperature dependence of Young's modulus is anomalous as it increases with temperature before T_g . Such a feature may be related to the amorphous silicon oxide (a-SiO₂), whose Young's modulus also has an anomalous temperature dependence [266]. Fig. 7.6 suggests that the BD model can simulate both the normal and anomalous temperature dependence of Young's modulus.

7.4.2 Relationship between relaxation time and mixing rules

As stressed by Medvedev *et al.* [65], mixing rules have influences on the predicted relaxation in a mean-field model. Now let us consider two basic cases.

(a) If the macro property (*e.g.* energy and volume) of glass equals the weighted average of the two state properties, that is, the arithmetic mean mixing rule, then

$$P = aP_1\lambda(t) + bP_2[1 - \lambda(t)], \quad (7.44)$$

where a and b are the weight parameters and P_1 and P_2 are the properties of the two states. The fundamental 'clock' of a BD model is controlled by the relaxation time, not by atomic vibration. Recall the hypothesis that the property relaxation depends on the departure of the equilibrium state,

$$\frac{dP}{dt} = \frac{P_{eq} - P(t)}{\tau}. \quad (7.45)$$

At a constant temperature, I substituted Eqs. (7.30) and (7.44) into Eq. (7.45) and obtained

$$\tau = J^{-1}. \quad (7.46)$$

Recall Eqs. (4.6) and (4.10) in Chapter 4; I showed that when the jump rate from one state to another satisfies $J = \tau_M^{-1}$. This consistency also indicates the validation of the BD model.

(b) If the macro property (*e.g.* density and electricity) follows the harmonic mean mixing rule, then

$$P^{-1} = aP_1^{-1}n_1 + bP_2^{-1}n_2. \quad (7.47)$$

Similar conductions lead to

$$\tau = \frac{P(t)}{P_{eq}} J^{-1}. \quad (7.48)$$

If the system state is not very far from the equilibrium, $P(t)/P_{eq} \approx 1$, Eqs. (7.46) and (7.48) were almost equivalent. This corresponds to the cases that was experimental found in Chapter 6 because Young's modulus changes a little during the aging period. However, if the system state is far from the equilibrium, it is expected that the effective relaxation time is time-dependent. This indicates that the mixing rule is essential for the relaxation process. In a mean-field theory with numerous different states, the jumping ratio can be pre-defined. Eq. (7.48) implies that even in the simplest case of two distinguishable states, the relaxation may drop into the non-exponential process. For the macro property, which intuitively follows the arithmetic mean mixing rule, for example, volume, practical mixing is not purely arithmetic due to the interactions affected by the stress contributed by the mismatch. This leads to the contributions of the harmonic mean. In the stochastic model of Robertson *et al.* [135] and Medvedev *et al.* [65], the local relaxation is assumed to be related to the macro volume due to the

interactions between different sub-regions. However, the question is as follows: Is the local relaxation affected by neighboring regions or the global system? Eq. (7.48) suggests that the global system is indeed participating in local relaxation if the sub-regions interact.

7.4.3 Distributions of the local elasticity heterogeneity due to VRH approximation

Recall the works of Yoshimoto *et al.* [257] and Mizuno *et al.* [255] who conducted MD simulations and calculated the bulk modulus K and shear modulus G at different scales. The probabilities of the elastic modulus at different scales were studied in both works and were found to have a Gaussian distribution. From the view of the combination of two different states of glass, the observed patches of the two states are possibly different at different scales, which leads to elasticity uncertainty in observations. To exhibit the relation in the BD model, I discuss the variance of Young's modulus as an example at the equilibrium state.

For Voigt's case, the following is derived

$$\sigma^2 [E_V] = \sigma^2 [\lambda_1 E_1 + \lambda_2 E_2] = \frac{1}{N} (E_1 - E_2)^2 \frac{J_1 J_2}{J^2}. \quad (7.49)$$

For Reuss' case,

$$\sigma^2 [E_R] = \sigma^2 \left[\frac{E_1 E_2}{\lambda_1 E_2 + \lambda_2 E_1} \right] = N^2 \left(\frac{E_1 E_2}{E_1 - E_2} \right)^2 \sigma^2 \left[\frac{1}{\varphi} \right], \quad (7.50)$$

where $\varphi = n - NE_1/(E_1 - E_2)$. Based on Eq. (7.17), $\langle n \rangle \sim B[N, J_2/J]$, which is a binomial distribution at the equilibrium state. Thus, $\varphi \sim B[N, p_\varphi]$ with $p_\varphi = J_2/J + E_1/(E_2 - E_1)$.

Therefore,

$$\begin{aligned}
\sigma^2 \left[\frac{1}{\varphi} \right] &= \left\langle \frac{1}{\varphi^2} \right\rangle - \left\langle \frac{1}{\varphi} \right\rangle^2 \\
&= \sum_{k=1}^N \frac{1}{\varphi^2} p_\varphi^k (1-p_\varphi)^{N-k} - \left[\sum_{k=1}^N \frac{1}{\varphi} p_\varphi^k (1-p_\varphi)^{N-k} \right]^2 \\
&= N p_\varphi (1-p_\varphi)^{N-1} {}_4F_3 \left(1, 1, 1, 1-N; 2, 2, 2; \frac{p_\varphi}{p_\varphi-1} \right), \\
&\quad - N^2 p_\varphi^2 (1-p_\varphi)^{2N-2} {}_3F_2 \left(1, 1, 1-N; 2, 2; \frac{p_\varphi}{p_\varphi-1} \right)^2
\end{aligned} \tag{7.51}$$

where ${}_L F_M(\{a_1, a_2, \dots, a_L\}; \{b_1, b_2, \dots, b_M\}; \varphi)$ is the generalized hypergeometric function of φ .

In addition, N is relatively large in a practical measurement; therefore, $\langle n \rangle \sim B[N, J_2/J]$ can be approximated to $\langle n \rangle \sim G[NJ_2/J, NJ_1J_2/J^2]$ is a Gaussian distribution with a mean of (NJ_2/J) and variance of (NJ_1J_2/J^2) . The mean of $1/\varphi$ can be found with Lecomte's method [267].

$$\left\langle \frac{1}{\varphi} \right\rangle = \sqrt{\frac{2J^2}{NJ_1J_2}} F_D \left[\sqrt{\frac{2N}{J_1J_2}} \left(J_2 - J \frac{E_1}{E_1 - E_2} \right) \right], \tag{7.52}$$

where $F_D[z] = \exp(-z^2) \int_0^z \exp(t^2) dt$ is the Dawson function [268]. The second-order moment of $1/\varphi$ is [267].

$$\left\langle \frac{1}{\varphi^2} \right\rangle = \frac{1}{N} \left(\frac{J}{J_2} - \frac{JE_2}{J_1E_1} \right) \left\langle \frac{1}{\varphi} \right\rangle - \frac{J^2}{NJ_1J_2} \tag{7.53}$$

Using Eqs. (7.52) and (7.53), one has

$$\begin{aligned}
\sigma^2 \left[\frac{1}{\varphi} \right] &= \left\langle \frac{1}{\varphi^2} \right\rangle - \left\langle \frac{1}{\varphi} \right\rangle^2 \\
&= \frac{J^2}{NJ_2J_1} \left\{ \sqrt{\frac{2(J_1E_1 - J_2E_2)^2}{NJ_1J_2E_1^2}} F_D \left[\sqrt{\frac{2N}{J_1J_2}} \left(J_2 - J \frac{E_1}{E_1 - E_2} \right) \right] \right. \\
&\quad \left. - 2F_D^2 \left[\sqrt{\frac{2N}{J_1J_2}} \left(J_2 - J \frac{E_1}{E_1 - E_2} \right) \right] - 1 \right\}.
\end{aligned} \tag{7.54}$$

Substituting Eq. (7.51) or Eq. (7.54) into Eq.(7.50), $\sigma^2[E_R]$ is obtained, and the variance determined by the VRH approximation is

$$\sigma^2[E] = \frac{1}{4}(\sigma^2[E_V] + \sigma^2[E_R]). \quad (7.55)$$

Based on the BD model, a local state follows a binomial distribution, as discussed in Section 7.3.3. With the increase in N , the binomial distribution gradually becomes a Gaussian distribution. Therefore, for the bulk modulus that follows the arithmetic mean, it is expected to obtain a Gaussian distribution. Nonetheless, Young's modulus or shear modulus contains harmonic mean effects that distort the distribution, Gaussian distribution should not be valid.

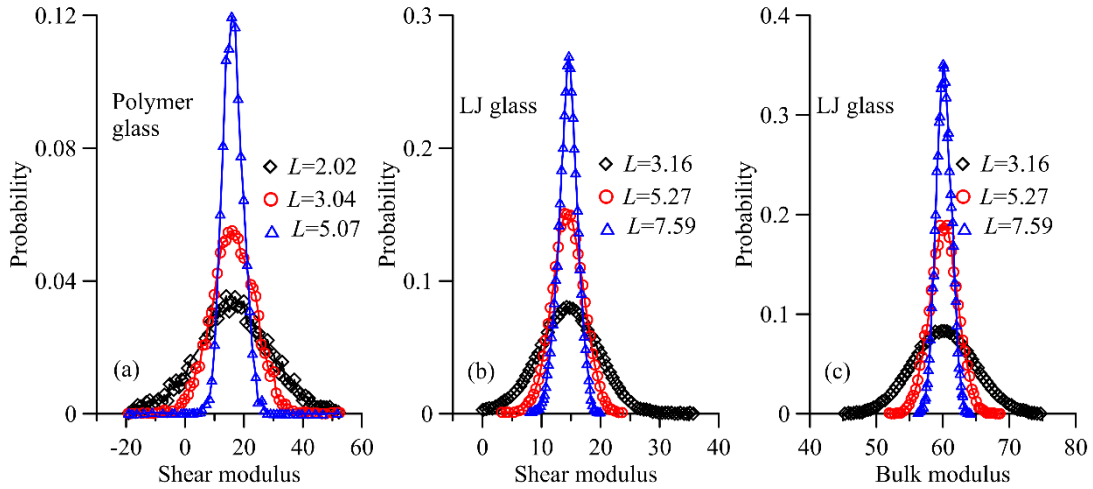


Fig. 7.7 The scale dependence of the distribution of elastic modulus. (a) shear modulus of the polymer glass by Mizuno *et. al* [255], and (b-c) shear and bulk moduli of the LJ glass by Yoshimoto *et. al* [257]

To clarify the difference between the prediction of BD model, and the previous upstanding, I collect the distribution of shear modulus of the polymer glass simulated by Mizuno *et. al* [255], and the distributions of shear and bulk moduli of the LJ glass

simulated by Yoshimoto *et. al* [257], and plot them in Fig. 7.7. In the plot, three different scales of L are considered with L being the side length of the investigated patch. The distribution is bell-shaped and becomes sharp with the increase of L . This seems consistent with Gaussian distribution. I collected the height (H) and the full width at the half maximum (W) from the reported data [255, 257]. Assuming that the average length of the studied patches in the BD model is L_0 , the number found in a patch is $(L/L_0)^3$. Based on the modulus variance of Eq.(7.49) that can result in a Gaussian distribution, the following relation is obtained:

$$W = \sqrt{8 \ln 2} \times \sigma \propto 1/\sqrt{N} \propto L^{-1.5}. \quad (7.56)$$

Besides, the peak height of the distribution $H = 1/(\sqrt{2\pi} \sigma)$. Therefore,

$$W \times H = \sqrt{8 \ln 2} \sigma \times \frac{1}{\sqrt{2\pi} \sigma} \approx 0.932. \quad (7.57)$$

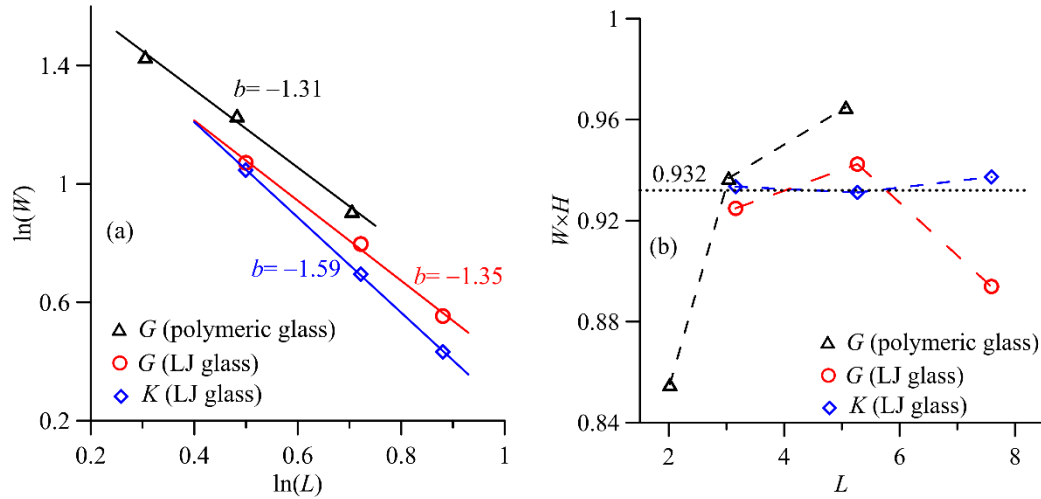


Fig. 7.8 Examination of Gaussian distribution of elastic modulus: (a) relaxation between $\ln(W)$ and $\ln(L)$ and (b) relation between $W \times H$ and L .

If the modulus distribution is Gaussian, Eq. (7.56) predicts a power index $b = \Delta \ln(W)/\Delta \ln(L) = -1.5$, and Eq. (7.57) predicts a constant value of 0.932. Now, let us examine the predictions. In Fig. 7.8(a), $\ln(W)$ is plotted versus $\ln(L)$, and in Fig. 7.8(b),

$W \times H$ is plotted versus L . In Fig. 7.8(a), the slope of the bulk modulus of LJ glass is -1.59 , which is close to the prediction. For the cases of shear modulus, the slopes of polymer glass and LJ glass are -1.31 and -1.35 , respectively, which deviate significantly from the prediction. For the cases of $W \times H$ in Fig. 7.8(b), the value of the bulk modulus of LJ glass is very close to the prediction of 0.932 , while the shear modulus for both glasses fluctuates significantly. That is, the mixing rules distort the distribution and change the scaling law, which simply follows the understanding of the BD model.

7.5 Conclusions

In summary, a birth–death model is derived based on rigid mathematics. The analytical prediction of the birth–death model completely agrees with the real stochastic processes under different thermal histories. In addition, the model can be applied to real experiments of Young’s modulus measurements. Using the model, I discussed the effects of the mixing rules on the effective relaxation time, and the distribution of elastic modulus at small scales.

Chapter 8 Conclusions and future works

In this thesis, glass relaxation was systematically and comprehensively investigated using experimental and theoretical inspections. Using the non-destructive IET, new phenomena of glass relaxation were found and then understood with both phenomenological and physical ideas. In this chapter, the main conclusions of the thesis are summarized, and the deliberate consideration of future works are discussed.

8.1 Conclusions

(1) The primary (α) relaxations of borosilicate and chalcogenide glasses were revealed using IET experiments. In the temperature-dependent measurements, the glass transition point (T_g) determined from Young's modulus was found to be close to that determined by the viscosity of borosilicate glasses. A non-destructive and instantaneous viscosity measurement method for borosilicate glasses was proposed for glasses with little non-exponentiality, which can be explained by the implicit features of the Burgers model as well as a newly proposed minimal model considering the solid-like to liquid-like behavior transition. A striking non-exponential relaxation was found in chalcogenide glass with the help of the Cole–Davidson (CD) function. This suggests a new method of determining the non-exponentiality in the glass.

(2) To describe the mechanical α and β relaxation in glassy materials, a viscoelastic model is established based on the normal mode analysis of the potential energy landscape, and the prediction of an apparent double-peak phenomenon in the Fourier spectrum has been validated by a ma-fluorosilicate glass beam. This suggests a new mechanism of secondary (β) mechanical relaxation and a new method of probing

β relaxation. The β relaxation in S-FSL5 was systematically investigated, and a negative temperature-dependent relaxation frequency was found, which can be explained based on the picture of fragmented oxide-network patches in liquid-like regions.

(3) The long-debated Kovacs' paradox associated with the nature of glass transition was investigated by monitoring the relaxation of Young's modulus of chalcogenide glass (As_2Se_3) in two-step aging experiments. The effective relaxation time at the quasi-equilibrium state is found to be dependent on the thermal history, which confirms the paradox in inorganic glass for the first time. An elasticity-based relaxation model was proposed to explain the relationship behavior, and the effects of thermal history were found to be related to the local survival parts of glass. Based on the MT analysis, the volume fraction of survival parts are found to experience a non-zero to zero transition around T_g .

(4) Finally, a birth–death model was proposed to reveal the coupling effects between elastic modulus relaxation and local heterogeneity. An analytical solution at arbitrary thermal histories was obtained. This model is available to capture the normal and anomalous relaxation of different glasses. After analysis of the scaling law of elastic modulus at small scales, the bulk modulus is found to be Gaussian, while the shear and Young's moduli are non-Gaussian owing to the difference in the mixing rules.

Overall, this thesis provides new phenomena and understanding of glass transition and relaxation. The methods used and the new findings should not only benefit industrial communities but also promote the understanding of glassy states.

8.2 Future works

8.2.1 Probing elasticity relaxation of glass by the birth–death model

Understanding the nature of structural glass transition has been a long journey for the glass research community. The relaxation of elasticity could be a new paradigm to this problem as the former is more sensitive to structural and dynamical heterogeneities in glass because of the nature of two-time autocorrelation [234, 235]. It is expected that either α or β relaxation can benefit from monitoring Young's modulus. In the loss modulus plot of a DMA spectrum at temperature scan, α relaxation generally corresponds to the main relaxation peak near T_g , relating to the main structural relaxation; β relaxation corresponds to the peak lower than T_g , relating to the local structural relaxations in a cage. Local α relaxations are generally found in amorphous materials with multiphase whose DMA spectrum contains several α relaxations [269]. However, these frequency peaks are dependent on the used frequency for scanning and bring uncertainty to some degree. While the instantaneous elasticity obtained from IET is hardly affected by the frequency of samples, thus can be considered as a more unique index of glass relaxations.

Elasticity relaxation also directly benefits the demands of the glass manufactory industry where the viscoelastic behavior of glass is needed in PGM. Therefore, a possible direction for future investigations is continually probing glass transition and relaxation through monitoring elastic modulus.

In Chapter 6, it was found that elasticity relaxation can probe the ergodicity breaking of glass after aging. This suggests a question of whether the glass transition is a critical phenomenon. It is thus necessary to interrogate whether the memory persistence below a glass transition point is universal by examining the elasticity

relaxation of other structural glasses. In Chapter 7, a simple birth–death model was established and proved to be adaptable to predict the relaxation behavior of elasticity and the microscopic distribution of elastic modulus. With more efforts, the birth–death model can be transformed into a random-walk model to reveal the weak ergodicity breaking as suggested in previous works [270].

The proposed birth–death model in Chapter 7 is mean-field, while the cooperative interactions between different parts of glass cannot be ignored in some situations. In previous studies, some additional parameters were introduced into mean-field theories, for example, the cooperative frequency in the coupling model [120], or the partition parameter x in Narayanaswamy’s relaxation function [108]. It will be noteworthy if the spatial interactions between different glass sub-systems can be directly investigated. Motivated by the distinguishable-particle lattice model [250], one possible development is to conduct simulations on a 2D or 3D configuration where every subsystem may transform among different states while they are affected by each other. This model will be similar to MD simulations but at a larger scale, rendering it possible to predict the long-time behavior of the elasticity relaxation. It would help to unveil how spatial constraints can lead to the observed memory effect and glass transition.

8.2.2 Mechanisms and applications of the rate-dependent viscosity of chalcogenide glasses

Chalcogenide glasses have very broad applications in infrared optics (e.g., thermal imaging, optical switches, etc. [22, 238, 271-273]). The chalcogenide products larger than $500\ \mu\text{m}$ can be manufactured by PGM. In recent years, the chalcogenide products

having micro/nano scale surface features are increasingly demanded [274]. These micro/nano scale surface features can be made by the direct imprint technique (DIT) [275]. Both PGM and DIT meet the ambivalent effects of temperature during molding. When the temperature is high, the chalcogenide glass is unstable and may oxidize, gasify or adhere to a mold surface; while when the temperature is low, the material has a high viscosity that may lead to insufficient deformations, excessive residual stresses, or fracture.

A possible approach to solve the dilemma is making use of the non-Newtonian performance of chalcogenide glasses. For example, experiments have shown that the viscosity of $\text{As}_x\text{Se}_{1-x}$ dramatically decreases when the shear rate is higher than 10^3 s^{-1} [274]. Similar non-Newtonian viscosity can also be found in other chalcogenide glass systems such as $\text{Ge}_x\text{Se}_{1-x}$ [276] and $\text{Ge}_3\text{As}_{52}\text{S}_{45}$ [277]. Therefore, the application of rate-dependent viscosity could reduce the molding temperature and maintain a required fluidity.

However, the non-Newtonian behavior in chalcogenide glasses can only be found in a few works of literature; the mechanisms and the approaches of exploitation need more explorations. A new technology of ‘impact print-type hot embossing process’ [278] may help to generate the high shear rate, while it has not been applied to chalcogenide glasses. Another approach to generate sustained high shear rate in a molding process is to make use of ultrasonic vibration. Traditional molding techniques generally used the additional heat flux of ultrasonic vibration [279]; the rate-dependent behavior of chalcogenide glasses in an ultrasound-assisted molding has not been investigated. Due to the significant and foreseeable applications of chalcogenide glasses, it is worth a

further investigation of the mechanism and the theoretical description of the rate-dependent behavior in them to develop a specific precision molding technology with a high yield.

References

- [1] W.S. Ishak, Glass-Based Optics For the Connected World, in: 2019 24th Microoptics Conference (MOC), 2019, pp. 26-27.
- [2] P. Fernandez, "Through the Looking Glass" The Infrastructure of Information, Library Hi Tech News, (2019).
- [3] M.J. Gorman, A Transparent Foundation?, *Science*, 298 (2002) 970-971.
- [4] T.C. Kriss, V.M. Kriss, History of the operating microscope: from magnifying glass to microneurosurgery, *Neurosurgery*, 42 (1998) 899-907.
- [5] J.C. Mauro, E.D. Zanotto, Two centuries of glass research: historical trends, current status, and grand challenges for the future, *International Journal of Applied Glass Science*, 5 (2014) 313-327.
- [6] D. Kennedy, C. Norman, What don't we know?, *Science*, 309 (2005) 75-75.
- [7] D.L. Anderson, Through the glass lightly, *Science*, 267 (1995) 1618-1618.
- [8] (!!! INVALID CITATION !!!).
- [9] K. Rao, *Structural chemistry of glasses*, Elsevier, 2002.
- [10] S.N. Sen, M. Chaudhuri, *Ancient glass and India*, Indian National Science Academy, 1985.
- [11] E. Fourcault, Apparatus for the manufacture of plate-glass by stretching, in, Google Patents, 1902.
- [12] I.W. Colburn, E. Washburn, Process and apparatus for the continuous production of sheet-glass, in, Google Patents, 1908.
- [13] L.A.B. Pilkington, Review lecture. the float glass process, *Proceedings of the Royal Society of London. Series A, Mathematical and Physical Sciences*, 314 (1969) 1-25.
- [14] A. Makishima, T. Tani, Preparation of Amorphous Silicas Doped with Organic Molecules by the Sol - Gel Process, *Journal of the American Ceramic Society*, 69 (1986).
- [15] A. Macfarlane, G. Martin, *Glass: a world history*, University of Chicago Press, 2002.
- [16] A. Neri, *L'arte vetraria*, Batti, 1679.
- [17] C.R. Kurkjian, W.R. Prindle, Perspectives on the history of glass composition, *Journal of the American Ceramic Society*, 81 (1998) 795-813.
- [18] L. Zhang, W. Liu, Precision glass molding: Toward an optimal fabrication of optical lenses, *Frontiers of Mechanical Engineering*, (2017) 1-15.
- [19] Y. Aono, M. Negishi, J. Takano, Development of large-aperture aspherical lens with glass molding, in: *Advanced Optical Manufacturing and Testing Technology 2000*, International Society for Optics and Photonics, 2000, pp. 16-24.
- [20] A.Y. Yi, A. Jain, Compression molding of aspherical glass lenses—a combined experimental and numerical analysis, *Journal of the American Ceramic Society*, 88 (2005) 579-586.
- [21] W. Liu, L. Zhang, Thermoforming mechanism of precision glass moulding, *Applied Optics*, 54 (2015) 6841-6849.
- [22] D.H. Cha, H.-J. Kim, H.S. Park, Y. Hwang, J.-H. Kim, J.-H. Hong, K.-S. Lee, Effect of temperature on the molding of chalcogenide glass lenses for infrared imaging applications, *Applied Optics*, 49 (2010) 1607-1613.
- [23] C. Springer, A. Hasanbeigi, Emerging energy efficiency and carbon dioxide emissions-reduction technologies for the glass industry, (2017).
- [24] X. Zhang, Y. Guimond, Y. Bellec, Production of complex chalcogenide glass optics by molding for thermal imaging, *Journal of Non-Crystalline Solids*, 326 (2003) 519-523.

- [25] M. Bertozzi, A. Broggi, C. Caraffi, M. Del Rose, M. Felisa, G. Vezzoni, Pedestrian detection by means of far-infrared stereo vision, *Computer vision and image understanding*, 106 (2007) 194-204.
- [26] A. Tverjanovich, Temperature dependence of the viscosity of chalcogenide glass-forming melts, *Glass Physics and Chemistry*, 29 (2003) 532-536.
- [27] P. Košťál, J. Šhánělová, J. Málek, Viscosity Measurements Applied to Chalcogenide Glass-Forming Systems, in: J. Šesták, J.J. Mareš, P. Hubík (Eds.) *Glassy, Amorphous and Nano-Crystalline Materials: Thermal Physics, Analysis, Structure and Properties*, Springer Netherlands, Dordrecht, 2011, pp. 165-178.
- [28] C.A. Angell, Formation of glasses from liquids and biopolymers, *Science*, 267 (1995) 1924-1935.
- [29] C.A. Angell, K.L. Ngai, G.B. McKenna, P.F. McMillan, S.W. Martin, Relaxation in glassforming liquids and amorphous solids, *Journal of Applied Physics*, 88 (2000) 3113-3157.
- [30] E.D. Zanotto, Do cathedral glasses flow?, *American Journal of Physics*, 66 (1998) 392-395.
- [31] L. Berthier, G. Biroli, Theoretical perspective on the glass transition and amorphous materials, *Reviews of Modern Physics*, 83 (2011) 587.
- [32] R. Zallen, *The physics of amorphous solids*, John Wiley & Sons, 2008.
- [33] W.H. Zachariasen, The atomic arrangement in glass, *Journal of the American Chemical Society*, 54 (1932) 3841-3851.
- [34] A. Cavagna, Supercooled liquids for pedestrians, *Physics Reports*, 476 (2009) 51-124.
- [35] E.D. Zanotto, J.C. Mauro, The glassy state of matter: Its definition and ultimate fate, *Journal of Non-Crystalline Solids*, 471 (2017) 490-495.
- [36] B.D. Coleman, Thermodynamics of materials with memory, *Archive for Rational Mechanics and Analysis*, 17 (1964) 1-46.
- [37] A. Samarakoon, T.J. Sato, T. Chen, G.-W. Chern, J. Yang, I. Klich, R. Sinclair, H. Zhou, S.-H. Lee, Aging, memory, and nonhierarchical energy landscape of spin jam, *Proceedings of the National Academy of Sciences*, 113 (2016) 11806-11810.
- [38] A.J. Kovacs, Transition vitreuse dans les polymères amorphes. Etude phénoménologique, in: *Fortschritte der hochpolymeren-forschung*, Springer, 1964, pp. 394-507.
- [39] R. Rendell, J. Aklonis, K. Ngai, G. Fong, Volume recovery near the glass transition temperature in poly (vinyl acetate): predictions of a coupling model, *Macromolecules*, 20 (1987) 1070-1083.
- [40] G. McKenna, M. Vangel, A.L. Rukhin, S.D. Leigh, B. Lotz, C. Straupe, The τ -effective paradox revisited: an extended analysis of Kovacs' volume recovery data on poly (vinyl acetate), *Polymer*, 40 (1999) 5183-5205.
- [41] L. Struik, Volume-recovery theory: I. Kovacs' τ_{eff} paradox, *Polymer*, 38 (1997) 4677-4685.
- [42] Q. Wang, J. Liu, Y. Ye, T. Liu, S. Wang, C. Liu, J. Lu, Y. Yang, Universal secondary relaxation and unusual brittle-to-ductile transition in metallic glasses, *Materials Today*, 20 (2017) 293-300.
- [43] L. Hu, Y. Yue, Secondary relaxation in metallic glass formers: its correlation with the genuine johari-goldstein relaxation, *The Journal of Physical Chemistry C*, 113 (2009) 15001-15006.
- [44] M. Vogel, P. Medick, E. Rössler, Secondary relaxation processes in molecular glasses studied by nuclear magnetic resonance spectroscopy, in: *Annual Reports on NMR Spectroscopy*, Elsevier, 2005, pp. 231-299.
- [45] A. Wisitsorasak, P.G. Wolynes, Dynamical heterogeneity of the glassy state, *The Journal of Physical Chemistry B*, 118 (2014) 7835-7847.
- [46] K.S. Schweizer, E.J. Saltzman, Activated hopping, barrier fluctuations, and heterogeneity in glassy suspensions and liquids, *Journal of Physical Chemistry B*, 108 (2004) 19729-19741.

- [47] W. Dmowski, T. Iwashita, C.-P. Chuang, J. Almer, T. Egami, Elastic heterogeneity in metallic glasses, *Physical Review Letters*, 105 (2010) 205502.
- [48] H. Ke, J. Zeng, C. Liu, Y. Yang, Structure heterogeneity in metallic glass: Modeling and experiment, *Journal of Materials Science & Technology*, 30 (2014) 560-565.
- [49] H. Sillescu, Heterogeneity at the glass transition: a review, *Journal of Non-Crystalline Solids*, 243 (1999) 81-108.
- [50] P.G. Debenedetti, F.H. Stillinger, Supercooled liquids and the glass transition, *Nature*, 410 (2001) 259-267.
- [51] J. Prins, *Physics of non-crystalline solids*, North-Holland Publishing Company, 1965.
- [52] E. Donth, *The glass transition: relaxation dynamics in liquids and disordered materials*, Springer Science & Business Media, 2013.
- [53] T.E.o.E. Britannica, Glass, in: *Encyclopædia Britannica*, Encyclopædia Britannica, inc, 2019.
- [54] J. Forrest, K. Dalnoki-Veress, J. Stevens, J. Dutcher, Effect of free surfaces on the glass transition temperature of thin polymer films, *Physical Review Letters*, 77 (1996) 2002-2005.
- [55] K. Nakazawa, Recrystallization of amorphous silicon films deposited by low - pressure chemical vapor deposition from Si₂H₆ gas, *Journal of Applied Physics*, 69 (1991) 1703-1706.
- [56] J. Willart, A. De Gusseme, S. Hemon, G. Odou, F. Danede, M. Descamps, Direct crystal to glass transformation of trehalose induced by ball milling, *Solid State Communications*, 119 (2001) 501-505.
- [57] C. Ban, M. Xie, X. Sun, J.J. Travis, G. Wang, H. Sun, A.C. Dillon, J. Lian, S.M. George, Atomic layer deposition of amorphous TiO₂ on graphene as an anode for Li-ion batteries, *Nanotechnology*, 24 (2013) 424002.
- [58] S. Bassnett, Y. Shi, G.F. Vrensen, Biological glass: structural determinants of eye lens transparency, *Philosophical Transactions of the Royal Society B: Biological Sciences*, 366 (2011) 1250-1264.
- [59] D. Bi, X. Yang, M.C. Marchetti, M.L. Manning, Motility-driven glass and jamming transitions in biological tissues, *Physical Review X*, 6 (2016) 021011.
- [60] J. Aizenberg, V.C. Sundar, A.D. Yablon, J.C. Weaver, G. Chen, Biological glass fibers: correlation between optical and structural properties, *Proceedings of the National Academy of Sciences of the United States of America*, 101 (2004) 3358-3363.
- [61] M. Bernaschi, A. Billoire, A. Maiorano, G. Parisi, F. Ricci-Tersenghi, Strong ergodicity breaking in aging of mean field spin glasses, *arXiv preprint arXiv:1906.11195*, (2019).
- [62] K. Biljaković, J. Lasjaunias, P. Monceau, F. Levy, Towards equilibrium ground state in charge-density-wave systems, *Physical Review Letters*, 67 (1991) 1902.
- [63] E.M. Mozur, A.E. Maughan, Y. Cheng, A. Huq, N. Jalarvo, L.L. Daemen, J.R. Neilson, Orientational Glass Formation in Substituted Hybrid Perovskites, *Chemistry of Materials*, 29 (2017) 10168-10177.
- [64] A. Larkin, V. Vinokur, Bose and vortex glasses in high temperature superconductors, *Physical Review Letters*, 75 (1995) 4666.
- [65] G.A. Medvedev, A.B. Starry, D. Ramkrishna, J.M. Caruthers, Stochastic model for volume relaxation in glass forming materials: Local specific volume model, *Macromolecules*, 45 (2012) 7237-7259.
- [66] M. Yang, X. Liu, H. Ruan, Y. Wu, H. Wang, Z. Lu, High thermal stability and sluggish crystallization kinetics of high-entropy bulk metallic glasses, *Journal of Applied Physics*, 119 (2016) 245112.
- [67] S. Wemple, Refractive-index behavior of amorphous semiconductors and glasses, *Physical Review B*, 7 (1973) 3767.
- [68] W. Liu, H. Ruan, L. Zhang, Revealing Structural Relaxation of Optical Glass Through the

- Temperature Dependence of Young's Modulus, *Journal of the American Ceramic Society*, 97 (2014) 3475-3482.
- [69] E. Le Bourhis, P. Gadaud, J.-P. Guin, N. Tournerie, X. Zhang, J. Lucas, T. Rouxel, Temperature dependence of the mechanical behavior of a GeAsSe glass, *Scripta Materialia*, 45 (2001) 317-323.
- [70] A.M. Glass, Investigation of the electrical properties of $\text{Sr}_{1-x}\text{Ba}_x\text{Nb}_2\text{O}_6$ with special reference to pyroelectric detection, *Journal of Applied Physics*, 40 (1969) 4699-4713.
- [71] A. Wright, A. Leadbetter, Diffraction studies of glass structure, *Physics and Chemistry of Glasses*, 17 (1976) 122-145.
- [72] J. Wong, C.A. Angell, *Glass: structure by spectroscopy*, M. Dekker New York, 1976.
- [73] A. Renninger, M. Reichtin, B. Averbach, Monte Carlo models of atomic arrangements in arsenic-selenium glasses, *Journal of Non-Crystalline Solids*, 16 (1974) 1-14.
- [74] J.C. Mauro, A.K. Varshneya, Multiscale modeling of arsenic selenide glass, *Journal of Non-Crystalline Solids*, 353 (2007) 1226-1231.
- [75] T. Rouxel, Elastic properties of glasses: a multiscale approach, *Comptes Rendus Mecanique*, 334 (2006) 743-753.
- [76] J.C. Phillips, Topology of covalent non-crystalline solids I: Short-range order in chalcogenide alloys, *Journal of Non-Crystalline Solids*, 34 (1979) 153-181.
- [77] J.E. Shelby JR, D.E. Day, Mechanical Relaxations in Mixed - Alkali Silicate Glasses: I, Results, *Journal of the American Ceramic Society*, 52 (1969) 169-173.
- [78] K. Ngai, M. Paluch, Classification of secondary relaxation in glass-formers based on dynamic properties, *The Journal of Chemical Physics*, 120 (2004) 857-873.
- [79] J. Bucaro, H. Dardy, High-temperature strain relaxation in silica by optical correlation spectroscopy, *Journal of Non-Crystalline Solids*, 24 (1977) 121-129.
- [80] A. Napolitano, P. Macedo, Spectrum of relaxation times in GeO_2 glass, *Journal of Research of the National Bureau of Standards. Section A, Physics and Chemistry*, 72 (1968) 425.
- [81] T. Shimada, T. Matsuo, H. Suga, F. Luty, Phase transition and glass transition in rubidium cyanide, *The Journal of Chemical Physics*, 85 (1986) 3530-3536.
- [82] R. Böhmer, K. Ngai, C.A. Angell, D. Plazek, Nonexponential relaxations in strong and fragile glass formers, *The Journal of Chemical Physics*, 99 (1993) 4201-4209.
- [83] G. Williams, D.C. Watts, Non-symmetrical dielectric relaxation behavior arising from a simple empirical decay function, *Transactions of the Faraday Society*, 66 (1970) 80-85.
- [84] J.D. Ferry, *Viscoelastic properties of polymers*, John Wiley & Sons, 1980.
- [85] M.L. Williams, R.F. Landel, J.D. Ferry, The temperature dependence of relaxation mechanisms in amorphous polymers and other glass-forming liquids, *Journal of the American Chemical Society*, 77 (1955) 3701-3707.
- [86] S. Arrhenius, Über die Reaktionsgeschwindigkeit bei der Inversion von Rohrzucker durch Säuren, *Zeitschrift für Physikalische Chemie*, 4 (1889) 226-248.
- [87] A.K. Varshneya, *Fundamentals of inorganic glasses*, Academic Press, INC, New York, 1994.
- [88] C. Walther, Ueber die Auswertung von Viskositätsangaben, *Erdöl und Teer*, 7 (1931) 382-384.
- [89] J.C. Maxwell, IV. on the dynamical theory of gases, *Philosophical Transactions of the Royal Society of London*, (1867) 49-88.
- [90] J.C. Dyre, N.B. Olsen, T. Christensen, Local elastic expansion model for viscous-flow activation energies of glass-forming molecular liquids, *Physical Review B*, 53 (1996) 2171.
- [91] M.D. Ediger, C. Angell, S.R. Nagel, Supercooled liquids and glasses, *The journal of physical*

- chemistry, 100 (1996) 13200-13212.
- [92] C.A. Angell, Perspective on the glass transition, *Journal of Physics and Chemistry of Solids*, 49 (1988) 863-871.
- [93] N. Mauro, M. Blodgett, M. Johnson, A. Vogt, K. Kelton, A structural signature of liquid fragility, *Nature Communications*, 5 (2014) 1-7.
- [94] Y. Yue, The iso-structural viscosity, configurational entropy and fragility of oxide liquids, *Journal of Non-Crystalline Solids*, 355 (2009) 737-744.
- [95] J.H. Gibbs, E.A. DiMarzio, Nature of the glass transition and the glassy state, *The Journal of Chemical Physics*, 28 (1958) 373-383.
- [96] G. Adam, J.H. Gibbs, On the temperature dependence of cooperative relaxation properties in glass-forming liquids, *The Journal of Chemical Physics*, 43 (1965) 139-146.
- [97] S. Edwards, Theory of glasses, *Polymer*, 17 (1976) 933-937.
- [98] M.H. Cohen, D. Turnbull, Molecular transport in liquids and glasses, *The Journal of Chemical Physics*, 31 (1959) 1164-1169.
- [99] G.S. Grest, M.H. Cohen, Liquids, glasses, and the glass transition: A free-volume approach, *Adv. Chem. Phys.*, 48 (1981) 455-525.
- [100] A.K. Doolittle, Studies in Newtonian flow. II. The dependence of the viscosity of liquids on free-space, *Journal of Applied Physics*, 22 (1951) 1471-1475.
- [101] J.C. Dyre, Colloquium: The glass transition and elastic models of glass-forming liquids, *Reviews of Modern Physics Supplement*, 78 (2006) 953.
- [102] J.-P. Bouchaud, Weak ergodicity breaking and aging in disordered systems, *Journal de Physique I*, 2 (1992) 1705-1713.
- [103] G. Diezemann, Aging in a free-energy landscape model for glassy relaxation, *The Journal of Chemical Physics*, 123 (2005) 204510.
- [104] A. Tobolsky, R.E. Powell, H. Eyring, Elastic-viscous properties of matter, *Frontiers in chemistry*, 1 (1943) 125-190.
- [105] M. Mooney, A theory of the viscosity of a Maxwellian elastic liquid, *Transactions of the Society of Rheology*, 1 (1957) 63-94.
- [106] J.C. Dyre, Source of non-Arrhenius average relaxation time in glass-forming liquids, *Journal of Non-Crystalline Solids*, 235 (1998) 142-149.
- [107] A.Q. Tool, Relation between inelastic deformability and thermal expansion of glass in its annealing range, *Journal of the American Ceramic Society*, 29 (1946) 240-253.
- [108] O. Narayanaswamy, A model of structural relaxation in glass, *Journal of the American Ceramic Society*, 54 (1971) 491-498.
- [109] C.T. Moynihan, A.J. Eastal, J. Wilder, J. Tucker, Dependence of the glass transition temperature on heating and cooling rate, *The Journal of Chemical Physics*, 78 (1974) 2673-2677.
- [110] A.J. Kovacs, J.J. Aklonis, J.M. Hutchinson, A.R. Ramos, Isobaric volume and enthalpy recovery of glasses. II. A transparent multiparameter theory, *Journal of Polymer Science Part B: Polymer Physics*, 17 (1979) 1097-1162.
- [111] L. Grassia, S.L. Simon, Modeling volume relaxation of amorphous polymers: modification of the equation for the relaxation time in the KAHR model, *Polymer*, 53 (2012) 3613-3620.
- [112] W. Ganze, *Complex dynamics of glass-forming liquids: A mode-coupling theory*, OUP Oxford Press, New York, 2008.
- [113] D.R. Reichman, P. Charbonneau, Mode-coupling theory, *Journal of Statistical Mechanics: Theory*

- and Experiment, 2005 (2005) P05013.
- [114] H. Cummins, The liquid-glass transition: a mode-coupling perspective, *Journal of Physics: Condensed Matter*, 11 (1999) A95.
- [115] A.C. Hanna, A Review of Liquid-Glass Transitions, (2006).
- [116] L. Janssen, Mode-coupling theory of the glass transition: A primer, *Frontiers in Physics*, 6 (2018) 97.
- [117] C. Roland, K. Ngai, Short time dynamics of glass - forming liquids, *The Journal of Chemical Physics*, 103 (1995) 1152-1159.
- [118] K. Ngai, Universal properties of relaxation and diffusion in condensed matter, *Chinese Physics B*, 26 (2017) 018105.
- [119] K. Ngai, Universality of low-frequency fluctuation, dissipation and relaxation properties of condensed matter. I, *Comments on Solid State Physics*, 9 (1979) 127-140.
- [120] K. Ngai, R. Rendell, Cooperative dynamics in relaxation: A coupling model perspective, *Journal of Molecular Liquids*, 56 (1993) 199-214.
- [121] A. Heuer, Exploring the potential energy landscape of glass-forming systems: from inherent structures via metabasins to macroscopic transport, *Journal of Physics: Condensed Matter*, 20 (2008) 373101.
- [122] G. Biroli, J.-P. Bouchaud, The random first-order transition theory of glasses: a critical assessment, *Structural Glasses and Supercooled Liquids: Theory, Experiment, and Applications*, (2012) 31-113.
- [123] G. Tarjus, S.A. Kivelson, Z. Nussinov, P. Viot, The frustration-based approach of supercooled liquids and the glass transition: a review and critical assessment, *Journal of Physics: Condensed Matter*, 17 (2005) R1143.
- [124] P.W. Anderson, B. Halperin, C.M. Varma, Anomalous low-temperature thermal properties of glasses and spin glasses, *Philosophical Magazine*, 25 (1972) 1-9.
- [125] P. Esquinazi, *Tunneling systems in amorphous and crystalline solids*, Springer Science & Business Media, 2013.
- [126] G. Aquino, A. Allahverdyan, T.M. Nieuwenhuizen, Memory effects in the two-level model for glasses, *Physical Review Letters*, 101 (2008) 015901.
- [127] K. Topp, D.G. Cahill, Elastic properties of several amorphous solids and disordered crystals below 100 K, *Zeitschrift für Physik B Condensed Matter*, 101 (1996) 235-245.
- [128] D. Tielbörger, R. Merz, R. Ehrenfels, S. Hunklinger, Thermally activated relaxation processes in vitreous silica: An investigation by Brillouin scattering at high pressures, *Physical Review B*, 45 (1992) 2750.
- [129] J. Classen, T. Burkert, C. Enss, S. Hunklinger, Beyond the tunneling model—Elastic properties of vitreous silica at low temperatures, *Advances in Solid State Physics* 40, (2000) 279-291.
- [130] S. Sahling, M. Koláč, V. Katkov, V. Osipov, Anomalous Tunneling Systems in Amorphous Organic Materials, *Journal of Low Temperature Physics*, 176 (2014) 64-81.
- [131] J.C. Dyre, Master-equation approach to the glass transition, *Physical Review Letters*, 58 (1987) 792.
- [132] J.C. Dyre, Energy master equation: A low-temperature approximation to bässler's random-walk model, *Physical Review B*, 51 (1995) 12276.
- [133] A. Prados, J. Brey, The Kovacs effect: a master equation analysis, *Journal of Statistical Mechanics: Theory and Experiment*, 2010 (2010) P02009.
- [134] H. Ruan, L. Zhang, A Monte - Carlo Approach for Modeling Glass Transition, *Journal of the American Ceramic Society*, 94 (2011) 3350-3358.

- [135] R.E. Robertson, R. Simha, J.G. Curro, Free volume and the kinetics of aging of polymer glasses, *Macromolecules*, 17 (1984) 911-919.
- [136] B.D. Coleman, W. Noll, Foundations of linear viscoelasticity, *Reviews of Modern Physics Supplement*, 33 (1961) 239.
- [137] S.R. Lustig, R.M. Shay Jr, J.M. Caruthers, Thermodynamic constitutive equations for materials with memory on a material time scale, *Journal of Rheology*, 40 (1998) 69.
- [138] J.M. Caruthers, D.B. Adolf, R.S. Chambers, P. Shrikhande, A thermodynamically consistent, nonlinear viscoelastic approach for modeling glassy polymers, *Polymer*, 45 (2004) 4577-4597.
- [139] G.A. Medvedev, J.M. Caruthers, Development of a stochastic constitutive model for prediction of postyield softening in glassy polymers, *Journal of Rheology*, 57 (2013) 949-1002.
- [140] D.S. Brauer, C. Rüssel, J. Kraft, Solubility of glasses in the system P2O5–CaO–MgO–Na2O–TiO2: Experimental and modeling using artificial neural networks, *Journal of Non-Crystalline Solids*, 353 (2007) 263-270.
- [141] Y. Sun, H. Bai, M. Li, W. Wang, Machine learning approach for prediction and understanding of glass-forming ability, *The journal of physical chemistry letters*, 8 (2017) 3434-3439.
- [142] D.R. Cassar, A.C. de Carvalho, E.D. Zanotto, Predicting glass transition temperatures using neural networks, *Acta Materialia*, 159 (2018) 249-256.
- [143] E. Alcobaça, S.M. Mastelini, T. Botari, B.A. Pimentel, D.R. Cassar, A.C.P. de Leon Ferreira, E.D. Zanotto, Explainable Machine Learning Algorithms For Predicting Glass Transition Temperatures, *Acta Materialia*, 188 (2020) 92-100.
- [144] K. Yang, X. Xu, B. Yang, B. Cook, H. Ramos, N.A. Krishnan, M.M. Smedskjaer, C. Hoover, M. Bauchy, Predicting the Young's Modulus of silicate Glasses using High-throughput Molecular Dynamics simulations and Machine Learning, *Scientific reports*, 9 (2019) 1-11.
- [145] D. Richard, M. Ozawa, S. Patinet, E. Stanifer, B. Shang, S. Ridout, B. Xu, G. Zhang, P. Morse, J.-L. Barrat, Predicting plasticity in disordered solids from structural indicators, *arXiv preprint arXiv:2003.11629*, (2020).
- [146] S.S. Schoenholz, E.D. Cubuk, D.M. Sussman, E. Kaxiras, A.J. Liu, A structural approach to relaxation in glassy liquids, *Nature Physics*, 12 (2016) 469-471.
- [147] R.J. Ivancic, R.A. Riggelman, Identifying structural signatures of shear banding in model polymer nanopillars, *Soft Matter*, 15 (2019) 4548-4561.
- [148] V. Bapst, T. Keck, A. Grabska-Barwińska, C. Donner, E.D. Cubuk, S. Schoenholz, A. Obika, A. Nelson, T. Back, D. Hassabis, Unveiling the predictive power of static structure in glassy systems, *Nature Physics*, 16 (2020) 448-454.
- [149] G. Biroli, Machine learning glasses, *Nature Physics*, 16 (2020) 373-374.
- [150] G. Roebben, B. Bollen, A. Brebels, J. Van Humbeeck, O. Van der Biest, Impulse excitation apparatus to measure resonant frequencies, elastic moduli, and internal friction at room and high temperature, *Review of Scientific Instruments*, 68 (1997) 4511-4515.
- [151] F. Förster, Ein neues Messverfahren zur Bestimmung des Elastizitätsmoduls und der Dämpfung, *Zeitschrift für Metallkunde*, 29 (1937) N2.
- [152] E. ASTM, Standard test method for dynamic Young's modulus, shear modulus, and Poisson's ratio by sonic resonance, in: *Annual Book of ASTM Standards*, 1875.
- [153] ISO, Methods of test for refractory products — Part 1: Determination of dynamic Young's modulus (MOE) by impulse excitation of vibration, in, Geneva, Switzerland, 2005.
- [154] G. Pickett, Equations for computing elastic constants from flexural and torsional resonant

- frequencies of vibration of prisms and cylinders, in, 1945.
- [155] S. Spinner, A method for determining mechanical resonance frequencies and for calculation elastic moduli from these frequencies, in: Proc. ASTM, 1961, pp. 1221-1238.
- [156] K. Heritage, C. Frisby, A. Wolfenden, Impulse excitation technique for dynamic flexural measurements at moderate temperature, Review of Scientific Instruments, 59 (1988) 973-974.
- [157] G. Roebben, B. Basu, J. Vleugels, J. Van Humbeeck, O. Van der Biest, The innovative impulse excitation technique for high-temperature mechanical spectroscopy, Journal of Alloys and Compounds, 310 (2000) 284-287.
- [158] E. Gregorová, W. Pabst, P. Dobl, V. Nečina, Temperature dependence of damping in silica refractories measured via the impulse excitation technique, Ceramics International, 44 (2018) 8363-8373.
- [159] G. Roebben, B. Basu, J. Vleugels, O. Van der Biest, Transformation-induced damping behavior of Y-TZP zirconia ceramics, Journal of the European Ceramic Society, 23 (2003) 481-489.
- [160] S. Bossuyt, S. Giménez, J. Schroers, Resonant vibration analysis for temperature dependence of elastic properties of bulk metallic glass, Journal of Materials Research, 22 (2007) 533-537.
- [161] M. Yang, X. Liu, Y. Wu, H. Wang, J. Wang, H. Ruan, Z. Lu, Elastic modulus change and its relation with glass-forming ability and plasticity in bulk metallic glasses, Scripta Materialia, 161 (2019) 62-65.
- [162] A. Kursumovic, M. Scott, The use of Young's modulus to monitor relaxation in metallic glasses, Applied Physics Letters, 37 (1980) 620-622.
- [163] J. Wang, H. Ruan, X. Wang, J. Wan, Investigating relaxation of glassy materials based on natural vibration of beam: A comparative study of borosilicate and chalcogenide glasses, Journal of Non-Crystalline Solids, 500 (2018) 181-190.
- [164] S. Adhikari, Structural dynamic analysis with generalized damping models: analysis, John Wiley & Sons, 2013.
- [165] S. Adhikari, Structural dynamic analysis with generalized damping models: identification, John Wiley & Sons, 2013.
- [166] F. Mainardi, G. Spada, Creep, relaxation and viscosity properties for basic fractional models in rheology, The European Physical Journal Special Topics, 193 (2011) 133-160.
- [167] P. Oswald, Rheophysics: the deformation and flow of matter, Cambridge University Press, New York, 2009.
- [168] H. Kobayashi, Y. Hiki, H. Takahashi, An experimental study on the shear viscosity of solids, Journal of Applied Physics, 80 (1996) 122-130.
- [169] A. Gent, Theory of the parallel plate viscometer, British Journal of Applied Physics, 11 (1960) 85.
- [170] J.C. Mauro, D.C. Allan, M. Potuzak, Nonequilibrium viscosity of glass, Physical Review B, 80 (2009) 094204.
- [171] M. Sellier, C.E. Hann, N. Siedow, Identification of relaxation functions in glass by mean of a simple experiment, Journal of the American Ceramic Society, 90 (2007) 2980-2983.
- [172] C.T. Moynihan, A.J. Easteal, J. Wilder, J. Tucker, Dependence of the glass transition temperature on heating and cooling rate, The journal of physical chemistry, 78 (1974) 2673-2677.
- [173] P. Mezeix, F. Cđarić, P. Houizot, Y. Gueguen, F. Munoz, T. Rouxel, Elasticity and viscosity of BaOTiO₂SiO₂ glasses in the 0.9 to 1.2 Tg temperature interval, Journal of Non-Crystalline Solids, 445 (2016) 45-52.
- [174] T. Hecksher, D.H. Torchinsky, C. Klieber, J.A. Johnson, J.C. Dyre, K.A. Nelson, Toward broadband mechanical spectroscopy, Proceedings of the National Academy of Sciences, (2017) 201707251.

- [175] I. Pereira, Overview on Determination of Elastic and Damping Properties of Different Materials using Impulse Excitation Technique, *U. Porto Journal of Engineering*, 3 (2017) 35-41.
- [176] W. Liu, L. Zhang, K. Mylvaganam, Relaxation oscillation of borosilicate glasses in supercooled liquid region, *Scientific reports*, 7 (2017) 15872.
- [177] J. Yan, T. Zhou, J. Masuda, T. Kuriyagawa, Modeling high-temperature glass molding process by coupling heat transfer and viscous deformation analysis, *Precision Engineering*, 33 (2009) 150-159.
- [178] G.W. Scherer, *Relaxation in glass and composites*, (1986).
- [179] F.T. Trouton, On the coefficient of viscous traction and its relation to that of viscosity, *Proceedings of the Royal Society of London. Series A, Containing Papers of a Mathematical and Physical Character*, (1906) 426-440.
- [180] C. Bernard, G. Delaizir, J.-C. Sangleboeuf, V. Keryvin, P. Lucas, B. Bureau, X.-H. Zhang, T. Rouxel, Room temperature viscosity and delayed elasticity in infrared glass fiber, *Journal of the European Ceramic Society*, 27 (2007) 3253-3259.
- [181] C. Perez, V. Alvarez, A. Vazquez, Creep behavior of layered silicate/starch-polycaprolactone blends nanocomposites, *Materials Science and Engineering: A*, 480 (2008) 259-265.
- [182] T. Zhou, J. Yan, J. Masuda, T. Kuriyagawa, Investigation on the viscoelasticity of optical glass in ultraprecision lens molding process, *Journal of Materials Processing Technology*, 209 (2009) 4484-4489.
- [183] T. Zhou, Q. Zhou, J. Xie, X. Liu, X. Wang, H. Ruan, Elastic - viscoplasticity modeling of the thermo - mechanical behavior of chalcogenide glass for aspheric lens molding, *International Journal of Applied Glass Science*, 9 (2018) 252-262.
- [184] Y. Gueguen, J.-C. Sangleboeuf, V. Keryvin, T. Rouxel, E.A. King, E. Robin, G. Delaizir, B. Bureau, X.-H. Zhang, P. Lucas, Sub-Tg viscoelastic behavior of chalcogenide glasses, anomalous viscous flow and stress relaxation, *Journal of the Ceramic Society of Japan*, 116 (2008) 890-895.
- [185] T. Kirkpatrick, D. Thirumalai, P.G. Wolynes, Scaling concepts for the dynamics of viscous liquids near an ideal glassy state, *Physical Review A*, 40 (1989) 1045.
- [186] R. Kubo, Statistical-mechanical theory of irreversible processes. I. General theory and simple applications to magnetic and conduction problems, *Journal of the Physical Society of Japan*, 12 (1957) 570-586.
- [187] W. Gotze, L. Sjogren, Relaxation processes in supercooled liquids, *Reports on Progress in Physics*, 55 (1992) 241.
- [188] D.W. Davidson, R.H. Cole, Dielectric relaxation in glycerol, propylene glycol, and n - propanol, *The Journal of Chemical Physics*, 19 (1951) 1484-1490.
- [189] C. Lindsey, G. Patterson, Detailed comparison of the Williams-Watts and Cole-Davidson functions, *The Journal of Chemical Physics*, 73 (1980) 3348-3357.
- [190] R. Böhmer, C.A. Angell, Correlations of the nonexponentiality and state dependence of mechanical relaxations with bond connectivity in Ge-As-Se supercooled liquids, *Physical Review B*, 45 (1992) 10091.
- [191] U. Senapati, A.K. Varshneya, Viscosity of chalcogenide glass-forming liquids: an anomaly in the 'strong' and 'fragile' classification, *Journal of Non-Crystalline Solids*, 197 (1996) 210-218.
- [192] P. Li, Y. Zhang, Z. Chen, P. Gao, T. Wu, L.-M. Wang, Relaxation dynamics in the strong chalcogenide glass-former of Ge₂₂Se₇₈, *Scientific reports*, 7 (2017) 40547.
- [193] G.P. Johari, M. Goldstein, Viscous liquids and the glass transition. II. Secondary relaxations in glasses of rigid molecules, *The Journal of Chemical Physics*, 53 (1970) 2372-2388.
- [194] G.P. Johari, M. Goldstein, Viscous liquids and the glass transition. III. Secondary relaxations in

- aliphatic alcohols and other nonrigid molecules, *The Journal of Chemical Physics*, 55 (1971) 4245-4252.
- [195] M. Kiebel, E. Bartsch, O. Debus, F. Fujara, W. Petry, H. Sillescu, Secondary relaxation in the glass-transition regime of ortho-terphenyl observed by incoherent neutron scattering, *Physical Review B*, 45 (1992) 10301.
- [196] J.C. Dyre, N.B. Olsen, Minimal model for beta relaxation in viscous liquids, *Physical Review Letters*, 91 (2003) 155703.
- [197] B. Jakobsen, K. Niss, N.B. Olsen, Dielectric and shear mechanical alpha and beta relaxations in seven glass-forming liquids, *The Journal of Chemical Physics*, 123 (2005) 234511.
- [198] E. Muzeau, J. Perez, G. Johari, Mechanical spectrometry of the beta-relaxation in poly (methyl methacrylate), *Macromolecules*, 24 (1991) 4713-4723.
- [199] J.C. Qiao, Q. Wang, D. Crespo, Y. Yang, J.M. Pelletier, Amorphous physics and materials: Secondary relaxation and dynamic heterogeneity in metallic glasses: A brief review, *Chinese Physics B*, 26 (2017) 016402.
- [200] Y. Ryabov, A. Gutina, V. Arkhipov, Y. Feldman, Dielectric relaxation of water absorbed in porous glass, *The Journal of Physical Chemistry B*, 105 (2001) 1845-1850.
- [201] T. Ichitsubo, E. Matsubara, T. Yamamoto, H. Chen, N. Nishiyama, J. Saida, K. Anazawa, Microstructure of fragile metallic glasses inferred from ultrasound-accelerated crystallization in Pd-based metallic glasses, *Physical Review Letters*, 95 (2005) 245501.
- [202] E. Schlosser, A. Schönhals, Recent development in dielectric relaxation spectroscopy of polymers, *Colloid and Polymer Science*, 267 (1989) 963-969.
- [203] T. Blochowicz, E. Rössler, Beta relaxation versus high frequency wing in the dielectric spectra of a binary molecular glass former, *Physical Review Letters*, 92 (2004) 225701.
- [204] P. Lunkenheimer, A. Loidl, *Glassy Dynamics: From Millihertz to Terahertz*, in: F. Kremer, A. Loidl (Eds.) *The scaling of relaxation processes*, Springer, Cham, 2018, pp. 23-59.
- [205] K. Grzybowska, A. Grzybowski, M. Paluch, Role of defects in the nonmonotonic behavior of secondary relaxation of polypropylene glycols, *The Journal of Chemical Physics*, 128 (2008) 134904.
- [206] K. Grzybowska, A. Grzybowski, M. Paluch, Peculiar Behavior of the Secondary Dielectric Relaxation in Propylene Glycol Oligomers near the Glass Transition, in: *AIP Conference Proceedings*, AIP, 2008, pp. 70-73.
- [207] K. Ngai, S. Pawlus, K. Grzybowska, K. Kaminski, S. Capaccioli, M. Paluch, Does the Johari-Goldstein β -Relaxation Exist in Polypropylene Glycols?, *Macromolecules*, 48 (2015) 4151-4157.
- [208] G. Johari, Localized molecular motions of β -relaxation and its energy landscape, *Journal of Non-Crystalline Solids*, 307 (2002) 317-325.
- [209] V. Novikov, Vibration anharmonicity and fast relaxation in the region of the glass transition, *Physical Review B*, 58 (1998) 8367.
- [210] W. Liu, L. Zhang, Mechanisms of the Complex Thermo-Mechanical Behavior of Polymer Glass Across a Wide Range of Temperature Variations, *Polymers*, 10 (2018) 1153.
- [211] T. Keyes, Normal mode theory of two step relaxation in liquids: Polarizability dynamics in CS₂, *The Journal of Chemical Physics*, 104 (1996) 9349-9356.
- [212] T. Keyes, Instantaneous normal mode approach to liquid state dynamics, *The Journal of Physical Chemistry A*, 101 (1997) 2921-2930.
- [213] H. Ruan, L. Zhang, Modeling of Random Relaxation Paths of Amorphous Material, *Journal of the American Ceramic Society*, 96 (2013) 1772-1778.
- [214] M. Cho, G.R. Fleming, S. Saito, I. Ohmine, R.M. Stratt, Instantaneous normal mode analysis of

- liquid water, *The Journal of Chemical Physics*, 100 (1994) 6672-6683.
- [215] P. Moore, B. Space, An instantaneous normal mode theory of condensed phase absorption: The collision-induced absorption spectra of liquid CO₂, *The Journal of Chemical Physics*, 107 (1997) 5635-5644.
- [216] B. Jakobsen, K. Niss, C. Maggi, N.B. Olsen, T. Christensen, J.C. Dyre, Beta relaxation in the shear mechanics of viscous liquids: Phenomenology and network modeling of the alpha-beta merging region, *Journal of Non-Crystalline Solids*, 357 (2011) 267-273.
- [217] T. Hecksher, N.B. Olsen, J.C. Dyre, Model for the alpha and beta shear-mechanical properties of supercooled liquids and its comparison to squalane data, *The Journal of Chemical Physics*, 146 (2017) 154504.
- [218] M. Vladkov, J.L. Barrat, Linear and nonlinear viscoelasticity of a model unentangled polymer melt: molecular dynamics and rouse modes analysis, *Macromolecular Theory and Simulations*, 15 (2006) 252-262.
- [219] V. Agrawal, K. Holzworth, W. Nantasetphong, A.V. Amirkhizi, J. Oswald, S. Nemat - Nasser, Prediction of viscoelastic properties with coarse - grained molecular dynamics and experimental validation for a benchmark polyurea system, *Journal of Polymer Science Part B: Polymer Physics*, 54 (2016) 797-810.
- [220] C. Liu, E. Pineda, D. Crespo, Mechanical relaxation of metallic glasses: an overview of experimental data and theoretical models, *Metals*, 5 (2015) 1073-1111.
- [221] H.-B. Yu, K. Samwer, Y. Wu, W.H. Wang, Correlation between β relaxation and self-diffusion of the smallest constituting atoms in metallic glasses, *Physical Review Letters*, 109 (2012) 095508.
- [222] S. Nemilov, Relaxation processes in inorganic melts and glasses: An elastic continuum model as a promising basis for the description of the viscosity and electrical conductivity, *Glass Physics and Chemistry*, 36 (2010) 253-285.
- [223] E. Orowan, Creep in metallic and non-metallic materials, in: *Proceedings of the First US National Congress of Applied Mechanics*, ASME, 1952.
- [224] S. Kolla, S.L. Simon, The τ -effective paradox: new measurements towards a resolution, *Polymer*, 46 (2005) 733-739.
- [225] L. Lundgren, P. Nordblad, P. Svedlindh, O. Beckman, Towards equilibrium in spin glasses, *Journal of Applied Physics*, 57 (1985) 3371-3376.
- [226] H. Mamiya, M. Ohnuma, I. Nakatani, S. Nimori, T. Furubayashi, Non-vanishing hysteresis in a spin-glass, *Philosophical Magazine Letters*, 85 (2005) 109-114.
- [227] L.F. Cugliandolo, J. Kurchan, Analytical solution of the off-equilibrium dynamics of a long-range spin-glass model, *Physical Review Letters*, 71 (1993) 173.
- [228] T. Castellani, A. Cavagna, Spin-glass theory for pedestrians, *Journal of Statistical Mechanics: Theory and Experiment*, 2005 (2005) P05012.
- [229] C. Moynihan, International discussion meeting on relaxations in complex systems, in, Iraklion, Crete, 1990.
- [230] S. Rekhson, International discussion meeting on relaxations in complex systems, in, Iraklion, Crete, 1990.
- [231] C. Moynihan, International discussion meeting on relaxations in complex systems, in, Vigo, Spain, 1997.
- [232] M. Goldstein, M. Nakonecznyj, Volume relaxation in zinc chloride glass, *Physics and Chemistry of Glasses*, 6 (1965) 126.

- [233] J.S. Haggerty, Thermal expansion, heat capacity and structural relaxation measurements in the glass transition region, in, Massachusetts Institute of Technology, 1966.
- [234] M. Parrinello, A. Rahman, Strain fluctuations and elastic constants, *The Journal of Chemical Physics*, 76 (1982) 2662-2666.
- [235] J. Lutsko, Stress and elastic constants in anisotropic solids: molecular dynamics techniques, *Journal of Applied Physics*, 64 (1988) 1152-1154.
- [236] S. Franz, M. Mézard, G. Parisi, L. Peliti, Measuring equilibrium properties in aging systems, *Physical Review Letters*, 81 (1998) 1758.
- [237] J. Yu, H. Luo, Y. Zhang, T.V. Nguyen, X. Jiang, J. Hu, A comprehensive study on frictional dependence and predictive accuracy of viscoelastic model for optical glass using compression creep test, *Journal of the American Ceramic Society*, 102 (2019) 6606-6617.
- [238] T. Zhou, Z. Zhu, X. Liu, Z. Liang, X. Wang, A review of the precision glass molding of chalcogenide glass (ChG) for infrared optics, *Micromachines*, 9 (2018) 337.
- [239] Z. Zmrhalová, P. Pilný, R. Svoboda, J. Šhánělová, J. Málek, Thermal properties and viscous flow behavior of As₂Se₃ glass, *Journal of Alloys and Compounds*, 655 (2016) 220-228.
- [240] D.S. McWilliams, Study of the effect of thermal history on the structural relaxation and thermoviscoelasticity of amorphous polymers, in, 1997.
- [241] G.A. Medvedev, J.M. Caruthers, Predictions of Volume Relaxation in Glass Forming Materials Using a Stochastic Constitutive Model, *Macromolecules*, 48 (2015) 788-800.
- [242] R. Rendell, K. Ngai, D. Plazek, Volume-dependent rate processes predicted by the coupling model, *Journal of Non-Crystalline Solids*, 131 (1991) 442-450.
- [243] S. Glasstone, K.J. Laidler, H. Eyring, *The theory of rate processes*, McGraw-hill, 1941.
- [244] L.F. Cugliandolo, J. Kurchan, L. Peliti, Energy flow, partial equilibration, and effective temperatures in systems with slow dynamics, *Physical Review E*, 55 (1997) 3898.
- [245] A.S. Keys, J.P. Garrahan, D. Chandler, Calorimetric glass transition explained by hierarchical dynamic facilitation, *Proceedings of the National Academy of Sciences*, 110 (2013) 4482-4487.
- [246] S. Suzuki, T. Kobayashi, H. Ohno, S. Kamiya, Viscosity of Glasses in the Systems As-Se and As-Se-X(X Equals I, S) in the Transition Region, *J. Soc. Mat. Sci. Japan*, 22 (1973) 134-139.
- [247] G. Shen, G. Hu, *Mechanics of Composite Materials*, Tsinghua University Press, Beijing, China, 2006.
- [248] D.W. Henderson, D.G. Ast, Viscosity and crystallization kinetics of As₂Se₃, *Journal of Non-Crystalline Solids*, 64 (1984) 43-70.
- [249] Y. Wang, D. Wei, D. Han, J. Yang, M. Jiang, L. Dai, Does structure determine property in amorphous solids?, *Chinese Journal of Theoretical and Applied Mechanics*, 52 (2020) 303-317.
- [250] L.-H. Zhang, C.-H. Lam, Emergent facilitation behavior in a distinguishable-particle lattice model of glass, *Physical Review B*, 95 (2017) 184202.
- [251] M. Lulli, C.-S. Lee, H.-Y. Deng, C.-T. Yip, C.-H. Lam, Spatial heterogeneities in structural temperature cause Kovacs' expansion gap paradox in aging of glasses, *Physical Review Letters*, 124 (2020) 095501.
- [252] D. Turnbull, M.H. Cohen, Free - volume model of the amorphous phase: glass transition, *The Journal of Chemical Physics*, 34 (1961) 120-125.
- [253] G. Tammann, *Der Glasszustand* (Leopold Voss, Leipzig, 1933), Sec. IV, 12.
- [254] Y. Liu, D. Wang, K. Nakajima, W. Zhang, A. Hirata, T. Nishi, A. Inoue, M. Chen, Characterization of nanoscale mechanical heterogeneity in a metallic glass by dynamic force microscopy, *Physical Review*

- Letters, 106 (2011) 125504.
- [255] H. Mizuno, S. Mossa, J.-L. Barrat, Measuring spatial distribution of the local elastic modulus in glasses, *Physical Review E*, 87 (2013) 042306.
- [256] O. Yamamuro, I. Tsukushi, A. Lindqvist, S. Takahara, M. Ishikawa, T. Matsuo, Calorimetric study of glassy and liquid toluene and ethylbenzene: Thermodynamic approach to spatial heterogeneity in glass-forming molecular liquids, *The Journal of Physical Chemistry B*, 102 (1998) 1605-1609.
- [257] K. Yoshimoto, T.S. Jain, K. Van Workum, P.F. Nealey, J.J. de Pablo, Mechanical heterogeneities in model polymer glasses at small length scales, *Physical Review Letters*, 93 (2004) 175501.
- [258] J. Ding, S. Patinet, M.L. Falk, Y. Cheng, E. Ma, Soft spots and their structural signature in a metallic glass, *Proceedings of the National Academy of Sciences*, 111 (2014) 14052-14056.
- [259] B. Sun, Y. Hu, D. Wang, Z. Zhu, P. Wen, W. Wang, C. Liu, Y. Yang, Correlation between local elastic heterogeneities and overall elastic properties in metallic glasses, *Acta Materialia*, 121 (2016) 266-276.
- [260] Z. Wang, B. Sun, H. Bai, W. Wang, Evolution of hidden localized flow during glass-to-liquid transition in metallic glass, *Nature Communications*, 5 (2014) 5823.
- [261] H. Wagner, D. Bedorf, S. KÜchemann, M. Schwabe, B. Zhang, W. Arnold, K. Samwer, Local elastic properties of a metallic glass, *Nature materials*, 10 (2011) 439-442.
- [262] M. Tsamados, A. Tanguy, C. Goldenberg, J.-L. Barrat, Local elasticity map and plasticity in a model Lennard-Jones glass, *Physical Review E*, 80 (2009) 026112.
- [263] R. Hill, The elastic behavior of a crystalline aggregate, *Proceedings of the Physical Society. Section A*, 65 (1952) 349.
- [264] W. Voigt, Ueber die Beziehung zwischen den beiden Elasticitätsconstanten isotroper Körper, *Annalen der Physik*, 274 (1889) 573-587.
- [265] A. Reuss, Berechnung der fließgrenze von mischkristallen auf grund der plastizitätsbedingung für einkristalle, *ZAMM - Journal of Applied Mathematics and Mechanics/Zeitschrift für Angewandte Mathematik und Mechanik*, 9 (1929) 49-58.
- [266] A. Polian, D. Vo-Thanh, P. Richet, Elastic properties of a-SiO₂ up to 2300 K from Brillouin scattering measurements, *EPL (Europhysics Letters)*, 57 (2002) 375.
- [267] C. Lecomte, Exact statistics of systems with uncertainties: an analytical theory of rank-one stochastic dynamic systems, *Journal of Sound and Vibration*, 332 (2013) 2750-2776.
- [268] H. Dawson, On the Numerical Value of $\int_0^1 \sin^2 \pi x dx$, *Proceedings of the London Mathematical Society*, 1 (1897) 519-522.
- [269] N. Wang, X. Wu, C. Liu, Opposite Effects of SiO₂ Nanoparticles on the Local α and Larger-Scale α' Segmental Relaxation Dynamics of PMMA Nanocomposites, *Polymers*, 11 (2019) 979.
- [270] G. Bel, E. Barkai, Weak ergodicity breaking in the continuous-time random walk, *Physical Review Letters*, 94 (2005) 240602.
- [271] A.L. Glebov, L. Huang, S. Aoki, M. Lee, K. Yokouchi, Two-dimensional microlens arrays in silicon-on-silicon planar lightwave circuit technology, *Journal of Micro/Nanolithography, MEMS, and MOEMS*, 2 (2003) 309-319.
- [272] P. Nussbaum, R. Voelkel, H.P. Herzig, M. Eisner, S. Haselbeck, Design, fabrication and testing of microlens arrays for sensors and microsystems, *Pure and applied optics: Journal of the European optical society part A*, 6 (1997) 617.
- [273] T.-W. Yeow, K.E. Law, A. Goldenberg, MEMS optical switches, *IEEE Communications magazine*, 39 (2001) 158-163.

- [274] W. Zhu, M. Marple, B. Aitken, S. Sen, Universality in the non-Newtonian viscous flow behavior of $\text{As}_x\text{Se}_{1-x}$ liquids: results from capillary rheometry, *Journal of Non-Crystalline Solids*, 453 (2016) 42-45.
- [275] N. Ostrovsky, D. Yehuda, S. Tzadka, E. Kassis, S. Joseph, M. Schwartzman, Direct Imprint of Optical Functionalities on Free - Form Chalcogenide Glasses, *Advanced Optical Materials*, 7 (2019) 1900652.
- [276] J.-P. Guin, T. Rouxel, V. Keryvin, J.-C. Sanglebœuf, I. Serre, J. Lucas, Indentation creep of Ge–Se chalcogenide glasses below T_g : elastic recovery and non-Newtonian flow, *Journal of Non-Crystalline Solids*, 298 (2002) 260-269.
- [277] S. Wang, C. Jain, L. Wondraczek, K. Wondraczek, J. Kobelke, J. Troles, C. Caillaud, M.A. Schmidt, Non-Newtonian flow of an ultralow-melting chalcogenide liquid in strongly confined geometry, *Applied Physics Letters*, 106 (2015) 201908.
- [278] D. Yun, J. Kim, M. Kim, D.Y. Kim, J. Kwon, J. Hwang, Impact Print - Type Hot Embossing Process Technology, *Advanced Engineering Materials*, 20 (2018) 1800386.
- [279] L. Nguyen, M.-H. Wu, C. Hung, Finite element analysis of ultrasonic vibration-assisted microstructure hot glass embossing process, *Australian Journal of Mechanical Engineering*, 17 (2019) 199-208.